Towards Understanding Solute and Solvent Dynamics in Mono and Dicationic Room Temperature Ionic Liquids Through Fluorescence and Nuclear Magnetic Resonance (NMR) Studies

By

PRABHAT KUMAR SAHU
CHEM11201104004

National Institute of Science Education and Research
Bhubaneswar, Odisha-751005

A thesis submitted to the
Board of Studies in Chemical Sciences

In partial fulfilment of requirements
For the degree of

DOCTOR OF PHILOSOPHY

of

HOMI BHABHA NATIONAL INSTITUTE
Mumbai, India

October, 2016

Homi Bhabha National Institute[1]

Recommendations of the Viva Voce Committee

As members of the Viva Voce Committee, we certify that we have read the dissertation prepared by Mr. Prabhat Kumar Sahu entitled "Towards Understanding Solute and Solvent Dynamics in Mono and Dicationic Room Temperature Ionic Liquids Through Fluorescence and Nuclear Magnetic Resonance (NMR) Studies" and recommend that it may be accepted as fulfilling the thesis requirement for the award of Degree of Doctor of Philosophy.

Chairman – Prof. Alagar Srinivasan	Date: 13.1.2017
Guide / Convener – Dr. Moloy Sarkar	Date: 13-01-2017
Co-guide - -------------------------------------	Date:
Examiner – Prof. Anunay Samanta	Date: 13.1.2017
Member 1- Dr. Sanjib Kar	Date: 13/01/2017
Member 2- Dr. Himansu Sekhar Biswal	Date: 13/01/2017
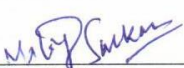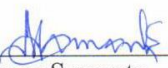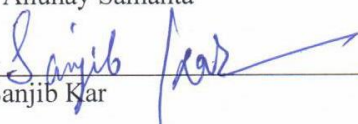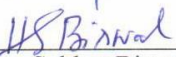
Final approval and acceptance of this thesis is contingent upon the candidate's submission of the final copies of the thesis to HBNI.

I/We hereby certify that I/we have read this thesis prepared under my/our direction and recommend that it may be accepted as fulfilling the thesis requirement.

Date: 13-01-2017

Place: Bhubaneswar
NISER, JATNI
CAMPUS

<Signature>

Co-guide (if applicable)

<Signature>

Guide

---

[1] This page is to be included only for final submission after successful completion of viva voce.

STATEMENT BY AUTHOR

This dissertation has been submitted in partial fulfilment of requirements for an advanced degree at Homi Bhabha National Institute (HBNI) and is deposited in the Library to be made available to borrowers under rules of the HBNI.

Brief quotations from this dissertation are allowable without special permission, provided that accurate acknowledgement of source is made. Requests for permission for extended quotation from or reproduction of this manuscript in whole or in part may be granted by the Competent Authority of HBNI when in his or her judgment the proposed use of the material is in the interests of scholarship. In all other instances, however, permission must be obtained from the author.

Prabhat Kumar Sahu

DECLARATION

I, hereby declare that the investigation presented in the thesis has been carried out by me. The work is original and has not been submitted earlier as a whole or in part for a degree / diploma at this or any other Institution / University.

Prabhat Kumar Sahu

List of Publications

1. Photophysical and density functional studies on the interaction of a new nitrobenzoxadiazole derivative with anions. S. K. Das**,** S. S. Mishra; **P. K. Sahu**, A. Nijamudheen, V. Mohan,; M. Sarkar. *Chem. Phys. Lett.* **2012**, *528*, 11.

2. Ion interactions with a new ditopic naphthalimide-based receptor: A photophysical, NMR and theoretical (DFT) Study. V. Mohan, A. Nijamudheen, S. K. Das, **P. K. Sahu**, U. P. Kar, A. Rahaman, M. Sarkar. *ChemPhysChem* **2012**, *13*, 3882.

3. *Picosecond solvation dynamics of Coumarin153 in Bis(1-Methyl-1h-Imidazol-3-Ium-3-Yl)dihydroborate cation containing room temperature ionic liquid and ionic liquid-dmf mixtures. **P. K. Sahu**, S. K. Das, M. Sarkar. *J. Appl. Sol. Chem. Model.*, **2013**, *2*, 47.

4. Synthesis, photophysics, live Cell imaging and aggregation behaviour of some structurally similar alkyl chain containing bromonaphthalimide systems: influence of alkyl chain length on the aggregation behaviour. M. Soni, S. K**.** Das, **P. K. Sahu**, U. P. Kar, A. Rahaman, M. Sarkar. *J. Phys. Chem. C* **2013**, *117*, 14338.

5. Probing the microscopic aspects of 1-butyl-3-methylimidazolium trifluoroacetate ionic liquid and its mixture with water and methanol: A photophysical and theoretical (DFT) study. S. K. Das, **P. K. Sahu**, M. Sarkar. *J. Fluoresc.* **2013**, *23*, 1217.

6. Diffusion-viscosity decoupling in solute rotation and solvent relaxation of coumarin153 in ionic liquids Containing fluoroalkylphosphate (FAP) Anion: A thermophysical and photophysical study. S. K. Das, **P. K. Sahu**, M. Sarkar. *J. Phys. Chem. B* **2013**, *117*, 634.

7. *Toward understanding solute−solvent interaction in room-temperature mono- and dicationic ionic liquids: A combined fluorescence spectroscopy and mass spectrometry analysis. **P. K. Sahu**, S. K. Das, M. Sarkar. *J. Phys. Chem. B* **2014**, *118*, 1907.

8. *Fluorescence response of a dipolar organic solute in a dicationic ionic liquid (IL): Is the behavior of dicationic IL different from that of usual monocationic IL? **P. K. Sahu**, S. K. Das, M. Sarkar. *Phys. Chem. Chem. Phys.* **2014**, *16*, 12918.

9. Probing the aggregation behavior of 4-aminophthalimide and 4-(N,N-dimethyl) amino-N-methylphthalimide: a combined photophysical, crystallographic, microscopic and theoretical (DFT) study. D. Majhi, S.K. Das, **P. K. Sahu**, S. Md Pratik, A. Kumar , M. Sarkar. *Phys. Chem. Chem. Phys.,* **2014**, *16*, 18349.

10. Analyte Interactions with a new ditopic dansylamide−nitrobenzoxadiazole dyad: a combined photophysical, NMR, and theoretical (DFT) study. A. K. Bhoi, S. K. Das, D. Majhi, **P. K. Sahu**, A. Nijamudheen, N. Anoop, A. Rahaman, M. Sarkar. *J. Phys. Chem. B* **2014**, *118*, 9926.

11. Studies on electronic energy transfer (EET) on a series of room temperature ionic liquids (RTILs):can the EET studies on RTILs be exploited to predict their structural organization? S. K. Das, **P. K. Sahu,** M. Sarkar. *RSC Adv.,* **2014**, *4*, 39184.

12. *Understanding structure-property correlation in monocationic and dicationic ionic liquids through combined fluorescence and pulsed-field gradient (PFG) and relaxation NMR experiments. **P. K. Sahu**, A. Ghosh, M. Sarkar. *J. Phys. Chem. B*, **2015,** *119*, 14221.

13. Investigating the influence of alkyl side chain length on the fluorescence response of C153 in a series of room temperature ionic liquids. S. K. Das, D. Majhi, **P. K. Sahu,** M. Sarkar. *RSC Adv.,* **2015**, *5*, 41585.

14. Combined photophysical, NMR and theoretical (DFT) study on the interaction of a multi component system in absence and presence of different biologically and environmentally important ions. A. K. Bhoi, **P. K. Sahu**, G. Jha. M. Sarkar. *RSC Adv.*, **2015**, *5*, 61258.

15. *Studies on intramolecular electron transfer reaction in donor-spacer-acceptor systems in room-temperature ionic liquids. **P. K. Sahu**, S. K. Das, M. Sarkar. *J. Mol. Liq.* **2016**, *214*, 24.

16. *Reorientational dynamics of charged and neutral solutes in 1-Alkyl-3-methylimidazoilum Bis(trifluoromethylsulfonyl)imide ionic liquids: Realization of ionic component of hydrogen bond. **P. K. Sahu**, M. Sarkar. *Chem. Phys. Lett.,* **2016**, 652, 177.

17. Studies on the mechanism of fluorescence quenching of cds quantum dots by 2-amino-7-nitrofluorene and 2-(n,n-dimethylamino)-7-Nitrofluorene. S. S. Dandpat, **P. K. Sahu**, M. Sarkar. *Chemistry Select*, **2016**,*1*, 2219.

18. Probing interactions of structurally similar but chemically distinguishable organic solutes with 1-ethyl-3-methylimidazolium alkylsulfate(alkyl = ethyl, hexyl and octyl) ionic liquids through fluorescence, NMR and Fluorescence Correlation Spectroscopy (FCS) study. D. Majhi, **P. K. Sahu**, S. Seth, M. Sarkar, *Phys. Chem. Chem. Phys.* **2016**, *18*, 22343.

19. *Nuclear magnetic resonance, fluorescence correlation spectroscopy and time-resolved fluorescence anisotropy studies of intermolecular interactions in Bis(1-methyl-1h-imidazol-3-ium-3-yl)dihydroboratebis(trifluoromethylsulfonyl)amide and its mixtures with various cosolvents. **P. K. Sahu**, R. Nanda, S. Seth, A. Ghosh, M. Sarkar. *Chem. Phys. Lett.*, **2016**, *661*, 100.

*pertaining to the present thesis.

Conferences

1. International symposium on Dynamics of Complex Chemical and Biological Systems (DCCBS-2014), during February 13-15, 2014 held at IIT Kanpur, India. Presented a poster entitled "Steady State and Time-resolved Fluorescence Response of a Dipolar Organic Solute in a Dicationic Ionic Liquid (IL): Is the Behavior of Dicationic IL Different from that of Usual Monocationic IL?"

2. 13th biennial DAE–BRNS "Trombay Symposium on Radiation and Photochemistry"- incorporating 6th "Asia-Pacific Symposium on Radiation Chemistry", (TSRP–APSRC–2016), organized by Bhabha Atomic Research Centre (BARC) in association with the Indian Society for Radiation and Photochemical Sciences (ISRAPS) during January 5–9, 2016 at BARC, Mumbai, India. Presented a poster entitled "Structure-Property Correlation In Mono And Dicationic ILs: Combined Fluorescence And NMR Studies"

3. International conference on Recent Advances in Molecular Spectroscopy (RAMS-2016), during March 2-4, 2016 held at University of Hyderabad, Hyderabad, India. Presented a poster entitled "Structure-Property Correlation In Mono And Dicationic ILs Through Combined Fluorescence And NMR Studies".

Prabhat Kumar Sahu

Dedicated to……

My Beloved Parents

ACKNOWLEDGEMENTS

Finally, I would like to express my heartfelt gratitude to my parents for their endless love, affection, support, and encouragement.

Above all, I thank the Almighty for showing me the right path always.

<div align="right">

Prabhat

</div>

CONTENTS

Chapter 3

Reorientational Dynamics of Charged and Neutral Solutes in 1-Alkyl-3-methylimidazoilum Bis(trifluoromethylsulfonyl)imide Ionic Liquids

Chapter 4

Intramolecular Photoinduced Electron Transfer Reaction in Donor-Spacer-Acceptor Systems in Room-Temperature Ionic Liquids

Chapter 5

Solute-Solvent and Solvent-Solvent Interaction in A Borate-Based Room Temperature Ionic Liquid and Its Binary Mixtures ith Various Cosolvents Through Fluorescence and NMR Study

Chapter 6

Solute and Solvent Relaxation Dynamics in Mono and Dicationic Room-Temperature Ionic Liquids: A Combined Fluorescence and NMR Study

SYNOPSIS

In recent times, ionic liquids (ILs) have attracted considerable attention both from academia and industry mainly due to their attractive physicochemical properties and their use in several applications.[1,2] Geminal dicationic ionic liquids (DILs), having two unit positive charge, are expected to be advantageous over traditional monocationic ionic liquids (MILs) as DILs have been shown to possess superior physicochemical properties in contrast to MILs.[3,4] In this regard, studies with an aim to understand the structure-dynamics correlation in these specialized media are of extreme importance for effective utilization of these systems. The present thesis is focused to understand the kinship among structure, intermolecular interactions and dynamics through solute and solvent dynamics study in mono and dicationic RTILs by employing steady-state and time-resolved fluorescence as well as Nuclear Magnetic Resonance (NMR) studies.

Organization of thesis

The present thesis has been systematically organized in six chapters to discuss the results obtained from different investigations during current research. The contents of the different chapters of the thesis are briefly mentioned below.

Chapter 1: Introduction

This chapter begins with a brief introduction about ILs and their physicochemical properties. Various applications of ILs both in academics and industries are outlined. Studies on solvation and rotational relaxation dynamics and photoinduced electron transfer reactions in RTILs are discussed in detail by highlighting recent literature reports. The utility of translational diffusion and spin-lattice relaxation measurements through NMR in understanding the structure-dynamics correlation are also described in this chapter. Objective of the present research work has been discussed at the end of this chapter.

Chapter 2: Instrumentations and Methods

Basic principles of various instrumental techniques employed in the present studies, such as absorption spectroscopy, steady-state and time-resolved spectrofluorimetry have been described briefly in this chapter. A detailed description of working principle of the time-correlated single photon counting (TCSPC) technique has been provided. Principles of solvation and rotational relaxation dynamics and various NMR techniques such as Pulsed-Field-Gradient NMR (PFG-NMR) and spin-lattice relaxation time (T_1) measurements are mentioned in detail. Methodologies employed to obtain the time-resolved emission spectra (TRES) from the decay curves; solvation and rotational relaxation time and analysis of rotational relaxation dynamics through different hydrodynamic models have also been discussed. Error limit for different experimental parameters are also provided at the end of this chapter.

Chapter 3. Reorientational Dynamics of Charged and Neutral Solutes in 1-Alkyl-3-methylimidazoilum Bis(trifluoromethylsulfonyl)imide Ionic Liquids

In this chapter, the effect of electrostatic interaction on solute rotation in ILs is discussed. Recent reports on rotational relaxation dynamics of charged solutes demonstrate the predominant role of solute-solvent hydrogen bonding interaction in slowing down the rotational diffusion of the concerned solute.[5,6] However, no evidence of role of electrostatic interaction on rotational dynamics has been observed.[5,6] To find out unambiguous role of electrostatic interaction towards solute rotation, we have studied rotational diffusion of some charged and neutral solutes in two structurally similar but chemically distinguishable ILs (Chart1). One of the IL contains a C2–methyl group (Chart 1) so that the H-bonding interaction due to C2–H is eliminated, and thereby the effect of electrostatic interaction on solute rotation is exclusively monitored. We have also chosen molecular probes with different unit charge so that the effect of variation in charge on solute rotation can also be followed in a systematic manner (Chart 1).
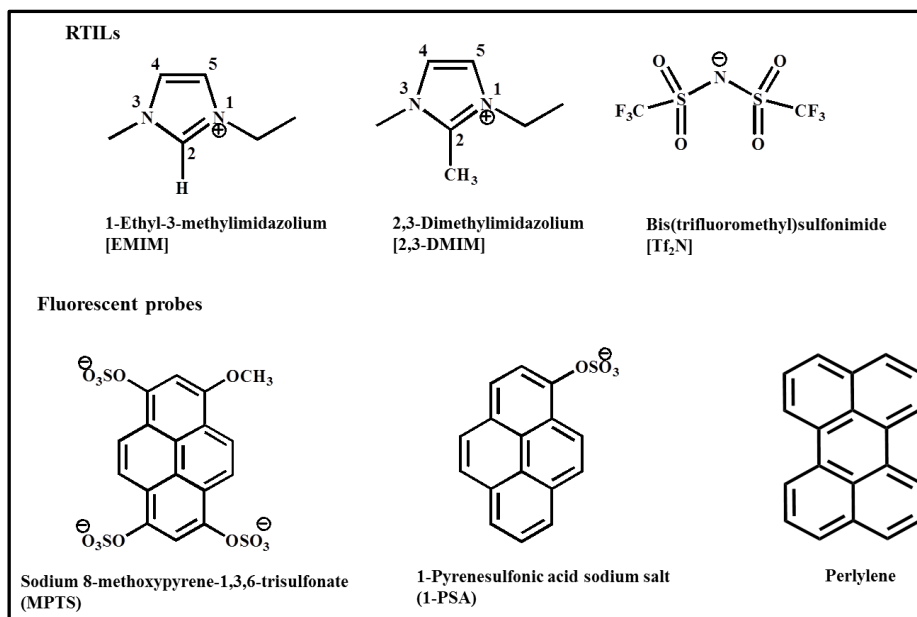
Chart 1: Molecular structures of the RTILs and different charged and neutral probes.

Table 1: Summary of the rotational relaxation parameters of MPTS, 1-PSA and perylene

Systems	Temp.(K)	[EMIM][Tf$_2$N]			[2,3-DMIM][Tf$_2$N]		
		Vis.(cP)	$<\tau_r>$(ns)	C_{rot}	Vis.(cP)	$<\tau_r>$(ns)	C_{rot}
MPTS	293	34.2	5.77	1.49	73.6	11.62	1.39
1-PSA	293	34.2	1.93	0.48	73.6	3.71	0.43
Perylene	293	34.2	0.51	0.15	73.6	1.04	0.13

Experimental error ±5%
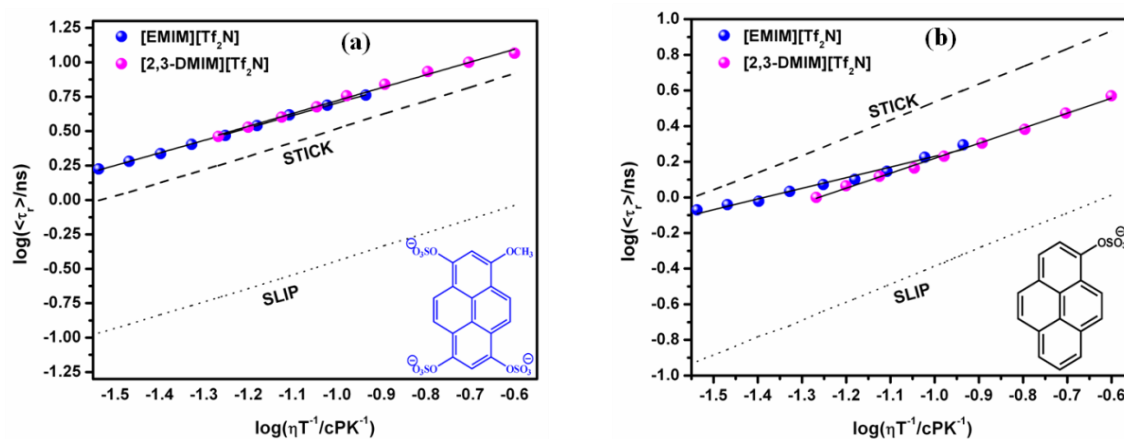
Figure 1. The log-log plots of τ_r vs. η/T for (a) MPTS and (b) 1-PSA. The solid black lines represent linear fit to the data points shown in symbols.

Analysis of the fluorescence anisotropy results in light of Stokes-Einstein-Debye (SED) hydrodynamic theory has revealed superstick hydrodynamics behaviour of MPTS in both ILs

(Figure 1a). Quite interestingly, rotational coupling constant (C_{rot}), is found to be similar (~1.6) for MPTS in both ILs (Table 1) even though [2,3-DMIM][Tf2N] cannot form stronger solute–solvent hydrogen bonding interaction owing to C2-methylation in the imidazolium moiety. This observation has indicated the role of electrostatic (ion-ion) interaction on rotational relaxation of MPTS in ILs. Rotational diffusion of the mononegative solute, 1-PSA, is observed to be faster than that has been observed for the tri-negative solute MPTS in both ILs (Figure 1, Table 1). The weakening of solute–solvent interaction due to reduction of total charge in 1-PSA can be reasoned behind such behaviour of 1-PSA. Rotational relaxation time of neutral perylene is found to be fastest among all the three probes under investigation. Similar C_{rot} values of perylene in the two ILs (Table 1) have indicated that it locates itself in a similar nonpolar environment in both the ILs. Additionally, translational diffusion coefficients of the probes, estimated through PFG-NMR experiments, have also corroborated the results obtained from anisotropy measurements. Results of the present investigations advocate the need of considering the electrostatic interaction between solute and solvent while explaining the rotational diffusion of charged solutes in RTILs.[7]

Chapter 4: Intramolecular Photoinduced Electron Transfer Reaction in Donor-Spacer-Acceptor Systems in Room-Temperature Ionic Liquids

This chapter describes the studies on intramolecular photoinduced electron transfer (PET) in flexible donor-spacer-acceptor (DSA) systems (Chart 2) in two imidazolium RTILs (Chart 2) and in acetonitrile. Two different flexible DSA systems are purposefully chosen so as to eliminate the effect of transport phenomenon on electron transfer process. The reaction kinetics have been followed via time-resolved fluorescence measurements and analyzed by using a two-state model.
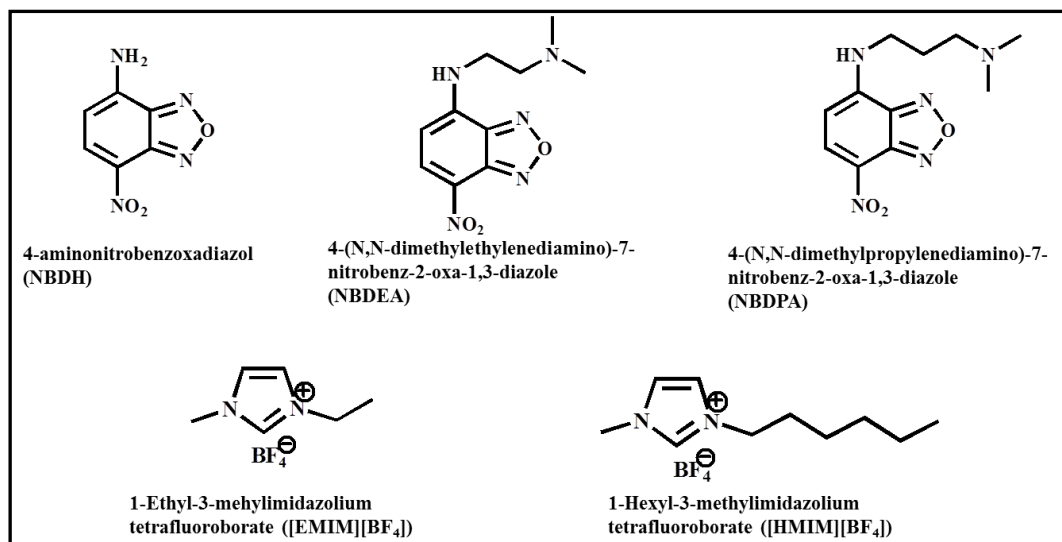
Chart 2: Molecular diagrams of the fluorescent probes and the RTILs.

Table 2: PET rate constants (k_{ET}) and average solvation times ($<\tau_s>$) in the RTILs for the DSA systems

Temp(K)	[EMIM][BF$_4$]			[HMIM][BF$_4$]		
	$^a k_{ET} (\times 10^7 \, S^{-1})$		$<\tau_s>$(ps)	$^a k_{ET} (\times 10^7 \, S^{-1})$		$<\tau_s>$(ps)
	NBDEA	NBDPA		NBDEA	NBDPA	
293	13.32	8.65	373	4.54	5.30	3680
303	16.12	13.55	238	7.16	7.06	1980
313	19.27	16.63	156	12.41	10.88	1130
323	23.15	20.63	113	15.60	13.92	686
333	26.90	24.50	81	18.64	17.03	460

^{a} Experimental error ±5%.

The results have indicated that PET rates are hindered in the RTILs compared to that in acetonitrile. Present study clearly demonstrates the consequences of rate of solvation in respective media in influencing the rate of electron transfer process (Table 2). It may be mentioned here that solvation dynamics in RTILS is quite complex and broadly distributed in time.[8] In the current study slow solvation rate in RTILs is believed to be responsible for slow rate of PET process in ionic liquids. [9]

Chapter 5: Solute-Solvent and Solvent-Solvent Interaction in A Borate-Based Room Temperature Ionic Liquid and Its Binary Mixtures With Various Cosolvents Through Fluorescence and NMR Study

The high viscosity, high manufacturing cost and difficulties in purification impose limitations to the effective use of RTILs. In this context binary mixtures of ILs with various cosolvents can be envisioned to be an alternative solvent system which may help in widening the applicability of ILs.[10] This chapter describes our effort in understanding IL-cosolvent systems by investigating the solute-solvent and solvent-solvent intermolecular interactions through fluorescence and NMR spectroscopy.

Specifically, solvation and rotational relaxation dynamics of Coumarin 153 (C153) has been studied in a borate-based imidazolium IL (Chart 3) and its binary mixtures with dimethylformamide (DMF). The addition of DMF to RTIL decreases the average solvation time due to a lowering of viscosity of the media. This also results in the faster rotational dynamics of C153.[11]

Bis(1-methyl-1H-imidazol-3-ium-3-yl)dihydroboratebis(trifluoromethylsulfonyl)amide

[BIMIMDBA][TF₂N]

Coumarin 153 (C153)
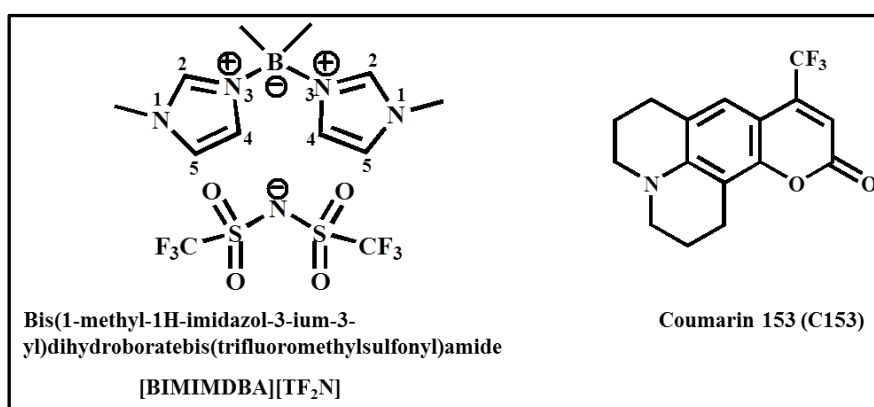
Chart 3: Molecular diagrams of the RTIL and C153.

Table 3. ^{1}H and ^{19}F chemical shifts (δ)/ppm of the cation and anion of the IL in neat and IL-molecular solvent binary mixtures

System	^{1}H Chemical shift (δ)/ppm			^{19}F chemical shift(δ)/ppm
	C2H	C4H, C5H	N-CH$_3$	
Neat IL	8.06	7.04	3.70	-81.18
IL + DMF	8.41	7.34, 7.28	3.89	-80.93
IL + DMSO	8.33	7.26, 7.21	3.83	-80.80
IL + MeOH	8.19	7.17, 7.15	3.80	-81.14
IL + Toluene	7.92	6.98, 6.87	3.53	-80.78

Further, intermolecular interactions between [BIMIMDBA][TF$_2$N] and its binary mixtures with DMF, dimethylsulfoxide (DMSO), methanol (MeOH) and toluene has been probed through NMR studies. Analysis of the ^{1}H and ^{19}F chemical shift (δ/ppm) of the IL in absence and presence of cosolvents (Table 3) indicates the presence hydrogen bonding and ion-π interaction along with ion-dipole interaction in these binary mixtures.
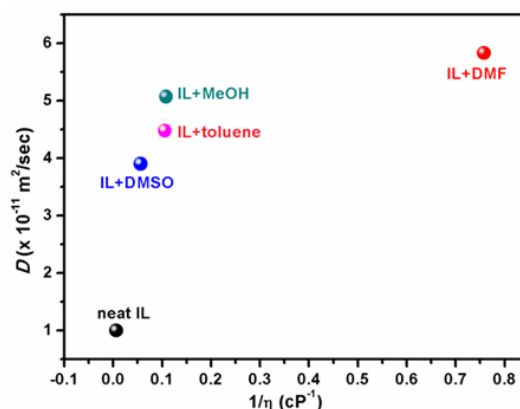
Figure 2. Diffusion coefficients (D) of the cation in neat IL [BIMIMDBA][TF$_2$N] and IL-cosolvent (1:1 molar ratio) binary mixtures.

Nonlinear variation of the translational diffusion coefficient (D) with medium viscosity (Figure 2) for different IL-cosolvent systems indicates the presence of different intermolecular interactions in different IL-cosolvent systems. Excitation wavelength dependent fluorescence anisotropy measurements have depicted that the structural organisation within IL-cosolvent binary mixtures could be very different due to the presence of different intermolecular interactions in different IL-cosolvent system in the present case.[12]

The outcome of the present study is expected to provide useful insight in designing a new borate IL-cosolvents system for newer applications.

Chapter 6: Solute and Solvent Relaxation Dynamics in Mono and Dicationic Room-Temperature Ionic Liquids: A Combined Fluorescence and NMR Study

The dicationic ILs (DILs) with their unique properties such as higher thermal stability, shear viscosity, surface tensions and larger liquid density are expected to be advantageous over the traditional monocationic ILs (MILs) as far as technological applications are concerned.[3,4] A comparative study of solute and solvation dynamics in both mono and dicationic ILs is expected to provide in-depth understanding about the relationship among structure, intermolecular interactions and dynamics which in turn may be helpful to exploit these dication-based systems in newer avenues.

This chapter discusses a comparative study on solute and solvent relaxation dynamics in a six-membered DIL and two MILs (Chart 4) having different alkyl chain length. The chapter is divided into two parts. The first part illustrates the rotational dynamics of some polar and nonpolar molecules in the mono and dicationic ILs whereas the second part describes the results of a combined fluorescence and NMR investigations in understanding the mechanism of dynamics of solvation in ILs.
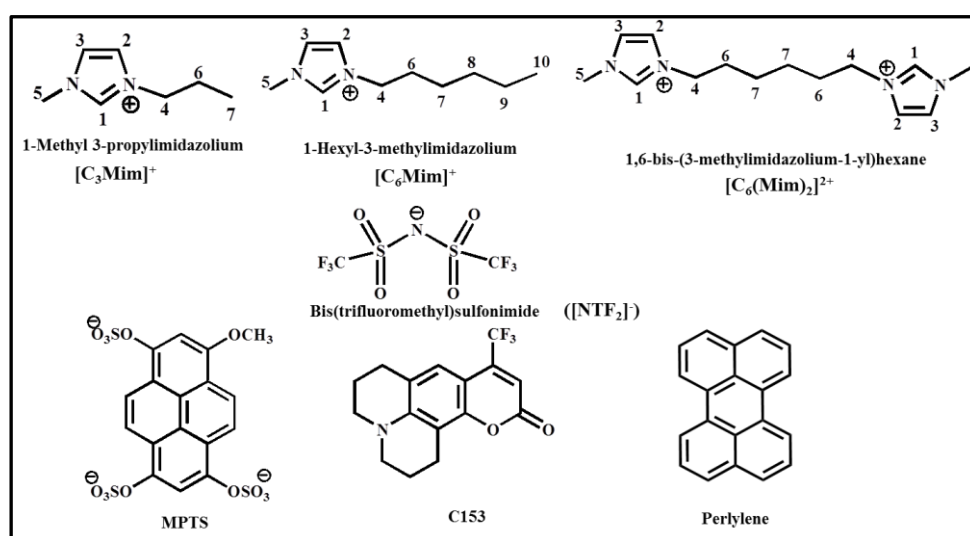
Chart 4: Molecular structures of RTILs and probes.
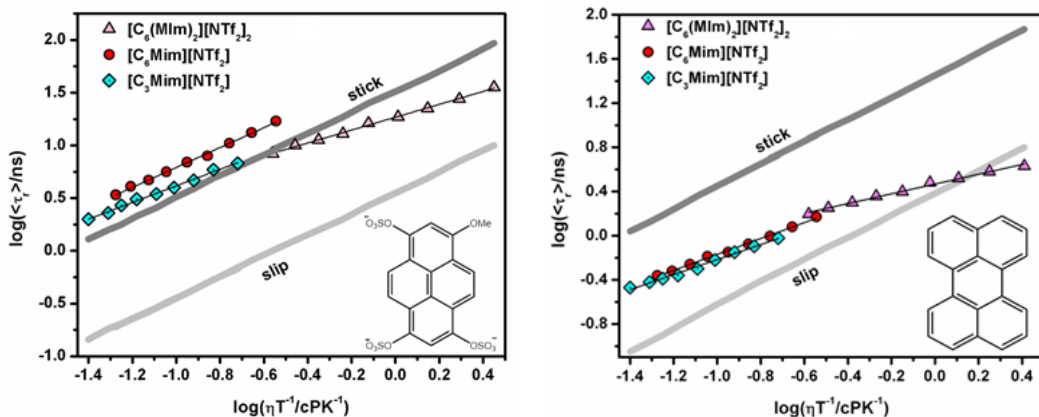
Figure 3. Log−log plots of $\langle \tau_r \rangle$ vs η/T for MPTS and perylene. The solid black line is the linear fit to the data points. Blue, red, and green dotted lines represent the boundary condition obtained from Gierer−Wirtz (GW) quasihydrodynamic theory[13] in [C$_3$Mim][NTf$_2$], [C$_6$Mim][NTf$_2$], and [C$_6$(MIm)$_2$][NTf$_2$]$_2$, respectively.

During the study of rotational dynamics, MPTS has shown a stronger interaction with [C$_6$MIm][NTf$_2$] than with [C$_3$MIm][NTf$_2$] or with [C$_6$(MIm)$_2$][NTf$_2$]$_2$. It has been demonstrated that relatively faster rotational behavior of MPTS in the DIL (Figure 3), despite the fact that of the DIL has a higher viscosity than the other two MILs, might arise due to stronger cation-counter anion interaction within the DIL. The nonpolar perylene shows a slip to sub-slip hydrodynamic behavior in the DIL (Figure 3) which indicates that it resides in the nonpolar domain of the media. Dipolar C153 follows normal SED hydrodynamics. Rotational coupling constants and average rotational relaxation times of C153 are found to be intermediate between the other two probes, which indicate that C153 is distributed in both polar and nonpolar regions of the media.[14,15] This study unveils distinctive features of solute−solvent interaction in the mono and dicationic ILs.

Table 4: Solvation relaxation parameters of C153 at $\lambda_{exc.}$ = 405nm

RTILs	Vis.(cP)/Temp.(K)	$\langle \tau_s \rangle$(ns)	$\Delta\nu_{obs}(10^3cm^{-1})$	$\Delta\nu_{est}(10^3cm^{-1})$	f_{obs}
[C$_3$MIm][NTf$_2$]	55/293	0.46	1.11	1.38	0.80
[C$_6$MIm][NTf$_2$]	84/293	0.73	1.07	1.32	0.81
[C$_6$(MIm)$_2$][NTf$_2$]$_2$	827/293	1.64	1.64	1.43	1.15

Experimental error ±5%. $f_{obs} = \Delta\nu_{obs}/\Delta\nu_{est}$.
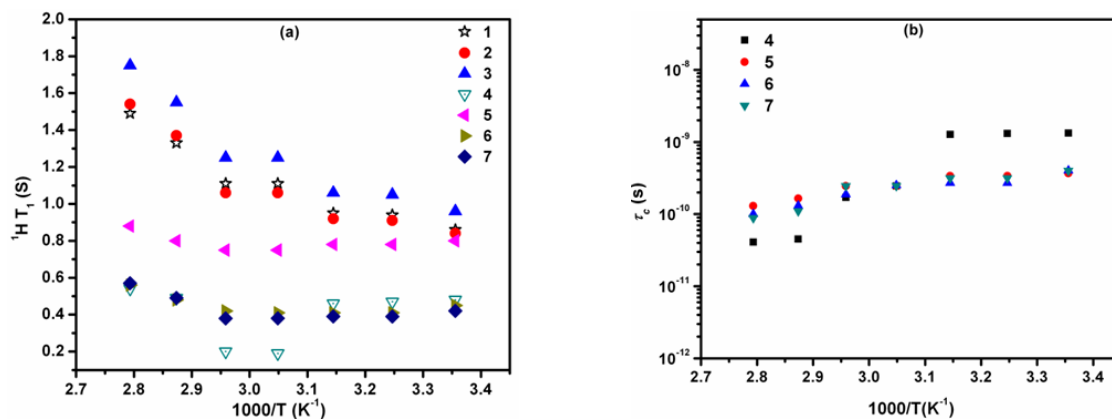
Figure 4. Temperature dependence of ^1H T_1 (a) and correlation time (τ_c) (b) of protons of the cation $[C_6(Mim)_2]^{2+}$.

Results of solvation dynamics study showed absence of any ultra-fast component of solvation in the DIL at lower temperature (Table 4). However at low viscous condition (higher temperature), ~32% of the total dynamics is found to be ultrafast in nature. This is a very interesting observation in a sense that such behaviour has not been observed for the imidazolium ILs. Moreover no proper explanation for origin of such observation is available. The present time-resolved fluorescence data indicates the reorientational motion of the cation can be responsible for the observed behaviour. In order to examine correlation between the reorientational motion of the imidazolium cation and dynamics of solvation NMR experiments have been carried out. PFG-NMR experiments have revealed distinctive features of translational diffusion of cations in the RTILs. ^1H spin−lattice relaxation experiments demonstrate a dissimilar reorientational dynamics of the cations of mono and dicationic ILs (Figure 4). Thus, from the outcomes of the NMR experiments it can be inferred that the role of reorientational motion of the imidazolium cation and consequently the contribution from dipole-dipole interaction influencing the ultrafast component of solvation in particular and solvation dynamics in general in ILs deserves serious consideration.[15,16]

In conclusion, the present study has demonstrated that the structure, intermolecular interactions and dynamics in MILs and DIL are quite different. The present work entails a significant step forward in understanding the structure-property relationship in mono and dicationic ILs.

The future prospects are also outlined at the end of the thesis.

References:

1. Hallett, J. P.; Welton, T. *Chem. Rev.* **2011**, *111*, 3508**.**

2. Plechkova, N. V.; Seddon, K. R. *Chem. Soc. Rev.* **2008**, *37*, 123.

3. Anderson, J. L.; Ding, R.; Ellern, A.; Armstrong, D. W. *J. Am. Chem. Soc.* **2005**, *127*, 593.

4. Shirota, H.; Mandai, T.; Fukazawa, H.; Kato, T. *J. Chem. Eng. Data* **2011**, *56*, 2453.

5. Prabhu S. R.; Dutt, G. B. *J. Phys. Chem. B* **2014**, *118*, 9420.

6. Khara, D. C.; Samanta. A. *Phys. Chem. Chem. Phys*. **2010**, *12*, 7671.

7. Sahu, P. K.; Sarkar, M. *Chem. Phys. Lett.,* **2016**, *652*, 177.

8. Jin, H.; Baker, G. A.; Arzhantsev, S.; Dong, J.; Maroncelli, M. *J. Phys. Chem. B* **2007**, *111*, 7291.

9. Sahu, P. K.; Das, S. K.; Sarkar, M. *J. Mol. Liq.* 2016, *214*, 24.

10. Nockemann, P.; Thijs, B.; Parac-Vogt, T. N.; Hecke, K. V.; Meervelt, L. V.; Tinant, B.; Hartenbach, I.; Schleid, T.; Ngan, V. T.; Nguyen M. T.; Binnemans, K. *Inorg. Chem.* **2008**, *47*, 9987.

11. Sahu, P. K.; Das, S. K.; Sarkar, M. *J. Appl. Sol. Chem. Model.*, **2013**, *2*, 47.

12. Sahu, P. K.; Nanda R.; Seth, S.; Ghosh, A.; Sarkar, M. *Chem. Phys. Lett.*, **2016**, *661*, 100.

13. Gierer, A.; Wirtz, K. Molekulare Theorie der Mikroreibung. Z. *Naturforsch., A: Phys. Sci.* **1953,** *8*, 532.

14. Sahu, P. K.; Das, S. K.; Sarkar, M. *J. Phys. Chem. B* **2014**, *118*, 1907.

15. Sahu, P. K.; Ghosh A.; Sarkar, M. *J. Phys. Chem. B* **2015**, *119*, 14221.

16. Sahu, P. K.; Das, S. K.; Sarkar, M. *Phys. Chem. Chem. Phys.* **2014**, *16*, 12918.

NBDPA (b) in ACN, [EMIM][BF$_4$] and [HMIM][BF$_4$].

16

with time for $[C_3Mim][NTf_2]$ and $[C_6(MIm)_2][NTf_2]_2$.

List of Tables

Glossary of Acronyms

ILs   ionic liquids

RTILs   room temperature ionic liquids

HF   hydrofluoric acid

NATO   North Atlantic Treaty Organization

MILs   monocationic ionic liquids

DILs   dicationic ionic liquids

Tf_2N^- / NTF_2^- bis(trifluoromethanesulfonyl)imide

BF_4^- Tetrafluoroborate

PF_6^- Hexafluorophophate

FAP   Fluoroalkylphosphate

Cl^- chloride ion

T_d thermal decomposition

T_g glass transition temperature

VFT   Vogel-Tammann-Fulcher

n_D refractive index

ε   static dielectric constant

$C_2mim[X]$ 1-ethyl-3-methylimidazolium halide

$C_4mim[Tf_2N]$ 1-butyl-3-methylimidazolium bis(trifluoromethylsulfonyl)imide

FT-IR   Fourier transform infrared spectroscopy

NMR   nuclear magnetic resonance

OHD-RIKES   Optical heterodyne-detected Raman induced Kerr effect

                            spectroscopy

MD	molecular dynamics
MALDI-MS	matrix-assisted laser desorption/ionization mass spectrometry
TSILs	Task specific ionic liquids
TDFSS	time-dependent fluorescence Stokes shifts
REES	red edge excitation shift
REE	red edge effect
PFG-NMR	Pulsed field gradiant nuclear magnetic resonance
PET	photoinduced electron transfer
DSA	donor-spacer-acceptor
[EMIM][TF$_2$N]	1-ethyl-3-methylimidazolium bis(trifluoromethylsulfonyl)imide
[EMIM][SCN]	1-ethyl-3-methylimidazolium thiocyanate
[BMIM][BF$_4$]	1-butyl-3-methylimidazolium tetrafluoroborate
NOE	Nuclear Overhouser Effect
[HMIM][Br].	1-hexyl-3-methylimidazolium bromide
[C$_4$mim][Br]	1-butyl-3-methylimidazolium bromide
[C$_4$C$_1$mim][Br]	1-butyl-2,3-dimethylimidazolium bromide
[BMIM][Tf$_2$N]	1-butyl-3-methylimidazolium bis(trifluoromethylsulfonyl)imide
CP-MAS	cross-polarization-magic angle spinning
C153	coumarin153
PMT	photomultiplier tube
TCSPC	time-correlated single photon counting
CFD	Constant Fraction Discriminator
TAC	Time to Amplitude Converter
MCA	Multichannel Analyzer
ADC	Analog-to-Digital Converter

FWHM	full width at half maximum
NLLS	nonlinear least squares
TRES	time-resolved emission spectra
MC	missing component
DFT	density functional theory
MPTS	sodium 8-methoxypyrene-1,3,6-sulfonate
1-PSA	1-pyrenesulfonic acid sodium salt
[2,3-DMIM][Tf$_2$N]	1-ethyl-2,3-dimethylimidazolium bis(trifluoromethylsulfonyl)imide
DMDPP	2, 5-dimethyl-1, 4-dioxo-3, 6-diphenylpyrrolo [3,4-*c*] pyrrole
PIET	photoinduced intermolecular electron transfer
NBDEA	4-(N,N-dimethylethylenediamino)-7-nitrobenz-2-oxa-1,3-diazole
NBDPA	4-(N,N-dimethylpropylenediamino)-7-nitrobenz-2-oxa-1,3-diazole
NBDH	4-aminonitrobenzoxadiazol
EtOAc	Ethylacetate
[EMIM][BF$_4$]	1-ehtyl-3-methylimidazolium Tetrafluoroborate
[HMIM][BF$_4$].	1-hexyl-3-methylimidazolium tetrafluoroborate
4NBD	4-(azetidinyl)-7-nitrobenz-2-oxa-1,3-diazole
[BIMIMDBA][TF$_2$N]	Bis(1-methyl-1-H-imidazol-3-ium-3-yl)dihydroborate bis(trifluoromethylsulfonyl)amide
C153	Coumarin 153
SPADs	single-photon avalanche photodiodes
ROESY	Rotating frame Overhauser Effect Spectroscopy
FCS	Fluorescence correlation spectroscopy
[C$_3$MIm][NTf$_2$]	1-methyl-3-propylimidazolium bis(trifluoromethylsulfonyl)amide

[C$_6$MIm][NTf$_2$]	1-hexyl-3-methylimidazolium bis(trifluoromethylsulfonyl)amide
[C$_6$(MIm)$_2$][NTf$_2$]$_2$	1,6-bis-(3-methylimidazolium-1-yl)hexane bis(trifluoromethylsulfonyl)amide
ANF	2-amino-7-nitrofluorene
PRODAN	6-propionyl-2-dimethylaminonaphthalene
QENS	quasi-elastic neutron scattering

Chapter 1

Introduction

In this chapter a brief discussion on structure, physicochemical properties and various applications of ionic liquids (ILs) has been provided. Basic principles of solvation and rotational dynamics are outlined followed by a discussion on some literature reports on solvation dynamics, rotational dynamics and photoinduced electron transfer process in ILs. The objective behind the present thesis is presented at the end of this chapter.

1.1 Ionic Liquids

Ionic liquids (ILs) are salts having melting point below 100°C.[1] The ILs which are liquid at ambient temperature and pressure are termed as Room Temperature Ionic Liquids (RTILs). ILs are composed of large and bulky cations and anions. The cations are usually organic moieties such as ammonium, imidazolium, pyrollidinium, pyridinium etc. whereas the anions can be organic or inorganic such as chloride, bromide, tertrafluoroborate, hexafluorophosphate etc. In these systems, the charge on the constituent ions is dispersed due to` their lager size and hence the charge density on the constituent ions is low. The large size of the constituent ions and the low charge density on them reduce the Coulombic forces between them and disrupt the lattice packing thereby preventing them to form a regular crystalline structure. Thus, low charge density on the constituent ions and inefficient packing make these systems liquid. The term 'ionic liquid' is coined for these liquids as their properties widely differ from the traditional high temperature molten salts.[2,3] ILs are different from the conventional organic solvents in terms of their distinctive physicochemical properties such as negligible vapour pressure, non-flammability, high thermal stability, wide electrochemical window and ability to dissolve a wide range of organic and inorganic compounds.[4-8] The tunability of the properties of an IL by varying the cation-anion

combination for a particular task gives them another advantage over traditional solvents. These interesting characteristics of IL make them a suitable alternative for organic solvents in organic synthesis, catalysis, and in various energy applications. [4-26]

Although the first IL ethyl ammonium nitrate was synthesized by German chemist Walden in 1914,[27] ILs came to limelight in the 1960s as a promising electrolytic material for advanced batteries.[1] The early examples of ILs based on chloroaluminate anions were moisture sensitive and highly reactive towards water which limited their application. This led to emergence of water-stable ILs in 1992 containing tetrafluoroborate, hexafluorophosphate, nitrate, sulfate, and acetate anions.[1, 10] However, these ILs are viscous and tetrfluoroborate known to produce HF on hydrolysis.[28] This problem was overcome by perfluorinated anion (such as $(CF_3SO_2)_2N^-$ and fluroalkylphosphate) based ILs which have low viscosity and high conductivity. But the problem with such ILs is that they are more expensive and have a high tendency to bind with metal ions. Again the presence of fluorine makes them toxic and harmful. [28-30] Later on cheaper and low coordinating, non-fluorinated orthoborate, carborane anion containing RTILs were developed.[31,32] A NATO workshop on "Green Industrial Applications of Ionic Liquids" held in Crete in 2000 gave a major thrust to the research activity on ILs. It was in this workshop that the definition of IL was reaffirmed and codified.[33] Interest and research activities on ILs have grown leaps and bounds since then with development of many new families of IL such as task specific ILs, germinal dicationic ILs (DILs) etc. Examples of various cations and anions of ILs are shown in Chart 1.1.

Cations

tetraalkylammonium   tetraalkylphosphonium   1,3-dialkylimidazolium

N-alkylpyridinium   N,N-dialkylpyrollidinium   N,N-dialkylmorpholinium

R= alkyl group

Anions

BF_4^-
tetrafluoroborate

PF_6^-
hexafluorophosphate

NO_3^-
nitrate

$CF_3CO_2^-$
trifluoroacetate

$(CF_3SO_2)_2N^-$
bis(trifluoromethylsulfonyl)imide
(Tf_2N)

$CH_3CO_2^-$
acetate
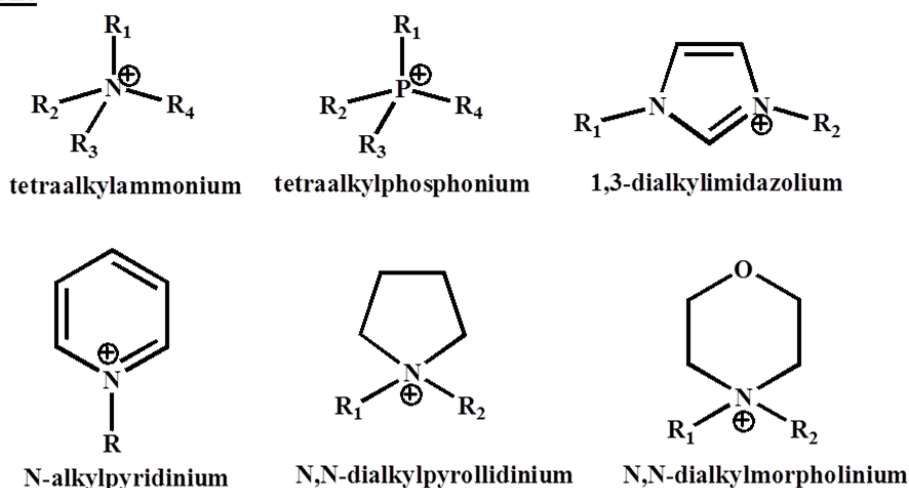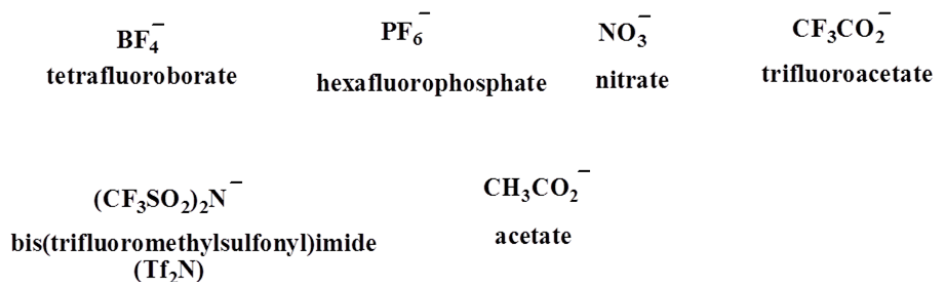
Chart 1.1. Structures of some common cations and anions of ILs.

1.1.1. Properties of ILs

As mentioned earlier some of the general properties of ILs which sets them apart from the conventional organic solvents are their negligible vapour pressure, high thermal and chemical stability, non-flammability, wide liquidous range, wide electrical conductivity, recyclability and ability to dissolve a large variety of organic and inorganic substances.[9-21, 34-36] Again these properties can be tuned by varying cation and anion combination for a desired purpose for which they are also known as "designer solvents'. These possibilities give them a special status both in fundamental and applied research. Molecular diagrams of some common ILs are shown in Chart 1.2. Physical properties of some commonly used ILs are provided in Table 1.1.

	n =	1	3	5
X= BF_4^-		EMIMBF$_4$	BMIMBF$_4$	HMIMBF$_4$
= PF_6^-			BMIMPF$_6$	
= $CF_3CO_2^-$		EMIMTFA	BMIMTFA	
= Tf_2N		EMIMTf$_2$N	BMIMTf$_2$N	HMIMTf$_2$N

n = 4	$[C_4(Mim)_2][Tf_2N]_2$
n = 6	$[C_6(Mim)_2][Tf_2N]_2$
n= 9	$[C_9(Mim)_2][Tf_2N]_2$
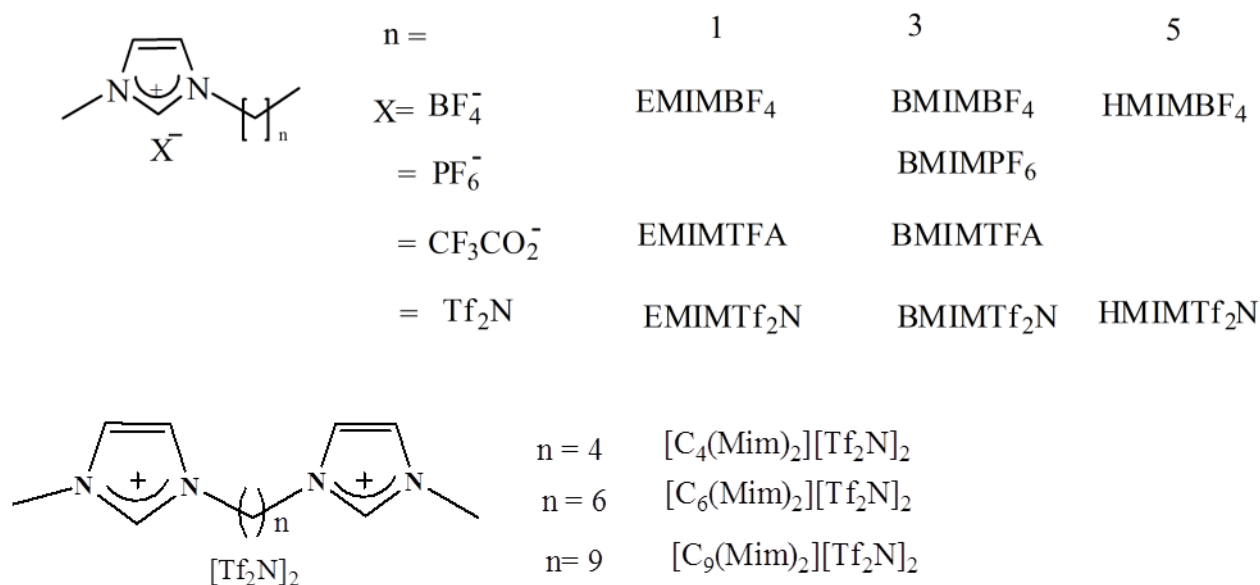
Chart 1.2. Molecular diagrams and abbreviation of some common imidazolium ILs.

Table 1.1. Physical properties of some common imidazolium ILs

RTILs	T_{mp}(°C)	T_d(°C)	η (cP)	ρ (g/CC)	$E_T(30)$	σ (ms/cm)
EMIMCl	86[a]	-	solid	solid	-	-
BMIMCl	65[a]	-	solid	solid	-	-
EMIMTf$_2$N	-3[b]	-	34[b]	1.52[b]	47.7[c]	8.8[b]
BMIMTf$_2$N	-4[b]	>400[d]	52[e]	1.43[e]	47.2[c]	3.9[e]
EMIMPF$_6$	60[f]	-	solid	solid	solid	5.2[g]
BMIMPF$_6$	-61[h]	-	371[i]	1.37[i]	52.3[j]	1.5[k]
BMIMBF$_4$	-81[h]	435[d]	154[i]	1.2[i]	48.9[l]	3.5[d]
$[C_4(Mim)_2][Tf_2N]_2$	59.5[m]	433.4[m]		-	-	-
$[C_6(Mim)_2][Tf_2N]_2$	-	427.1[m]	649.5[m]	1.546[m]	-	-
$[C_9(Mim)_2][Tf_2N]_2$	-	421.3[m]	678.8[m]	1.479[m]	-	-

T_{mp}: melting point, T_d: decomposition temperature, η: viscosity, ρ: density, σ: specific conductivity, $E_T(30)$: microscopic solvent polarity parameter. (a) ref 13; (b) at 20°C, ref 37; (c) ref 38; (d) ref 39; (e) ref 40; (f) ref 41; (g) at 25°C, ref 42; (h) ref 43; (i) at 20°C, ref 11; (j) ref 44; (k) ref 45; (l) ref 46. (m) ref 47.

Melting points*:* ILs have a wide liquidus range characterized by their low melting points as well as high decomposition points. Melting occurs when the crystal structure disrupts and the

molecules or ions fall out of their crystal lattice. Most of the ILs do not possess a sharp melting point as they can undergo supercooling.[18] As the properties of the ILs depend on the nature of constituents, attempts have been made to correlate the melting point of the ILs to the nature of their cation or anion.[42,48] It has been observed that ILs with symmetric cation exhibits the highest melting point. With increasing alkyl chain length the melting point of ILs is observed to decrease.[42,48] The melting point of ILs generally decreases with increasing anionic radius.[49]

Thermal stability and decomposition temperature: Thermal stability of an IL is strongly dependent on the nature of its constituent ions.[18] ILs are generally thermally stable up to ~450 °C with decomposition temperatures around 300–500 °C. It has been observed that with the increase of hydrophobicity of anion, the thermal decomposition temperature of ILs decreases.[35] ILs with halide anions have reduced thermal stability as compared to the ILs with nonhalide anions. Relative thermal stability of ILs with different anion decreases in the order $PF_6^- > Tf_2N^- \approx BF_4^- >$ halides.[18,35] The trend of thermal stability with respect to cation is observed to be in the order as follows: phosphonium >imidazolium > tetraalkyl ammonium > pyrrolidinium.[18]

Glass transition temperature: The glass transition temperature (T_g) gives an indication of the strength of cohesive forces within a salt. The cohesive interactions generally decrease due to electron repulsion and increases through the attractive Coulomb and van der Waals interactions.[50] Hence, variation in the cation-anion combination in the IL can change T_g with variation in the cohesive energy within an IL. It has been observed that decrease in the cation size and increase in asymmetry of the cation lowers the value of T_g due to reduction of packing and reduction of cohesive energy of the ILs.[51]

Density: Density of ILs depends on close packing of the ionic constituents of the ILs. Almost all ILs are denser than water with density ranging from 1.0 to 1.6 g cm^{-3} depending on their ion structure. The density has been observed to decrease with increasing alkyl chain length on the cation for alkylammonium and alkylimidazolium ILs.[52, 53] Similarly, in the sulfonium salts, the density decreases with increasing alkyl chain length. With variation in the cationic moiety, density generally decreases in the order of pyridinium ILs > imidazolium ILs > aliphatic ammonium ILs and piperidinium ILs. Nature of anion also affects the densities of ILs. With increasing alkyl chain length of the anion the density of ILs decreases a trend similar to that has been observed for cations. Introduction of bulky chain such as fluoroalkyl chains also increases density of ILs. For example, for ILs with 1-ethyl-3-methylimidazolium ([EMIM]) cation density follows the order: $CH_3SO_3^- < BF_4^-$ and $CF_3COO^- < CF_3SO_3^- < (CF_3SO_2)_2N^- < (C_2F_5SO_2)_2N^-$. Interestingly, for lactum based ILs with fluorinated anions, density is found to decrease with increasing the ring carbon number of the cation. This has been attributed to the perturbation in the cation-anion interaction due to the increase in the cation size.[54]

Viscosity: Viscosities of ILs are significantly higher (typically 10 to 100 times) than that of conventional organic solvents.[37] Viscosity of a fluid is a result of various molecular/ionic interaction (intra/inter) such as Coulombic, van der Walls interaction and hydrogen bonding interactions within the constituents of the fluid. Hence, like many other properties, the viscosity of ILs is also affected by the nature of cations and anions of the ILs. It has been observed that increase in alkyl chain length in the cation leads to an increase in viscosity due to stronger van der Waals interactions.[37] The viscosity of the IL is also affected by relative basicity and the ability of the anion to participate in hydrogen bonding interaction.[55,56] It has been observed that ILs containing PF_6^- and BF_4^- ions are more viscous due to strong H⋯F interactions than those IL with the weakly basic Tf_2N^- ion, in which the negative charge is

quite dispersed over the two sulfoxide groups.[57] Viscosity variation may also occur due to variation in the size, shape, and molar mass of anion with smaller, lighter, and more symmetric anions leading to more viscous ILs. Viscosities of ILs are strongly affected by impurities like halide and water.[57] The viscosities of ILs generally obeys Vogel-Tammann-Fulcher (VFT) equation which is given below.[58]

$$\ln(\eta) = \ln(\eta_0) + \frac{DT_C}{T - T_C} \tag{1.1}$$

In the above relation η_0 is the viscosity at infinite temperature, D is the fragility parameter and T_c is the characteristic temperature at which viscosity diverges.

Conductivity: The ionic conductivity (specific conductivity) of a medium is of vital importance for any electrochemical application. ILs have reasonably good ionic conductivities compared with those of organic solvents/electrolyte systems (up to 10 mS cm^{-1}).[59,60] However, at room temperature their high viscosity causes reduction in the conductivity values because of the fact that conductivity of any electrolytic solution not only depends on the number of charge carriers but also on their mobility.[40] The larger size of the constituent ions as well as association between the ionic species of ILs reduces the ion mobility which, in turn, leads to lower conductivities. Aggregation is another factor which brings reduction in the conductivity. Hence, because of these factors ILs having higher viscosity values exhibit lower conductivity. Conductivity of the ILs can be enhanced by mixing them with various cosolvents.[61,62]

Electrochemical Potential Window: For any medium to be used in electrochemical measurements, the electrochemical potential window (potential region without significant background current) is one of the key criterion to be looked into. ILs generally exhibit a wide potential window, a desirable property for application in various electrochemical

31

applications. ILs are known to show a typical windows of 4.5–5 V.[24][63] Overall, this potential window range exceeds that accessible in conventional electrolytic solutions.

Polarity: ILs are considered as polar solvents as they are composed of ions. Early investigation on polarity of ILs using solvatochromic dye method showed that imidazolium-based ILs possess a polarity close to that of short chain alcohols.[64, 65] Polarity of ILs was further determined through various methods such as fluorescent dye method,[66,67] EPR spectroscopy,[68] microwave spectroscopy,[69] FT-IR spectroscopic probe method[70] and FT-IR combined with density functional calculations (DFT).[71] All these investigations point out that despite following various methods a definitive standard has not been established for IL polarity. The polarity of ILs is responsible for their ability to dissolve solutes. It has also been demonstrated through solubility test of various nonpolar substances including hydrogen,[72] carbon dioxide[73] and fullerene[74] that ILs can dissolve not only polar solutes or charged solute via ionic liquid structure design, but also various non-polar compounds.

Other properties: Other important properties of ILs are surface tension and refractive index. In general it has been observed that variation in either the cationic or anionic moieties have a similar effect on surface tension.[75] With increase in packing efficiency the surface tension is found to decrease whereas increase in ionic interaction or hydrogen bonding interaction increases the surface tension of ILs. The refractive index (n_D) values indicate that ILs can be considered to be moderately polar media like acetonitrile but less polar than short chain alcohol. Refractive index is found to decrease slowly with increase in alkyl length, while the addition of a hydroxyl group leads to an increase in the n_D value.[75]

The ability to mix with water and other organic solvents is another important property of ILs. Solubility of an IL is mainly governed by the anion moieties. For examples ILs containing PF_6^-, Tf_2N^- anions are hydrophobic where as BF_4^-, sulfates and halide salts are

hydrophilic in nature. Increase in alkyl chain length of the cation increases the hydrophobicity of the ILs.[42,48,55] But addition of a hydroxyl group in the alkyl chain increases the solubility in water.

1.1.2. Structural and Dynamic Heterogeneity of ILs

Information about structural features of ILs is extremely important to understand their complex physical, chemical, and dynamic behaviour. ILs, like traditional molecular liquids, were initially thought to be homogeneous.[76] However, recent experimental and theoretical investigations have suggested that structures of ILs vary from supramolecular (ion pairs, ion clusters) assemblies to mesoscopic (H-bond networks and micelle-like) pattern.

Weingärtner et al.[77] have determined the ion pair association constants from conductivity measurements for ethylammonium nitrate (EAN) in n-octanol and suggested that a chemical equilibrium is established between ion pairs and "free" ions: $EA^+[NO_3^-] \rightleftharpoons EA^+ + NO_3^-$. Likewise multinuclear NMR studies on $C_2mim[X]$ ILs (where $X=Cl^-$, Br^-, and I^-) have suggested contact ion pairs formation in the pure ILs.[78] Studies on transport properties of dialkylimidazolium ILs also provided indirect evidence for ion pair formation.[79] Another important study by Gebbie et al.[80] indicated the presence of coordinated cation+anion network in $C_4mim[Tf_2N]$. However, this picture of ion pair model for IL bulk structure lacks the weight of scientific evidence. More recent dielectric spectroscopic investigations on both protic and aprotic ILs have revealed no evidence in support of ion pair formation. [81-84] As this technique is highly sensitive to liquid dynamics in picosecond-to-nanosecond time scale it would be possible to follow the reorientational relaxations of ion pairs or similar aggregates, if present, in ILs. Similarly, NMR measurements have also not detected any ion pairs in ILs.[85] These conclusions have also been supported by recent molecular dynamics (MD) simulations studies.[86-88]

Information about structures of some ILs has also been investigated through X-ray diffraction methods.[89, 90] These recent reports have shown the presence of an extended network of cations and anions through hydrogen bonding interactions in solid state.[89, 90] Later on, the evidence of hydrogen bonding assisted network of ionic components of ILs has also been obtained through neutron diffraction,[91] IR,[92] Raman spectroscopy,[93] NMR[94] and mass spectrometry studies.[95, 96] Investigations on X-ray diffraction measurements on ILs have shown that ILs can exist in micellar and reverse micellar structure.[97, 98]

Mesoscopic structural features of ILs was first proposd by Schröder et al.[99] based on diffusion coefficient measurements of three electro-active solutes dissolved in aprotic ILs as a function of water content. The authors have suggested that the IL-water binary mixture can be considered as heterogeneous system with polar and nonpolar regions. Computational studies by many researchers have suggested self-assembled solvent nanostructure of neat ILs. These reports have indicated towards self-aggregation of alkyl chains to form spatially heterogeneous domains in ILs.[100-103] Recently, heterogeneous solvent structure of ILs has also been shown through optical heterodyne-detected Raman induced Kerr effect (OHD-RIKES) studies.[104]

Later, both experimental and theoretical studies have shown that ILs are not only structurally but also dynamically heterogeneous. Heterogeneous nature of ILs has been proved through excitation wavelength dependent fluorescence study of several probes in ILs by Samanta and coworkers[105] and MD simulation studies by Hu and Margulis.[106] Investigations on excitation wavelength dependent solvation dynamics in neat IL and IL microemulsion through time-resolved fluorescence studies by Maroncelli[107] and Bhattacharyya[108] have also revealed the dynamic heterogeneity of the ILs with different polar and nonpolar domains. Very recently, Hunger and coworkers[109] have also successfully probed the dynamic heterogeneity of protic alkylammonium-based ILs through femtosecond

IR spectroscopy. However, since ILs are complex media, further studies based on theoretical and experimental investigations are necessary to understand the relationship between structural variation of ions and heterogeneity of these media.

1.1.3. Applications of ILs

ILs with unique physicochemical properties have shown a great promise as a replacement of volatile organic solvents (VOCs) in many chemical reactions and catalysis.[110-113] They have also been used in separation technology, for example, as a stationary phase in gas-liquid chromatography or as a mobile phase in liquid chromatography.[114] ILs are also as used as an ionic in laser desorption/ionization mass spectrometry (MALDI-MS).[115, 116] As ILs have the potential to dissolve a wide range of compounds, they are sometimes used to dissolve and crystallize proteins and other hydrophobic ligands.[117] Interestingly many unknown chemical products are obtained from chemical reactions those are carried out in ILs.[118] It has been proposed that micro-heterogeneous behaviour of the ILs could be responsible for this observation.[119] Apart from this, the high conductivity, low reactivity, and wide electrochemical window of ILs make them an promising candidate to be used as an electrolyte in various electrochemical applications.[36, 120, 121]

It may also be noted that ILs have also been exploited in various other industrial applications such as lubricants and rocket propellants.[122] In the past decades, "task-specific" ionic liquids (TSILs) have been used in catalysis,[123] organic synthesis,[4] and separation of specific materials,[4] synthesis of nanomaterials,[124] and ion conductive materials, scavenging SO_2 and CO_2 etc.[125]

Geminal dicationic ILs are another important class of ILs which have exhibited superior physicochemical properties than the traditional MILs in terms of higher thermal stability, higher shear viscosity, higher surface tensions and larger liquid density.[47, 126-135] The greater structural variability in DILs is expected to result in diverse physiochemical

properties of DILs, compared to MILs, making them even more tunable and versatile.[47] Recent studies have reported that DILs, similar to the monocationic ILs (MILs), can be used effectively as catalysts,[136-139] solvents,[140] lubricants[141, 142] and electrolytes[143, 144] especially at high temperatures due to their high thermal stability.

1.1.4. Photophysical Studies in ILs

Molecular level understanding of the structure and dynamics of ILs is extremely important for their effective utilization in various applications. Scientific communities around the world have made attempts to understand structure-property relationship[100-108] in ILs through experimental[38, 105, 107, 108, 145-205] and theoretical investigations.[206-211] Photophysical[212-226] and photochemical[119] studies are found to be attractive perhaps because of their sensitivity to the micro-heterogeneous nature of the ILs.[100, 105-108, 145-150, 185-189] Some of the important photophysical studies in ILs relevant to the present thesis work are discussed in the following sections.

Excitation wavelength dependence fluorescence study: Emission spectrum of a fluorescent molecule is expected to be independent of excitation wavelength according to Kasha's rule which states that fluorescence emission originates from the lowest vibrational energy level of the lowest excited state of the same spin multiplicity.[227] However, under certain circumstances emission spectrum of a fluorophore is observed to be shifted towards longer wavelength particularly when the fluorophore is excited at the red end of its absorption spectrum.[228-234] This phenomenon is generally known as "red-edge effect" (REE).[231, 232] REE phenomenon is observed under specific conditions.[228, 229] Firstly, there must be a distribution of energetically different assemblies of molecules in the ground state. This leads to inhomogeneous broadening of the absorption spectrum. Secondly, the excited sate relaxation of the fluorescent probe should be slower or comparable to its excited state lifetime. This leads to distribution of different solvent environments in the systems exhibiting "REE" effect.

REE effect has been observed in ILs for some organic fluorescent molecules.[105] This phenomenon is illustrated schematically in Scheme 1.1. REE effect in a medium like IL can provide qualitative idea about the microhetrogeneous nature of the ILs.
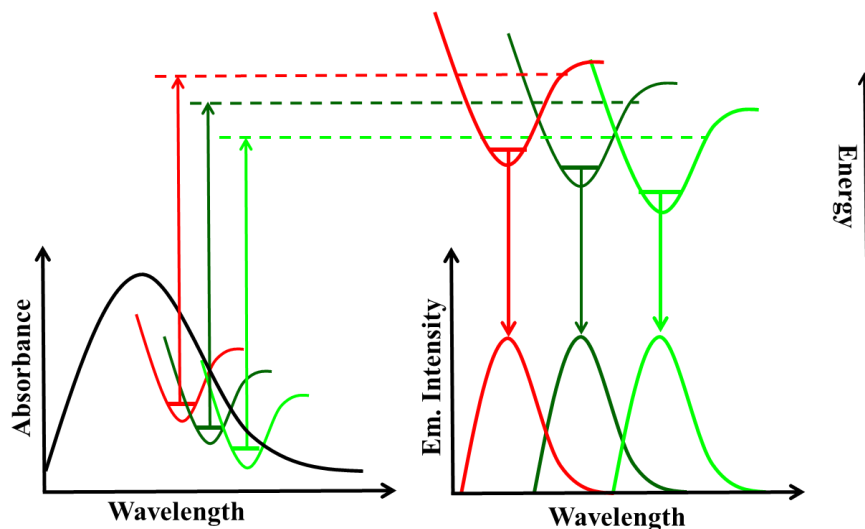
Scheme 1.1. Pictorial representation of red-edge effect (REE).

*Solvation dynamics***:** The phenomenon of time-dependent response of a solvent system towards the perturbation to a solute's charge distribution is termed as "Solvation Dynamics". Solvation dynamics has a strong influence on dynamics of many chemical reactions. Thus studies on solvent relaxation processes are fundamentally important as it can provide a full characterization of the static as well as dynamic properties of solute-solvent interactions. The most exploited method to study solvation dynamics is Time-dependent fluorescence Stokes shift (TDFSS) measurement.[151-189] This process is schematically depicted in Scheme 1.2. At first, a solute molecule is promoted to the first excited state S_1 by a pulsed light with sufficient energy. The dipole moment of the solute in S_1 state is considerably higher than the ground state S_0. In this process the equilibrium between the solute and solvent molecules present before the pulsed excitation, is perturbed. Then the solvent molecules try to stabilize the S_1 state by rearranging themselves around the newly created dipole. The solvent relaxation process leads continuous red shift of the emission spectra of the probe with time.[235]

By following this energy relaxation due to solvent reorganisation at different times through time-resolved spectroscopy, the idea about solvation dynamics can be obtained.

The molecular probes for TDFSS measurements should satisfy the following characteristics. Firstly, there should be a large change in the dipole moment of the probe upon photoexcitation. Secondly, the probe molecule should show long excited state lifetime. Thirdly, the probe molecules should not undergo any excited state phenomena other than solvation process.[235] Molecular structures of some well-known fluorescent probes are shown in Chart 1.3[161, 183]

Coumarin 153 (C153) **Coumarin 480 (C480)**

Prodan **4-aminophthalimide (AP)**
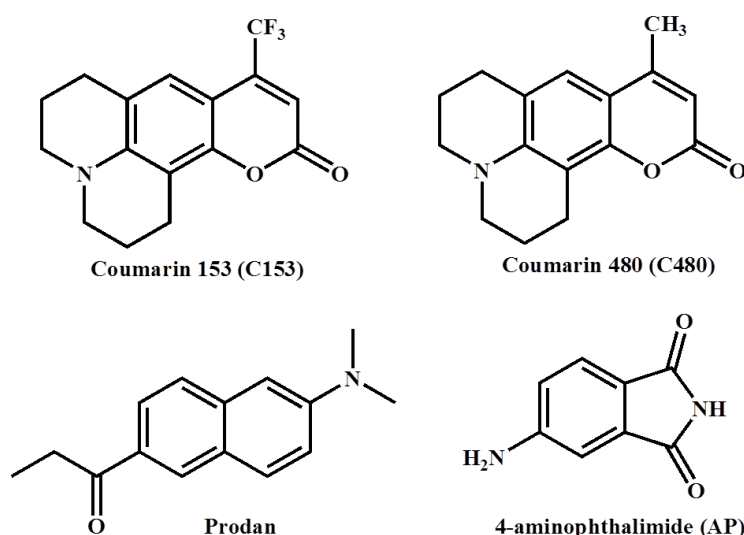
Chart 1.3. Structures of some dipolar molecules used to study solvation dynamics.
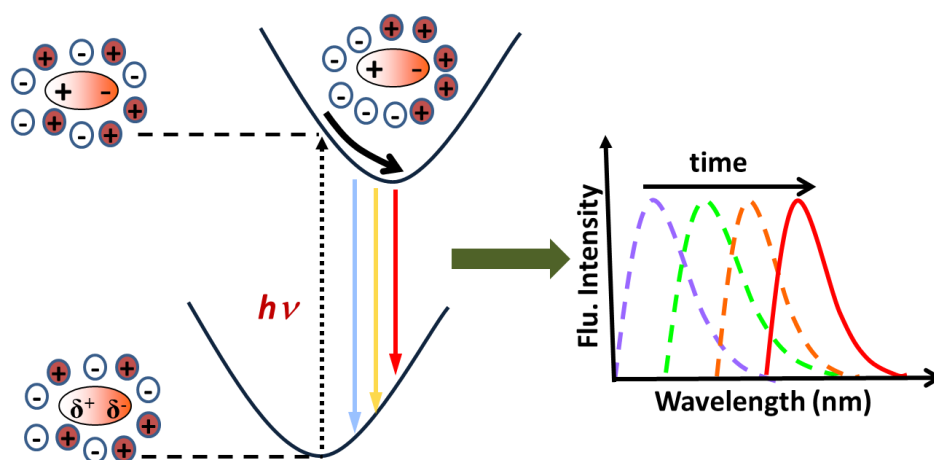
Scheme 1.2. Schematic representation of time-dependent fluorescence Stokes shift in ILs.

Since ILs are polar,[45, 46] TDFSS measurements in ILs have been studied by using dipolar probe molecules in ILs. Some of the pioneering works on solvation dynamics in ILs have been carried out by Samanta[151-159] and Maroncelli.[160-170] Many other researchers like Sarkar,[171-177] Petrich,[178,179] Biswas[180-184] and Bhattacharyya[236,237] and have also contributed significantly to this area. The key findings of these works are described in the recent review articles.[154, 155, 158] Essentially, these investigations have revealed that solvation dynamics in ILs is slow compared to that of the common molecular solvents. Moreover, the time-resolvable component of the dynamics is observed to be bi-exponential with a slow component and a fast component.[158] Some researchers prefer to consider the dynamics to be non-exponential in nature.[168] In addition to this, it has been observed that the average solvation time is primarily dependent on the viscosity of the media and almost 50% of the solvent relaxation dynamics is observed to be quite fast (<25 ps).[158]

The mechanism of solvation process in ILs is known to be quite different from that in conventional polar solvents.[155] While primary contribution towards solvent stabilization in dipolar solvents comes from dipolar reorientation of solvent molecules around the photoexcited probe, in ILs, translational motion of the ionic constituents contributes significantly to the solvation process. This is because, with change in dipole moment of the probe molecule upon photoexcitation, the ionic species of the ILs experience a net force which makes them move from their original position. The ionic constituents then try to reorganize themselves around the photoexcited probe.[155] The mechanism of solvation in an oversimplified form has been illustrated in Scheme 1.3.
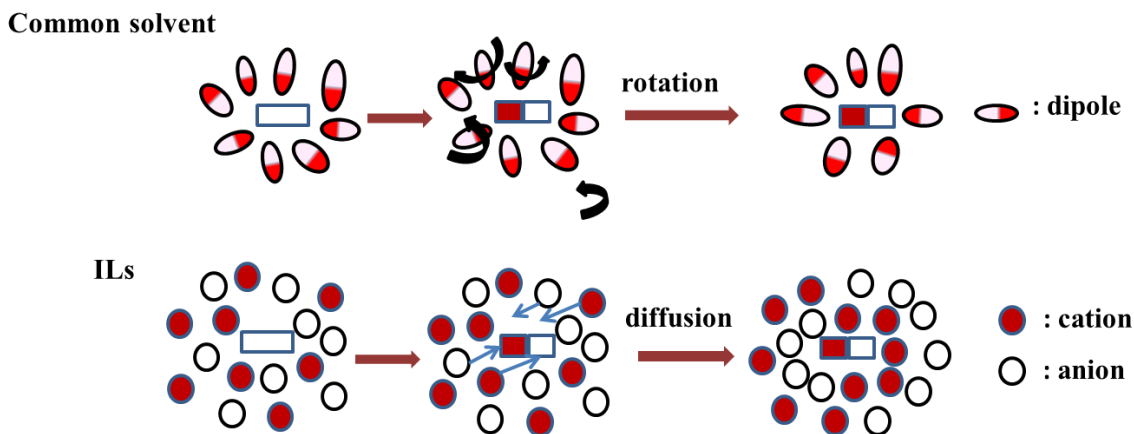
Figure 1.3. Oversimplified illustration of fundamental difference in mechanism of solvation in conventional molecular solvents and ILs.

Attempts have also been made to understand the dynamics of solvation in ILs through simulation studies. However, the results of these studies differ significantly. While Shim et al.[206] have shown the translational motion of the anions to be responsible for the fast component of solvation, Kobrak and Znamenskiy demonstrated that the collective cation-anion motion is responsible for the observation of fast component.[207,208] In another study, Shim et al.[209] have attributed the ultrafast dynamics to the fluctuation in the local density of the ions in the immediate vicinity of the probe molecule. The authors have shown that when the local density is high, the ultrafast component is observed because of the motion of the ions in close proximity to the probe molecule and when the local density is low, the ions away from the probe molecules are responsible towards ultrafast component of solvation. In a very recent study, Biswas and coworkers[181] have shown that the dipolar rotation of the cation of the IL is mainly responsible for the observation of ultrafast solvation component and its contribution towards total dynamics can be as much as 40%.

Rotational relaxation dynamics: Rotational dynamics of a fluorescent probe in a medium is studied through recording fluorescence anisotropy decay of the molecule in the concerned medium. Fluorescence anisotropy study is the measurement of emission depolarization of a fluorescent molecule after photoexcitation by a beam of polarised light. Rotational diffusion

of the photoexcited probe leads to emission depolarization.[238] The isotropic distribution of molecules in a homogeneous solution is perturbed by polarized light beam, and molecules whose dipole moment vectors are aligned with the electric vector of the polarized light are selectively excited. This introduces an anisotropic distribution of molecules in the system. The average angular displacement of dipole of the fluorophore between the absorption and the subsequent emission due to rotational diffusion is detected through anisotropy measurements. Again, rotational diffusion of a molecule depends upon its size and shape as well as on the local microenvironment (viscosity etc.) of the medium. Moreover, since rotational motion of a solute will also depend on the solute-solvent interaction (H-bonding, electrostatic interaction etc.), studies on rotation of solute molecule, therefore, can provide proper understanding of the micro-picture of liquids and solutions.[239]

To analyse the data obtained from rotational dynamics study, hydrodynamic theories such as Stokes-Einstein-Debye (SED) theory has been extensively used. SED theory has been observed to be successful in explaining the rotational diffusion of medium sized solute molecules when the coupling between solute and solvent is purely hydrodynamic in nature.[240] According to this theory rotational time (τ_r^{SED}) of non-interacting solute can be related to the medium viscosity η by the following expression.[240]

$$\tau_r^{\ SED} = \frac{\eta V f C}{k_B T} \qquad (1.2)$$

In the above relation V is the van der Waals volume of the molecule, f is its shape factor, C is the boundary condition parameter, T is the absolute temperature and k_B is the Boltzmann constant. The shape factor f represents the extent of departure of the shape of molecule from spherical nature. For a spherical solute f is unity, and is greater than 1 for an asymmetric ellipsoid. The two extremes of the boundary conditions of SED models are called

stick and slip limits. When the solute molecules are larger in size than the solvent molecules C becomes unity which sets the stick boundary condition. C less than unity represent the slip boundary condition and come into picture when size of the solute molecule is smaller or comparable to that of the solvent molecule. SED theory considers solute molecules as either symmetric or asymmetric ellipsoids. SED theory is helpful for the calculation of rotational coupling constants (C_{rot}) which measure the departure from the normal hydrodynamic behaviour.

However, SED theory is found not to be suitable for a scenario where solvent size is greater than solute size. In that scenario quasihydrodynamic theories[241, 242] are invoked as they take care of the solvent size along with the solute size. Similarly models other than SED theory such as "Solventberg"[243] or "Nee-Zwanzig model"[244] are employed to explain rotational dynamics of a solute molecule.

Investigations on rotational relaxation dynamics in ILs have been widely carried out basically to gain idea about the nature of various solute-solvent and solvent-solvent interactions prevailing in ILs.[193-205] Recently, various research groups have shown that apart from medium viscosity specific solute-solvent interactions significantly hinders the solute rotation in ILs.[156, 193, 194] Solvent size has also been observed to influence solute rotation in absence of any specific interaction.[194] Since ILs are composed of ions, rotational dynamics of charged probes have also been investigated with an aim to understand the role of electrostatic interaction towards solute rotation.[6, 193] These studies have revealed that medium viscosity and specific solute-solvent hydrogen bonding interactions are the predominant factor in controlling solute rotation in ILs.[6, 193] Interestingly no clear cut evidence on influence of charge-charge interaction on solute rotation has been observed.[6, 193]

Photoinduced electron transfer: Understanding of the process of electron transfer is extremely important for development of new systems for various electrochemical and energy

related applications.[245-247] As ILs are being exploited for various electrochemical and energy applications it is pertinent to understand the electron transfer process in ionic liquid media. Some of the key studies on intramolecular and intermolecular photoinduced electron transfer (PET) process carried out in ILs are discussed below.

Study on intermolecular PET by Paul and Samanta[223] have revealed that the mechanism of electron transfer is strongly influenced by the microscopic properties of the ILs. The authors have demonstrated that the PET rate constant determined from fluorescence quenching (k_q) is higher than the diffusion controlled rate constant (k_{diff}) suggesting that the microviscosity around the donor-acceptor pair largely differs from the bulk viscosity of the ILs. Interestingly, similar results have also been reported by Maroncelli[248] and Vauthey[249] independently in conventional organic solvents having comparably high viscosities, indicating that this behaviour is not unique to ILs and rate of electron transfer is not faster in ILs compared to conventional solvents.

Effect of solvation on PET in ILs have also been investigated through study of intramolecular PET by many research groups.[213-217] In this context, reports by Samanta[213, 214] and Manocelli[215] have demonstrated that PET reactions are solvent controlled in ILs. Recent report by Wu[216] and Wishart[217] have shown that rate of intramolecular PET reactions in ILs is slow compared to the conventional solvents. Such observation has been attributed to the slow solvent relaxation in ILs.[216, 217] These studies have also revealed that intramolecular electron transfer reaction in RTILs should be treated using a solvent controlled electron-transfer model where solvent relaxation time has a significant role in controlling this process.

1.1.5. NMR Investigations in ILs

Chemical shift measurements are routinely carried out to characterize ILs. Simple ^{1}H NMR chemical shifts has been found to be useful in detecting perturbations to the environment around the cations and anions, especially IL–solute interactions.[249] For example,

[1]H chemical shifts of [EMIM][TF$_2$N] as a function of benzene and fluorinated benzene has been studied by Dias et al. to probe charge-induced structuration of ILs.[251] Apart from measuring chemical shifts for characterization of ILs, multinuclear NMR has also been used extensively for investigating diffusion, relaxation, and other physiochemical properties in ILs.[251]

Pulsed field gradient NMR (PFG-NMR) technique has been very popular in determining diffusion coeffiecients of cations and anions of IL.[250] Measurement of self-diffusion in combination with other bulk properties, such as viscosity, density, and electrical conductivity, provides a thorough understanding of molecular transport in ILs. Field cycling NMR has also been used to determine self-diffusion coefficients.[252] Cation self-diffusion coefficients of [EMIM][SCN] and [BMIM][BF$_4$] are reported using ^{1}H relaxation data, and both cation and anion diffusion coefficients are calculated for [BMIM][PF$_6$] using ^{19}F relaxation data. In another study Grey and coworkers[253] have utilized NMR line shape as a sensitive probe to determine the effective diffusion rate of ions to understand supercapacitor charging dynamics in ILs.

Generally in PFG-NMR measurements in ILs, ^{1}H and ^{19}F are typically used due to their large gyromagnetic ratio and relative abundance. However, recently [7]Li, [11]B, and ^{13}C have also been used to measure diffusion coefficients.[254, 255] Also the viscosity of ILs causes difficulties in measuring self-diffusion coefficients using standard NMR probes and gradient hardware. However at elevated temperatures, measurements can be performed. Stray field NMR is an alternative to measure slow diffusion by exploiting the static gradient present in the fringe field of any NMR magnet, although there are few reports available.[256] Systematic investigations on water confined in ILs have been performed by Saihara et al. through PFG-using a mixture of H$_2$O and D$_2$O.[257] They found that water molecules were situated in close proximity to each other and loosely confined inside the IL. Transport properties of ILs in the

presence of solvents such as dimethyl carbonate,[258] polyethylene glycol,[259] hexane,[260] DMSO[261] and polar aprotic[262] solvents have also been reported recently. Similarly, the effects of inorganic salt addition on the transport properties of ILs and the salt are reported in several publications using PFG-NMR.[263-266]

Apart from PFG-NMR, spin–lattice (T_1) and spin–spin (T_2) relaxation measurements have been found to be extremely helpful in getting further insight into atomic level interactions. NMR combined with Nuclear Overhouser Effect (NOE) experiments have been used extensively to investigate reorientation dynamics in ILs.[267-272] Recently, a number of studies have been reported for site selective dynamics of ILs in order to understanding inter- and intramolecular interactions.[267-272] To get a complete description of the reorientation ion dynamics, Driver and Ingman[273] have used spin– lattice NMR relaxation and NOE data at multiple field strengths to develop a simple analytical procedure to determine the diagonalized rotational diffusion tensor for the cation in [HMIM][Br].

Endo et al.[274] have employed relaxation NMR technique to investigate rotational dynamic effects of methylation by comparing rotational correlation times in [C$_4$mim][Br] and [C$_4$C$_1$mim][Br]. It has been shown that methylation near the butyl group would cause an inhibition of butyl group rotation and in turn increase viscosity or melting point. From rotational correlation time (τ_c), the authors have shown that the decrease in stable anion interaction sites plays a major role in controlling the rotational diffusion.[274] The same group also investigated ionic dynamics in [BMIM][Tf$_2$N] in the glassy and liquid states. For glassy states, below the melting point of [BMIM][Tf$_2$N], they utilized ^{13}C CP-MAS (cross-polarization-magic angle spinning) solid-state NMR to investigate ion dynamics.[275]

1.2. Objective Behind the Thesis

Though extensive photophysical studies have been undertaken on ILs in the past one and half decade, many challenges concerning ILs have not been fully resolved. Some of the key issues regarding ILs which still remain as challenges are;

- Proper understanding of the micro-heterogeneous behaviour of various ILs.

- Nature of various interactions (solute-solvent and solvent-solvent) prevailing in ILs that can influence their physicochemical properties and reactivity.

- Understanding of the relationship between rate of solvation and electron transfer process. This is fundamentally important to employ ILs to their full potential in various electrochemical and energy storage devices.[24]

- The origin of ultrafast component of solvation in ILs is to be fully understood as the solute reactivity depends on the dynamics of solvation.

Apart from these, studies that focus on understanding of structure and dynamics of germinal DILs are very limited. In particular studies on solvation and rotational relaxation dynamics are limited to monocation-based systems. As DILs are known to possess advantageous physicochemical properties over the traditional MILs,[126-135] it is extremely important to have a thorough understanding of structure-property relationship in DILs so that they can be effectively used for newer applications.

The current thesis work has been carried out primarily to address the above mentioned challenges. In this thesis work, attempts have been made to understand the relationship among structure, intermolecular interactions and dynamics in various types of mono and dicationic ILs through solvation and rotational relaxation dynamics studies.

Rotational diffusion of some charged and neutral solutes in two structurally similar but chemically distinguishable imidazolium ILs have been investigated. This study has been

aimed to find out unambiguous role of electrostatic interaction towards solute rotation. In this study, one of the IL contains a C2–methyl group so that the H-bonding interaction due to imidazolium C2–H is eliminated, and thereby the effect of electrostatic interaction on solute rotation is exclusively monitored (Chapter 3).

Investigations have been carried out towards understanding the role of solvents on intramolecular PET kinetics by employing two nitrobenzoxadiazole-based flexible donor-spacer-acceptor (DSA) derivatives in two room temperature ILs (Chapter 4). The flexible DSA systems are purposefully chosen so as to eliminate the effect of transport phenomenon on electron transfer process. The results obtained in ILs have been further compared with a conventional organic solvent acetonitrile.

The high viscosity, difficulties in purification and high manufacturing cost are some of the limitations which restrict the effective use of ILs. This problem can be overcome by using binary mixtures of ILs with various cosolvents which may help in widening the applicability of ILs.[276] In this thesis work attempts have been made to understanding IL-cosolvent systems by investigating the solute-solvent and solvent-solvent intermolecular interactions through fluorescence and NMR spectroscopy. The study has been described in detail in chapter 5.

The last chapter of the present thesis (Chapter 6) discusses a combined fluorescence and NMR investigations in structurally similar imidazolium-based mono and dicationic ILs, carried out with an aim to understand the structure-property relationship in DILs. In particular NMR studies have been performed with an objective to understand the origin of ultrafast component of solvation in ILs.

The outcome of the present thesis work is expected to entail a significant step forward in our understanding of structure, intermolecular interaction and dynamics in ionic liquid medium.

Chapter 2

Instrumentations and Methods

This chapter describes details of various experimental techniques employed in the present research work. Various methodologies adopted to analyse the experimental data have also been mentioned in this chapter.

2.1. Purification of ILs

ILs used in the present studies were purchased from Merck (Germany), Frontier Scientific (USA) and Iolitech (USA). The ILs were purified by activated charcoal treatment and kept in high vacuum overnight before use in any spectroscopic study. Purity of ILs were checked by NMR spectroscopy and mass spectrometry and their optical purity were verified through absorption spectroscopy. A geminal dicationic IL (DIL) has also been synthesised and purified by following a literature.[47] The details of the synthetic procedure, purification and characterization of the DIL is described in chapter 6.

2.2. Sample Preparation for Spectroscopic Measurements

For steady-state and time-resolved fluorescence measurements, ILs were taken in different long-necked quartz cuvettes of 1 cm path length. Requisite amount of the fluorescence probe was added to the ILs at room temperature so that the optical density of the probe below 0.4 was maintained to avoid problems due to the inner filter affects. Proper precaution was taken to avoid moisture absorption by these ILs during sample preparation. The cuvettes were sealed by rubber septum and parafilm to avoid moisture adsorption by these ILs.

2.3. Instrumentations

2.3.1. Instruments Used for Chemical Characterisation of Samples

Bruker Avance 400 MHz NMR spectrometer has been used for characterization of the compounds through NMR spectra. The viscosities of the ILs have been measured by a LVDV-III Ultra Brookfield Cone and Plate viscometer (accuracy: 1% and repeatability: 0.2%). For temperature dependent viscosity measurements a Julabo water circulator bath has been used.

2.3.2. Instrumental Techniques for Absorption and Steady State Emission Measurements

2.3.2.1. Absorption Measurements

UV-visible absorption spectroscopy is the commonly used technique to get information about the ground electronic state of choromophoric systems. One can get an idea about the various natures of electronic transitions possible in the ground state of the chromophore by looking at the wavelength of different absorption bands and molar extinction coefficient at different wavelength. This allows the characterization or the identification of various chromophoric systems and their surrounding microenvironments.[227, 280, 281] In addition, absorption profile of an absorbing species is often influenced by solvent polarity, polarizability and hydrogen bonding interaction in the ground state. Hence, UV-visible absorption spectroscopy can provide more useful information regarding the nature of interactions between the chromophoric species and its surrounding microenvironment in the ground electronic state.

According to Lambert Beer's law, absorbance (A_λ) of an absorbing species in a solution at an wavelength λ, is directly proportional to the concentration (*C)* of the species in the solution and its molar extinction coefficient (ε_λ) at that particular wavelength. It can be expressed by the following relation[227, 238, 280, 281]

$$A_\lambda = log\ (I_0/I) = \varepsilon_\lambda Cl \tag{2.1}$$

where I_0 and I are the intensities of the incident and transmitted light, respectively, and l is the path length for the light beam passing through the sample.

In present thesis work, absorption spectra for different samples have been recorded using Perkin Elmer (Lambda 750) spectrophotometer. The minimum wavelength resolution for Perkin Elmer (Lambda 750) spectrophotometer is 0.15 nm and lowest absorbance measurable is ~0.005.

2.3.2.2. Steady State Fluorescence Measurements

Fluorescence spectroscopy is an extremely powerful technique to investigate various photophysical and photochemical processes occurring in the excited state of the fluorescent molecules. It is a very sensitive technique. Subtle changes in the energetics and various interactions in the excited state of emitting species are reflected through the changes in the intensity, position of the emission maximum and shape of the emission profile of the concerned species.[227, 238, 280, 281] Thus, this technique provides a better idea about the surroundings of the emitting species. In the present thesis, investigations on steady state fluorescent measurements have been carried out using a Perkin Elmer (LS55) fluorescence spectrometer equipped with a high pressure xenon lamp as the excitation source and a R-928F (Hamamatsu) photomultiplier tube (PMT) as the photodetector. Temperature of the sample holder was controlled by the Perkin Elmer, PTP1 peltier temperature programmer by the circulation of water through the sample holder.

2.3.3. Instrumental Techniques for Time-resolved Studies

2.3.3.1. Fluorescence Lifetime Measurements

Time-resolved fluorescence techniques are extremely useful in providing information about the dynamics and kinetics of various photophysical and photochemical processes. In this technique a fluorescent molecule is excited with a very short pulse of light which creates

an initial population (n_0) of fluorophore in the excited state. This excited state population decays with a rate ($k_r + k_{nr}$) according to following equation[227, 238, 280-285]

$$-\frac{dn(t)}{dt} = (k_r + k_{nr})n(t)$$
(2.2)

where $n(t)$ is the number of excited molecule at time t following the excitation of fluorophore molecule with the very short pulse light, k_r and k_{nr} are the radiative and nonradiative decay rate constant respectively. The probability of emission from each excited fluorophore in a given period of time is same. The excited state population decays in an exponential fashion as per the relation

$$n(t) = n_0 \exp(-t/\tau)$$
(2.3)

As florescence intensity is directly proportional to the number of excited molecules present in the solution, Equation 2.3 can be alternatively expressed in terms of the time dependent intensity $I(t)$ and the integration of the resulting equation gives the following expression

$$I(t) = I_0 \exp(-t/\tau_f)$$
(2.4)

where I_0 is the intensity at zero time and τ_f is the fluorescence lifetime of the sample. τ_f is related to the radiative and nonradiative decay rate constants as per the equation

$$\tau_f = \frac{1}{k_r + k_{nr}}$$
(2.5)

Excited state fluorescence lifetime is generally estimated through time-correlated single photon counting (TCSPC) technique. Here it should be kept in mind that different molecules spend different scale of times in the excited states. Thus some molecules in the excited state may emit at very short times while others may take a longer time than the measured τ_f values to emit. Thus a time distribution of these emitted photons is created which represents the measured fluorescence decay of the sample under investigation. Hence, the estimated lifetime

actually represents the statistical average of the times that the molecules spend in the excited state.

Time-resolved measurements in the present thesis work have been carried out using Edinburgh OB920 TCSPC setup. The basic working principles of the TCSPC technique is provided below.

2.3.3.2. Basic Principle of TCSPC Technique

TCSPC working principle is based on the detection of a single photon from a sample after a pulsed excitation. The time dependent probability distribution of the single photon emission from an excited fluorophore following its excitation is equivalent to the time dependent changes in the fluorescence intensity of the sample following its excitation by the short light pulse.[282-285] The working principle of TCSPC technique (operated in forward mode) is shown by a schematic diagram in Scheme 2.1.

As depicted in Scheme 2.1, an excitation pulse is used to excite the sample. A signal corresponding to this excitation pulse is directed to a start PMT. The optical signal at the start PMT generates an electrical START pulse, which is then passed through the Constant Fraction Discriminator (CFD) which accurately measures the arrival time of the pulse. This signal is passed through START input to the Time to Amplitude Converter (TAC), which generates a voltage ramp which increases linearly with time. Photons emitted from the sample after pulsed excitation are then detected one by one by the stop PMT to generate electrical STOP pulses for each of the individual photons received. The STOP pulses thus generated in the stop PMT are also routed through a CFD and a variable delay line to the STOP input of the same TAC unit. After detecting the first STOP pulse, the TAC unit stops the generation of voltage ramp. Now, the TAC contains a voltage which is proportional to the time delay (Δt) between the excitation and emission signals. The TAC output pulse is then routed through PGA (Pulsed gain amplifier) to an Analog-to-Digital Converter (ADC). The

ADC generates a numerical value proportional to the height of the TAC output pulse and the signal (count) is stored in a memory address (channel) in the MCA (multichannel analyser).
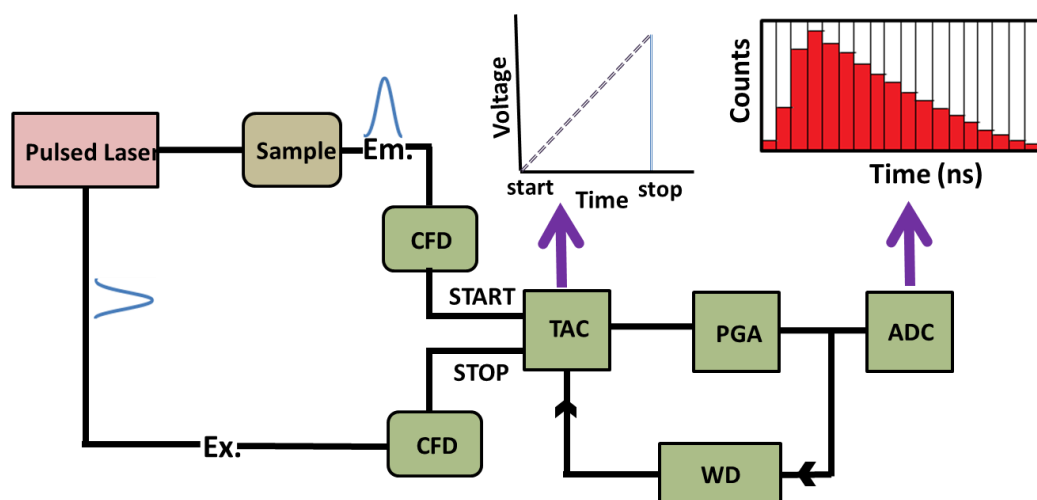
Scheme 2.1. A Schematic diagram for the working principle of TCSPC setup.

The above cycle (from the triggering of the pulsed excitation light source to the data storage in the MCA) is repeated again and again for a large number of times and thus a histogram of counts is collected in the MCA channels. Scheme 2.1 has shown for a TCSPC technique which is operated in forward mode. However, presently almost all TCSPC measurements are performed in the "reverse mode"[238]. In the present work also we have used the TCSPC setup in "reverse mode". This process is almost same as described above except that the emission pulse is used to start the TAC and the excitation pulse is used to stop the TAC. This procedure is used because of the high repetition rate of modern pulsed-light sources. The TAC has to be reset and set to zero before each start pulse, which takes a finite amount of time. The TAC can be constantly in reset mode if the start signals arrive too rapidly. The emission signals occur about 1 per 100 excitation pulses, and thus much less frequently than the excitation pulses. These emission pulses are used to start the TAC, and the next laser pulse is used to stop the TAC. Present electronics for TCSPC setup only allow the detection of the first arrival photon. A brief description of important electronic

components of TCSPC setup is described below. For estimation of fluorescence lifetime from the measured fluorescence decay curves, suitable analysis procedure is discussed later.

2.3.3.3. Important Components of a TCSPC Setup

(i) Pulsed excitation source: Different diode lasers (EPL 375nm, 405nm, 445nm) had been used as the excitation sources to excite the fluorophore. The instrument response function (IRF) for this TCSPC setup is around 100 ps which has been measured from full width at half height maximum (FWHM) of IRF pulse and it is varied with the excitation source. The repetition rate for excitation pulses was usually kept at 1 MHz.

(ii) Constant fraction discriminator(CFD): The main function of the CFD is to improve the signal to noise ratio (S/N) by discarding the signals below a threshold height such that the counts recorded by the instrument are actually due to the photons detected by the PMTs and not due to spurious electrical noises. It also records the correct timing information for the START and STOP inputs to the TAC unit such that the timing jitter in the detection is minimized. As the leading edge discriminators are always associated with significant timing errors, the CFDs are recognized to be the best suited discriminators for the TCSPC measurements to obtain the accurate timing information for the START and STOP signal.

(iii)Time-to-amplitude converter (TAC): In TCSPC setup, time correlation between the START and STOP pulse is carried out by using the TAC unit which is considered as the heart of this setup. On receiving the START pulse, following the preset delay which is already set in the TAC itself, a timing capacitor in the TAC start charging linearly with time from a constant current source. When the charging is discontinued upon receiving a STOP pulse, the charging process is stopped and TAC unit generates an output pulse. The amplitude of charge accumulated on the TAC capacitor is proportional to the measure of time difference between the arrivals of START pulse and STOP pulse, because the charging process of the capacitor in the TAC is linear with time. In the present Edinburgh TCSPC setup, the TAC range can be

varied from 2.5 ns to 50 μs. A suitable TAC range was judicially selected for a particular TCSPC measurement depending on the expected fluorescence lifetime of the sample used.

(v) Multichannel analyzer (MCA): The MCA used in a TCSPC setup can be operated in two modes: (i) Pulse Height Analysis (PHA) mode for measuring fluorescence decays, (ii) Multichannel Scaling (MCS) mode for measuring time-resolved emission spectra. The data stored in the MCA channels are transferred to a computer for further analysis and processing.

*(vi) START and STOP PMTs***:** Though in a typical TCSPC instrument suitable start and stop PMTs are used to carry out the measurements, only a single PMT with very high gain and low transit time is used in the present Edinburgh OB920 instrument to detect the emission photons from the sample. Thus the only photodetector used in the present instrument is a special Hamamatsu (R3809U-50) PMT, used in combination with a Quantum, North West (TC 125) temperature controller. The detector is having a spectral response from ~300 to 800 nm. In this instrument the measurement is in fact made in a reverse mode, i.e., the signal from the special PMT is used as a start pulse for the TAC unit and an electrical signal synchronized with the pulsed diode laser is used as the stop pulse. This reverse mode is adopted especially for faster data collection using high repetition rate of the excitation pulses (0.5 or 1 MHz). This reverse mode of detection is essential to avoid unnecessary charging of the TAC unit by the high repetition rate excitation pulses. In this context, it should be mentioned that in Edinburgh OB920 model TCSPC set up a PC based TCC card is used which incorporates both TAC and MCA directly and has been used for the data collection. PC monitor is used to display the measured decay curve. Suitable analysis software is used to fit the measured decay curves and obtain the fluorescence lifetimes of the samples.

2.4. Methods

2.4.1. Analysis of the Fluorescence Decay Curves

2.4.1.1. Data Analysis

Fluorescence lifetime values were estimated from the fluorescence decay curves by employing reconvolution least squares method.[286] The excitation pulse can be expressed as a δ-function when the measured decay time is longer than the pulse-width of the excitation source. However, when the excited state lifetime is short, experimental data can be distorted by several factors such as the finite decay time of the source pulse, response time of the photomultiplier tube (PMT) and related electronics. Hence the instrument response function depends on decay time of the lamp pulse and response time of the detector (PMT) and associated electronics. The measured decay function is convolution of the true fluorescence decay and instrument response function. Hence, it is necessary to deconvolute the instrument response function from the experimental decay to get the fluorescence lifetime. The procedure can be mathematically described as[280, 281, 287-289]

$$I_m(t) = \int_0^t I_R(t - t')R(t')dt'$$

$$(2.6)$$

where, $I_m(t)$ is the fluorescence intensity at time t, $I_R(t-t')$ is the response function of the experimental system and $R(t')$ is the intensity of the exciting pulse at time t'. Instrument response function was measured using a dilute Ludox solution and deconvolution algorithm was done through iterative reconvolution method.

A nonlinear least squares (NLLS) data processing method is then applied to fit the ideal decay with some assumed functional form. This procedure is adopted to test whether a chosen mathematical method is consistent with the real data points or not. The least square analysis is only applicable if the data points satisfy certain assumptions. The main assumptions are that there should be enough independent data points, the uncertainties in the

experimental data points are Gaussian distributed and there should be no systematic error in the experimental data points. Experimentally, one can obtain both $I_m(t)$ and $R(t')$ from the TCSPC setup. During analysis, a decay function $G(t)$ is first assumed for the sample and this function is deconvoluted with the observed $R(t')$ according to equation 2.6 to obtain a calculated curve $Y(t)$, which is then compared with the experimentally observed decay curve $I_m(t)$.[238, 280, 281, 287, 289] The variables in the function $G(t)$ is iteratively changed until a good comparison (best fit) between the $Y(t)$ and $I_m(t)$ is obtained. The function $G(t)$ is usually assumed to be a sum of exponentials in such a way that,

$$G(t) = \sum_i B_i \exp(-t/\tau_i)$$

(2.7)

where B_i is the pre-exponential factor for the ith component and τ_i is the corresponding fluorescence lifetime constant. The success of an analysis and accordingly the acceptance of a fit to the observed decay curve are determined from the judicial judgments of the following statistical parameters.

2.4.1.2. Reduced Chi-square (χ^2) Values

Reduced χ^2 values are looked upon to judge the goodness of an iterative analysis and its value approaches unity if the model does fit the data. It is defined as

$$\chi^2 = \frac{\sum_i W_i \{Y_i - I_i\}^2}{n - p}$$

(2.8)

where Y_i is the count of ith channel of the calculated curve, I_i is the count at the ith channel of the experimentally measured curve. W_i [$W_i = I/I_i$], is the weighting factor of the counts in the ith channel, n is the number of channels used for the decay to be analyzed and p is the number of degrees of freedom in the decay function consider for the analysis which is equal to the number of variables in the function $G(t)$. For a very good fit, the χ^2 values should be close to unity.

2.4.1.3. Distribution of Weighted Residuals

The weighted residuals represent the deviation of the measured decay function from the fitted function. It is one of the most important parameters for the judgments of the success of an analysis of TCSPC data set and defined by the following relation

$$r_i = \sqrt{W_i} \{Y_i - I_i\}$$

(2.9)

where W_i, Y_i and I_i are as defined earlier. The random distribution of the weighted residuals about the zero line for the whole data range represents a good fit to the experimental data. In the present work F900 software has been used for deconvolution of the instrument response function and to fit each decay curve to a suitable mathematical function maintaining the χ^2 values between 1 and 1.2.

2.4.2. Construction and Fitting of Time-resolved Emission Spectra (TRES)

For the construction of TRES a set of procedure has been followed. Around 25-30 decay profiles were recorded at magic angle (54.7°) at 5/10 nm intervals across the entire range of the steady state emission profile.[238] F900 programme has been used to deconvolute of the instrument response from each decay curve. The decay curves were fitted by using a multiexponential decay function according to equation equation 2.10 maintaining the χ^2 value between 1 and 1.2. During this process random distribution of weighted residuals were also inspected to get a good fit.

$$I(\lambda,t) = I_o \sum_i a_i(\lambda) \exp[-\frac{t}{\tau_i(\lambda)}], \quad \sum_i a_i(\lambda) = 1$$

(2.10)

The time-resolved emission spectra (TRES) at different times are obtained from the appropriately normalized decay function $I'(\lambda, t)$ for different wavelengths and at different times where $I'(\lambda, t) = H(\lambda) \times I(\lambda, t)$. Here $H(\lambda)$ values is calculated by the following relation[225]

$$H(\lambda) = \frac{I_{ss}(\lambda)}{\sum_i \alpha_i(\lambda)\tau_i(\lambda)}$$

(2.11)

where $I_{ss}(\lambda)$ is the steady state intensity, $\alpha_i(\lambda)$ is the preexponential coefficient, and $\tau_i(\lambda)$ is the decay time at that wavelength with $\sum \alpha_i(\lambda)=1$. Each wavelength dependent emission spectra are then converted to frequency based spectra. Then, emission peak frequency at each time, $v(t)$ is obtained by fitting the spectrum to a log-normal line-shape function as given below[291]

$$I'(\lambda,t) = h\exp[-\ln 2\left\{\frac{\ln(1+\alpha)}{\gamma}\right\}^2] \text{ for } \alpha > \text{-}1, \alpha = \frac{2\gamma(v-v_p)}{\Delta}$$

$$= 0 \quad \text{for } \alpha \leq \text{-}1$$

(2.12)

In the above expression h, γ, v_p and Δ are the peak height, asymmetry parameter, peak frequency and width parameters of the spectra respectively.

2.4.3. Solvation Dynamics and Missing Component (MC) Calculation

For solvation time calculation the normalized Stokes shift correlation function $C(t)$ (also called solvent correlation function) is obtained from the following relationship.[290]

$$C(t) = \frac{v(t) - v(\infty)}{v(0) - v(\infty)}$$

(2.13)

In this expression $v(0)$ is the peak frequency at time $t = 0$, just after the electronic excitation and $v(t)$ is the peak frequency at time t, $v(\infty)$ is the peak frequencies at $t = \infty$ when solvent molecules are in the equilibrium position around the photoexcited probe molecule. The $C(t)$ vs. t curve is fitted by a bi-exponential function of the form[158, 159]

$$C(t) = a_1 e^{-t/\tau_1} + a_2 e^{-t/\tau_2}$$

(2.14)

where τ_1 and τ_2 are the solvent relaxation time and a_1 and a_2 are normalized pre-exponential factors. Then average solvation time is calculated from the relation

$$\langle \tau_s \rangle = a_1\tau_1 + a_2\tau_2$$

(2.15)

$C(t)$ vs t curve can also be fitted by the stretched exponential function as given below[160-170]

$$C(t) = exp(-(t/\tau_{solv})^{\beta}) \qquad \text{where } 0<\beta\leq1 \qquad (2.16)$$

to get the value of τ_{solv} and β. Then the average solvation time was calculated from the relation.

$$\langle\tau_{st}\rangle = \frac{\tau_{solv}}{\beta}\Gamma(\beta^{-1})$$

$$(2.17)$$

where, Γ is the gamma function and τ_{st} is solvation time considering $C(t)$ is stretched exponential function.

The finite time resolution of TCSPC setup puts constraints on the accurate estimation of the time-zero spectra and thereby estimation of dynamic Stokes shift. Therefore a semi-emperical method developed by Fee and Maroncelli[291] have been used to get time-zero spectrum. This method is based on steady state absorption and emission spectra of the fluorophore. The basic assumption of this method is that prior to solvent relaxation the Stokes shift of a given fluorescent probe in a polar and nonpolar solvent should be same. An approximate time zero frequency, $\nu(0)$ can be calculated by the following relation

$$\nu_p(0) \cong \nu_p(abs)-\{\nu_{np}(abs)-\nu_{np}(emi)\} \qquad (2.18)$$

where the subscripts "p" and "np" represent the polar solvent of interest and a reference nonpolar solvent, respectively. The choice of nonpolar solvent depends on the peak position of absorption of probe molecule in the polar solvent under investigation. Then, the percentage of missing component in dynamics of solvation can be calculated by the following relation.[291]

Percentage of missing component (MC) $= [\{\nu_{cal}(0)-\nu_{obs}(0)\}/ \{\nu_{cal}(0)-\nu_{obs}(\infty)\}] \times 100$ (2.19)

2.4.4. Time-resolved Fluorescence Anisotropy Measurements

The dynamics of angular displacement between absorption and subsequent emission of a fluorophore is monitored through time-resolved fluorescence anisotropy study. The pictorial representation of fluorescence anisotropy measurement is illustrated in Scheme 2.2. Molecules whose dipole moment vectors are aligned with the electric vector of the excitation pulse, are selectively excited. Then the emission intensities corresponding to different excitation and emission polarizer orientation are collected. Here I_{vv} represents the emission intensity observed with parallel polarization (excitation and emission polarizer are in vertical position) and I_{VH} indicates the intensity of perpendicularly polarized emission (excitation and emission polarizer are in vertical and horizontal position respectively). The ideal anisotropy, r(t), is expressed as,

$$r(t) = \frac{I_{vv}(t) - I_{VH}(t)}{I_{VV}(t) + 2I_{VH}(t)}$$

(2.20)

The difference between parallel and perpendicular emission is normalized by the total emission intensity, so the anisotropy is a dimensionless quantity and independent of the fluorophore concentration as well as the total emission intensity.
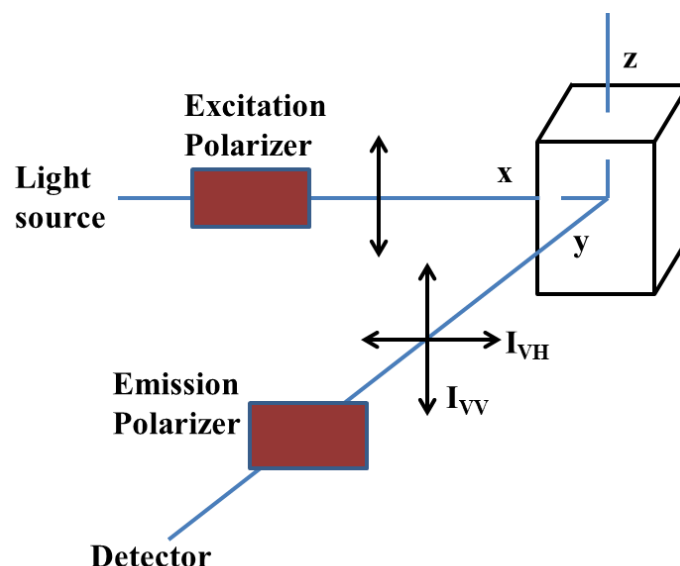
Scheme 2.2. Simplified pictorial representation of fluorescence anisotropy measurement with the help of time-resolved fluorescence anisotropy.

In TCSPC technique, sensitivity of experimental setup and electronics can influence the real anisotropy measurement. Hence it is necessary to include a correction factor *G* in the expression for *r(t)*. This G value represents the relative sensitivity of the detection system to these different polarizations. *G* varies with the emission wavelength and the band pass of the monochromator. It can be determined by

$$G = \frac{I_{HH}}{I_{HV}}$$

(2.21)

where I_{HH} and I_{HV} are the emission intensities when the excitation and emission polarizers are in horizontal-horizontal, horizontal-vertical position respectively. In the present study, the G factor is calculated from the ratio between I_{HH} and I_{HV} at the emission maxima. G factor can also be calculated experimentally from the tail matching of the measured anisotropy decay curve of a standard sample in a known standard solution. The measured anisotropy is then calculated by the following equation

$$r(t) = \frac{GI_{vv}(t) - I_{VH}(t)}{GI_{VV}(t) + 2I_{VH}(t)}$$

(2.22)

In the present study, Edinburgh OB920 TCSPC set up has been used for time-resolved fluorescence anisotropy measurements. The emission intensities were collected alternatively at parallel and perpendicular polarization (with respect to the vertically polarized excitation laser beam) for an equal interval of time until the count difference between the two polarizations (at t = 0) is ∼5000. For G-factor calculation, the same procedure was adopted but with 5 cycles and horizontal polarization of the exciting laser beam. The time-resolved fluorescence anisotropy, r(t) can be fitted by various functions. Generally, we preferred to fit it by single or bi-exponential function which is varied from sample to sample and the functional form is given below.

$$r(t) = r_0 \exp(-\frac{t_i}{\tau_i})$$

(2.23)

It is worth mentioning that the initial anisotropy value, r_0 should be within the range -0.20 to 0.40 for any single-photon excitation.[229]

2.5. NMR Measurements

2.5.1. Translational diffusion measurements

NMR experiments have been carried out using a 9.4 Tesla Bruker Avance NMR spectrometer at Larmor frequencies of 400.1MHz for ^{1}H and 376.5MHz for ^{19}F. Stimulated echo bipolar pulse-gradient pulse (stebpgp) sequence has been applied for the determination of translational diffusion coefficients, D, at different temperature (298 K to 338K). The echo heights were recorded at 16 equal intervals with variation of gradient pulse strength from 2 to 95% of the maximum gradient pulse strength (50 G/cm). The echo heights were then fit to the equation

$S(g) = S(0) \exp[−D\gamma^2\delta^2 g^2(\varDelta − \delta/3)]$ (2.24)

where $S(g)$ and $S(0)$ are the echo height at the gradient strength g and 0, respectively, γ is the

gyromagnetic ratio of the proton, δ is gradient pulse length, and Δ is the duration between the two gradient pulses.

2.5.2. Spin-lattice Relaxation Time (T$_1$) Measurements

T$_1$ data were acquired using inversion recovery method[292] and were fit to the Bloembergen−Purcell−Pound (BPP) relationship[293] (Eq.2.25) to obtain rotational correlation time, τ_c for each resolved NMR resonance peak.

$$\frac{1}{T_1} = \frac{6}{5}\frac{\gamma^4 h^2}{b^6}I(I+1)\left[\frac{\tau_c}{1+\omega_0^2\tau_c^2} + \frac{4\tau_c}{1+4\omega_0^2\tau_c^2}\right] \qquad (2.25)$$

where γ is the gyromagnetic ratio of the proton ($2\pi\cdot42.576$MHz/Tesla), $\hbar$ is reduced Planck's constant, b ($= \Sigma r$) is the summed distance between protons and the sum runs over all protons that are dipolar coupled to the proton evaluated, I is nuclear spin number of the proton ($= 1/2$). $\omega_0 = 2\pi\nu_0$, where ν_0 is 400.1 MHz at 9.4 Tesla, the proton observation frequency, and τ_c is the rotational correlation time. Equation 2.25 is derived under the isotropic motion approximation and applies in the extreme narrowing limit (T$_1$ = T$_2$). The only other unknown quantity in Eq. 2.25, other than τ_c, is b. To calculate b for a proton, T$_1$ measurements were repeated for varying temperature, so that T$_1$ can be measured for different τ_c. It can be easily shown from Eq. 2.25 that T$_1$ passes through a minimum where $\omega_0\tau_c$ becomes equal to 0.616, which corresponds to τ_c of 2.45×10^{-10}s for 400.1 MHz proton frequency. The distance term, b, can there from be calculated using minimum value of T$_1$.[292] As the distance term involves only near neighbour protons (within 5 Å), it is assumed that b remains unaltered with change in temperature. The summed distance b was therefore used to calculate τ_c from T$_1$ data taken at all temperatures.

^{19}F T_1 measurements were also carried out to obtain T_1 values for anions of some ILs by employing same methodology as mentioned above. However τ_c values were not calculated for anions.

2.6. Standard Error Limits

Standard error limits involved in the experimental results were

Viscosity (η)	$\pm 2\%$
Density (ρ)	$\pm 2\%$
λ_{max} (abs./flu.)	± 1 nm
τ_f (> 1ns)	$\pm 5\%$
Rotational relaxation time	± 5-10%
Solvent relaxation time	$\pm 5\%$
Rate of intramolecular PET	± 5-10%

Chapter 3

Reorientational Dynamics of Charged and Neutral Solutes in 1-Alkyl-3-methylimidazoilum Bis(trifluoromethylsulfonyl)imide Ionic Liquids

Role of electrostatic interaction on rotational relaxation dynamics of two charged solutes, sodium 8-methoxypyrene-1,3,6-trisulfonate (MPTS), 1-pyrenesulfonic acid sodium salt (1-PSA) and neutral perylene has been studied in two structurally similar but chemically distinguishable imidazolium-based ionic liquids (ILs). Analysis of the results reveals that rotational relaxation of MPTS is significantly hindered even in the IL where acidic C2–H of the imidazolium moiety is replaced by the methyl group. Moreover, rotational relaxation of neutral perylene is found to be faster than mononegative 1-PSA which is again observed to be faster than that of tri-negative MPTS in the same ILs.

3.1. Introduction

Ionic liquids (ILs) have gathered considerable attention over the past decade both from academia and industry owing to their interesting physicochemical properties such as low vapour pressure, large electrochemical window and capacity to solubilize large range of organic and inorganic materials etc.[4-8] It is also known that the constituents of ILs can play significant role in determining their physicochemical properties.[9] Moreover, these properties are observed to be tuneable with the variation of the constituents that they are composed off. For example, it has been observed that substitution at C2 position of the imidazolium cation can help in controlling the physicochemical properties of ILs.[203] Reichardt has demonstrated the role of the hydrogen bonding interaction of the C2- hydrogen in shaping the micro-polarity of several imidazolium-based ILs.[44] He has also shown that the C(2)-alkylated imidazolium ILs are less polar than those comprising the C2- hydrogen.[44] C2-H hydrogen of imidazolium cation is also quite acidic (pK_a=23.0).[294] It has also been shown that C2-

methylation increases the viscosity and melting point but decreases the conductivity.[37, 295-297] Since intermolecular interactions such as electrostatic interactions, van der Waals forces and hydrogen bonding interactions are known to have profound influence on many physicochemical properties of liquids and solution[287, 298-300], many other researcher have also investigated the role of C2 methylation in imidazolium cation in determining the physicochemical properties of the ILs by carrying out theoretical and experimental studies.[301-303] Essentially these studies have demonstrated that the intermolecular interaction among solute-solvent, solvent-solvent plays important role in controlling the properties of liquids and solution[298] and interplay among these forces may induce a non-trivial behaviour in ILs.[109, 162] Thus, understanding of solute-solvent interaction as well as cation-anion interactions within the IL is of great importance not only to understand the fundamentals of their action but also to effectively use them in applications such as solvent for reaction,[304-306] separation media[307] and electrochemical applications etc.[308]

Studies on rotational relaxation dynamics involving an organic solute by exploiting time-resolved anisotropy measurements is proven to be a very useful tool in providing a great deal of information about intermolecular interactions in solution.[298] In recent past, studies on solute rotation in a variety of ILs have helped in understanding the various interactions that are present within the ILs and also between added solute and ILs.[192-205] Recent studies have demonstrated the role of specific solute-solvent interaction in controlling rotational motion of organic solutes in ILs.[192-205] Since ILs are composed of ions, attempts have also been made to find out the role of electrostatic interaction in influencing the rotational dynamics[192, 193] In this context the work by Fruchey and Fayer by employing charged solute, sodium 8-methoxypyrene-1,3,6-sulfonate (MPTS) in a series of N-alkyl-N-methylimidazolium ionic liquids is noteworthy.[193] The authors have demonstrated that the hydrogen bonding interaction between MPTS and C2-H can play an important role in slowing down the rotation

of MPTS in the RTILs. The results indicated that MPTS is bound to RTILs. The increased volume of MPTS, due to solvent association, is believed to be responsible for its slow reorientational motion. On the similar objective, Samanta and his co-workers[192] have investigated the rotational relaxation dynamics of cationic and anionic solutes, ethidium bromide (EB) and 1-anilinonaphthalene-8-sulfonate (ANS) in imidazolium-based ILs. The rotational behaviour of the ionic solutes is observed to be very similar in ILs and glycerol under isoviscous conditions. Essentially their results have also demonstrated that the solute-solvent hydrogen bonding interaction is primarily responsible for slowing down the solute rotation. No evidence of electrostatic interaction between solute and solvent in slowing down the solute rotation has been observed. It should be noted here that the above studies have been carried out in imidazolium-based ILs where the acidic C2-H is involved in solute-solvent hydrogen bonding interaction. Perhaps because of this issue no straight forward correlation between solute rotation and electrostatic interaction was found from the above studies. One possible approach to find out unambiguously the role of electrostatic interaction towards solute rotation in imidazolium-based ILs, C2-H of the imidazolium cation can be substituted with a suitable group like "methyl" so that the H-bonding interaction due to C2-H is eliminated, and thereby the effect of electrostatic interaction on solute rotation is monitored.

It is in this context the present study has been conducted. We have carried out the present study with the tri-anionic probe MPTS and mono-anionic 1-pyrenesulfonic acid sodium salt (1-PSA) and nonpolar perylene in two ILs. The choice of the probe is made in such a way so that a systematic variation in total charge on the solutes is maintained. ILs used in this study are purposefully chosen so that, 1-ethyl-3-methylimidazolium bis(trifluoromethylsulfonyl)imide [EMIM][Tf$_2$N] can form intermolecular hydrogen bond via C2-H of the imidazolium moiety with the negatively charged sulfonate group of the

solute, whereas 1-ethyl-2,3-dimethylimidazolium bis(trifluoromethylsulfonyl)imide [2,3-DMIM][Tf$_2$N] cannot form such interaction as the acidic C2-H is replaced with the methyl group in the latter case. Time-resolved fluorescence anisotropy measurements by employing these three probes in these two ionic liquids have been carried out. The results from the rotational anisotropy measurements have been analyzed with the help of Stokes−Einstein−Debye (SED) hydrodynamic theory.[240] Solute-solvent interactions have been investigated further by measuring translational diffusion of the probes in the ILs by PFG-NMR technique. Molecular structures of the ILs and the probes are presented in Chart 3.1.
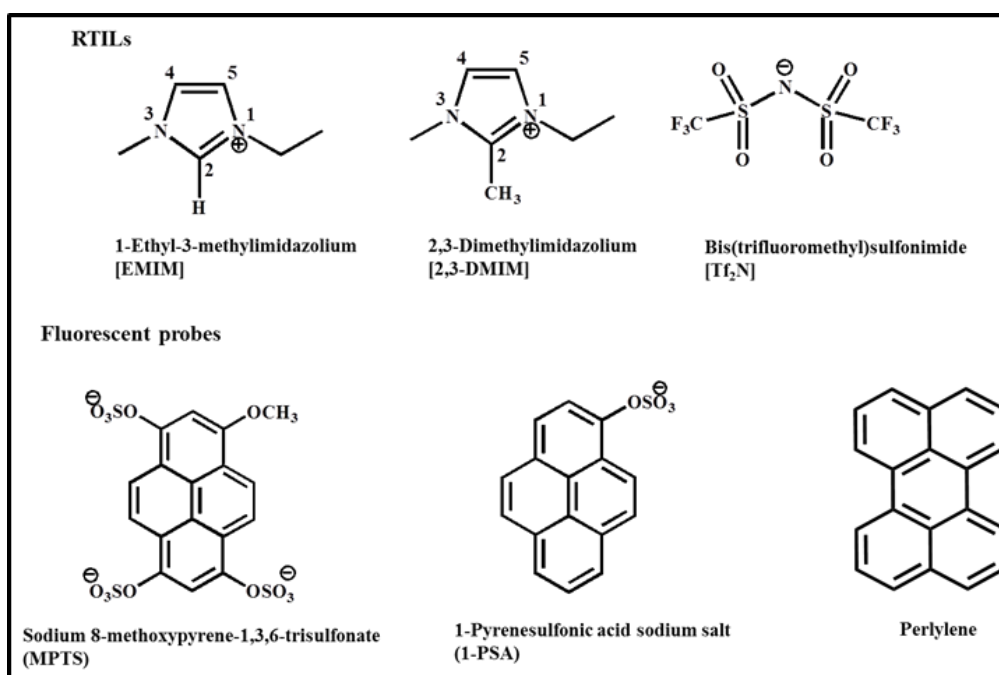
Chart 3.1. Molecular structures of the ILs and molecular probes.

3.2. Experiments and Methods

MPTS, 1-PSA and perylene were purchased from Fluka, Sigma-Aldrich and used as received. The RTILs [EMIM][Tf$_2$N] and [2,3-DMIM][Tf$_2$N] were obtained IOLITECH, USA (>98% purity) and used as received. Procedures of sample preparation and experimental methods for steady-state and time-resolved studies, translational diffusion measurement through NMR and viscosity measurements are described in detail in Chapter 2.

3.3. Results and Discussion

3.3.1. Steady-State Absorption and Emission Spectra

Representative absorption and emission spectrum of 1-PSA in the two ILs are shown in Figure 3.1. The absorption and emission spectra of the probes in the two ILs are found to be very close. This observation indicates that the bulk polarities of the ILs are very similar. The absorption and emission maxima of any of the probes are found not be affected by varying temperature from 293 K-333 K.
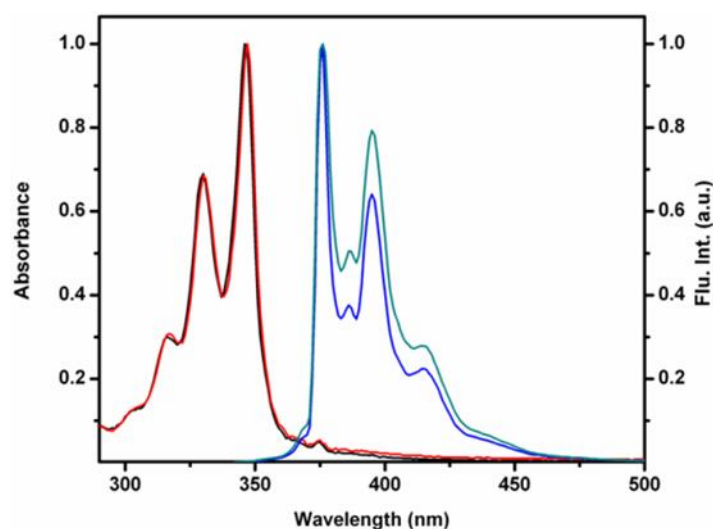
Figure 3.1. Combined absorption and emission spectra (λ_{exc} =330 nm) of 1-PSA in the ILs. Absorption and emission spectra are represented by black and blue lines in [EMIM][Tf$_2$N] and red and green lines in [2,3-DMIM][Tf$_2$N].

3.3.2 Rotational Relaxation Dynamics

Time-resolved fluorescence anisotropy measurements of all three probes (MPTS, 1-PSA and perylene) have been carried out over the temperature range 293 K to 333 K. Representative anisotropy decay profiles of MPTS in [EMIM][Tf$_2$N] and [2,3-DMIM][Tf$_2$N] is shown in Figure 3.2. The rotational relaxation times are calculated from single exponential fit to anisotropy decay data for MPTS and 1-PSA and biexponential fit to the anisotropy decay data for perylene. In the present case, single and biexponential fittings of the anisotropy decay profiles of the respective systems can be ascribed to the symmetry properties of the molecules.[192] Rotational relaxation parameters of MPTS, 1-PSA and perylene in both ILs at different temperatures are presented in Table 3.1. For perylene, individual component of the biexponential fitting parameters for the anisotropy decay profiles are provide in Table 3.2.
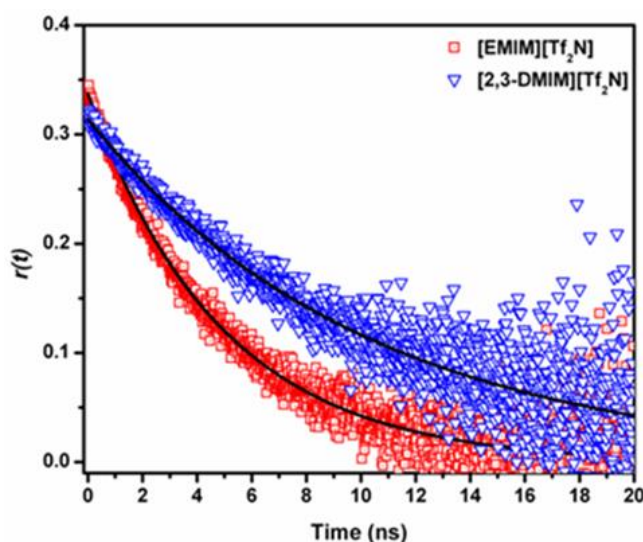
Figure 3.2. Time resolved fluorescence anisotropy decay of MPTS in [EMIM][Tf$_2$N] and [2,3-DMIM][Tf$_2$N].

Table 3.1. Rotational relaxation parameters of MPTS, 1-PSA and perylene in [EMIM][Tf$_2$N] and [2,3-DMIM][Tf$_2$N] at different temperatures

Systems	Temp.(K)	[EMIM][Tf$_2$N]			[2,3-DMIM][Tf$_2$N]		
		Vis.(cP)	$<\tau_r>$(ns)	C_{rot}	Vis.(cP)	$<\tau_r>$(ns)	C_{rot}
[a]MPTS	293	34.2	5.77	1.49	73.6	11.62	1.39
	298	28.4	4.87	1.54	59.0	10.01	1.52
	303	23.7	4.15	1.60	48.4	8.56	1.62
	308	20.4	3.47	1.58	39.6	6.92	1.62
	313	17.5	2.94	1.59	33.0	5.71	1.63
	318	15.0	2.53	1.62	28.4	4.74	1.60
	323	13.1	2.17	1.61	24.2	4.00	1.61
	328	11.3	1.91	1.67	20.6	3.37	1.62
	333	9.97	1.68	1.69	18.0	2.89	1.61
[a]1-PSA	293	34.2	1.93	1.49	73.6	3.71	0.43
	298	28.4	1.68	0.51	59.0	2.97	0.44
	303	23.7	1.40	0.51	48.4	2.41	0.44
	308	20.4	1.26	0.54	39.6	2.01	0.45
	313	17.5	1.18	0.61	33.0	1.70	0.47
	318	15.0	1.08	0.66	28.4	1.46	0.48
	323	13.1	0.95	0.68	24.2	1.31	0.53
	328	11.3	0.91	0.77	20.6	1.16	0.54
	333	9.97	0.85	0.86	18.0	1.00	0.54
Perylene	293	34.2	0.51	0.15	73.6	1.04	0.13
	298	28.4	0.41	0.15	59.0	0.89	0.15
	303	23.7	0.38	0.17	48.4	0.74	0.14
	308	20.4	0.33	0.17	39.6	0.64	0.14
	313	17.5	0.30	0.18	33.0	0.54	0.16
	318	15.0	0.26	0.19	28.4	0.50	0.16
	323	13.1	0.23	0.20	24.2	0.46	0.16
	328	11.3	0.21	0.21	20.6	0.35	0.17
	333	9.97	0.20	0.23	18.0	0.31	0.18

[a]Rotational relaxation times for MPTS and 1-PSA were calculated from single-exponential decay function.

Table 3.2. Rotational relaxation parameters of perylene in [EMIM][Tf$_2$N] and [2,3-DMIM][Tf$_2$N] at different temperatures

	Temp.(K)	Vis.(cP)	a_1	τ_1(ns)	a_2	τ_2(ns)	$<\tau>$(ns)	C_{rot}
[EMIM][Tf$_2$N]	293	34.2	0.37	0.13	0.63	0.70	0.51	0.15
	298	28.4	0.40	0.11	0.60	0.61	0.41	0.15
	303	23.7	0.51	0.16	0.49	0.61	0.38	0.17
	308	20.4	0.53	0.16	0.47	0.53	0.33	0.17
	313	17.5	0.51	0.13	0.49	0.48	0.30	0.18
	318	15.0	0.47	0.10	0.53	0.40	0.26	0.19
	323	13.1	0.49	0.10	0.51	0.37	0.23	0.20
	328	11.3	0.65	0.11	0.35	0.40	0.21	0.21
	333	9.97	0.63	0.11	0.37	0.36	0.20	0.23
[2,3-DMIM][Tf$_2$N]	293	73.6	0.45	0.38	0.55	1.58	1.04	0.13
	298	59.0	0.50	0.36	0.50	1.42	0.89	0.15
	303	48.4	0.45	0.30	0.55	1.10	0.74	0.14
	308	39.6	0.44	0.21	0.56	0.98	0.64	0.14
	313	33.0	0.42	0.17	0.58	0.80	0.54	0.16
	318	28.4	0.37	0.15	0.63	0.71	0.50	0.16
	323	24.2	0.41	0.15	0.59	0.67	0.46	0.16
	328	20.6	0.54	0.14	0.46	0.59	0.35	0.17
	333	18.0	0.53	0.13	0.47	0.52	0.31	0.18

As can be seen from Table 3.1 rotational relaxation time (τ_r) for all the three probes in both ILs decreases with increase in temperature as medium viscosity gradually decreases upon increase in temperature. At a particular temperature, τ_r for all the probes, is fund to be lower in [EMIM][Tf$_2$N] than in [2,3-DMIM][Tf$_2$N] as the viscosity of the later is higher at any given temperature. It has also been observed that τ_r increases proportionately with increase in viscosity on going from [EMIM][Tf$_2$N] to [2,3-DMIM][Tf$_2$N]. In fact at a similar η/T (for example, at 308 K in [EMIM][Tf$_2$N] and 328 K in [2,3-DMIM][Tf$_2$N]), τ_r values are found to be very close for all the solutes. Quite interestingly, a close inspection of the data in

Table 3.1 reveals that τ_r values are higher for the charged solutes (MPTS and 1-PSA) than the uncharged perylene at any given temperature. Again, among the charged solutes, τ_r value is observed to be significantly higher for MPTS (with three units –ve charge) than that for 1-PSA (one unit –ve charge) in both ILs. The present data on rotational relaxation time (τ_r) points out that rotation of a charged solute experiences relatively stronger hindrance than the uncharged one and the such hindrance decreases with reduction in the total charge (here negative) of the solute molecules.

To obtain a better understanding of the nature of rotational diffusion of the charged and uncharged solutes the results from the rotational anisotropy measurements have been analysed further with the help of SED hydrodynamic theory.[240] SED theory helps us to correlate reorientation time with the medium viscosity as per the following equation 1.2. As mentioned in Chapter 2, the two limiting boundary conditions in SED theory are stick and slip.[240] For calculation of slip boundary condition paremeter (C_{slip}), the probe properties that are available in literature[34] have been used. In case of 1-PSA, optimized structure (from Gaussian 09 software [309]) has been used to calculate volume and thereby C_{slip}. Details of the calculation have been described in Chapter 2. The van der Waals volumes (V), shape factor (f), and calculated slip boundary condition parameter (C_{slip}) for the probe molecules are listed in Table 3.3.

Table 3.3. van der Waals volumes, shape factor, and slip boundary condition parameters

Systems	van der Waals volume(Å^3)	f	C_{slip}
MPTS	343	1.33	0.11
1-PSA	286	1.65	0.12
Perylene	225	1.76	0.085
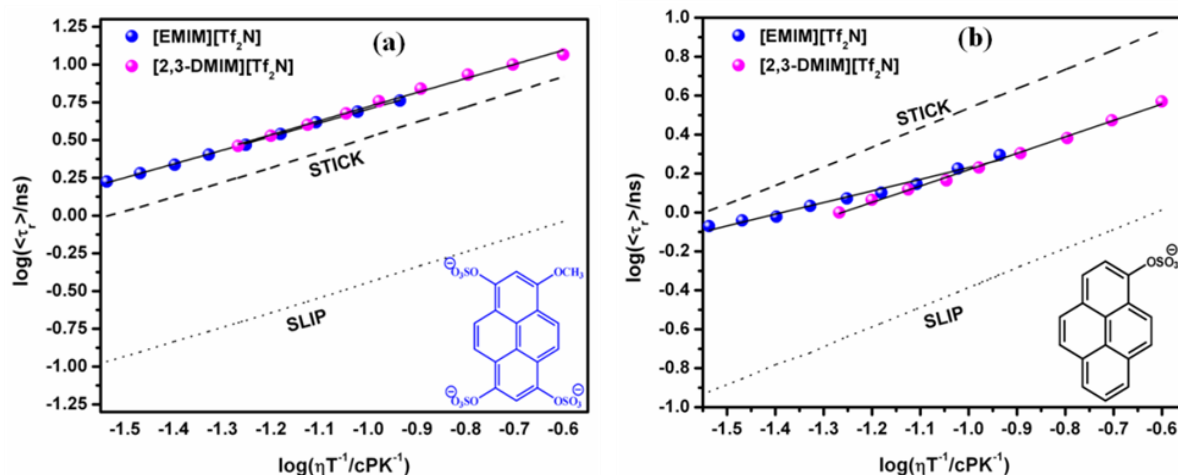
Figure 3.3. The log-log plots of τ_r vs. η/T for MPTS (a) and 1-PSA (b). The solid black lines represent linear fit to the data points.

Figure 3.3(a)-(b) represents the log-log plots of τ_r vs. η/T for MPTS and 1-PSA respectively. Slopes of the linear fit to the τ_r vs η/T plot, are found to be the similar (equation 3.1 and 3.2).

MPTS in [EMIM][Tf$_2$N]

$$\tau_r = (1.61 \pm 0.01)(\eta/T)^{(0.90 \pm 0.01)} \text{ (N=9, R=0.99)} \tag{3.1}$$

MPTS in [2,3-DMIM][Tf$_2$N]

$$\tau_r = (1.65 \pm 0.02)(\eta/T)^{(0.93 \pm 0.02)} \text{ (N=9, R=0.99)} \tag{3.2}$$

MPTS has been observed to show superstick behaviour in both the ILs (Figure 3.3(a)). It is well documented in literatures that superstick behaviour arises due to specific solute-solvent interaction between acidic C2-H of imidazolium moiety and negatively charged anions.[190, 193] The present data indicate that the strength of solute-solvent interaction is same in both ILs. Note that C_{rot} value of MPTS in [2,3-DMIM][Tf2N] (1.52 at 298K) is found to be very close to that in [EMIM][Tf2N] (1.54 at 298K) (Table 3.1) despite the fact that [2,3-DMIM][Tf2N] does not contain acidic hydrogen (C2-H).

This is an interesting observation in a sense that hydrogen-bonding interaction between MPTS and [2,3-DMIM] cation can be ruled out because of C2-methylation. It may be mentioned here that while explaining the superstick behavior of MPTS in a series of 1-alkyl-3-methyl-imidazolium based ILs, Fruchey and Fayer[193] demonstrated that the superstick behaviour cannot be ascribed to a non-specific solute-solvent interaction. We would also like to note here that superstick behaviour in hydrodynamics is traditionally explained on the basis of solventberg[243] and Nee-Zwanzig dilectric friction[244] models. While solventberg model consider the increase in rotor volume due to specific solute-solvent interaction, dilectric friction considers the torque between a dipole and the reactive field of the surrounding dielectric cavity. Interestingly, Maroncelli[310] in case of alcoholic solvents has demonstrated that solventberg model dominates over dielectric friction model. Another report by Kurnikova *et al.*[311] through time-resolved optical heterodyned polarization spectroscopy and molecular dynamics study on solute-solvent interaction in dimethylesulfoxide (DMSO) has revealed different rotational diffusion of cationic (thionine), anionic (resorufin) and neutral (resorufamine) probes which are of similar size. The authors have found that while the rotational diffusion of resorufamine follows in-between slip and stick boundary conditions, the anionic resorufin obeys slip boundary condition and the positively charged molecule, thionine shows superstick behaviour. This observation has been rationalized by hydrogen bonding interaction between thionine and DMSO. Thionine has been found to be associated with the solvent much more strongly compared to the other systems. In the present case, even though the hydrogen bonding interaction between MPTS in [EMIM][Tf$_2$N] cannot be neglected, it is interesting to observe the superstick behaviour for MPTS also in [2,3-DMIM][Tf$_2$N] where C2-H proton is replaced by methyl group. In this context it should be mentioned that the ionic component of the hydrogen bond between the charged solute and cation of the IL is known to have significant contribution in determining the polarity scale of

ILs as demonstrated by Welton and coworkers'.[300] In another report, the authors, through *ab initio* calculations, have demonstrated that the hydrogen bond in the ionic liquid 1-butyl-3-methylimidazolium chloride ($[C_4C_1im]Cl$) is primarily ionic in nature and the Coulombic interaction is the dominant stabilizing force.[312] In light of the above discussions, our present results certainly illustrates the predominant role of ionic component of hydrogen bonding interaction during rotation of an ionic solute.

To get the systematic idea about the influence of electrostatic interaction, rotational relaxation behaviour of another charged solute, having total negative charge less than the tri-negative MPTS molecule, a mono-negative 1-PSA is also employed. Figure 3.2(b) reveals that the rotational relaxation dynamics of 1-PSA is different from MPTS and is observed to lie between hydrodynamic stick and slip limits. While C_{rot} values for MPTS in the two ILs are found to be similar, the same for 1-PSA, in the two ILs are found to be somewhat different. C_{rot} values for 1-PSA is estimated to be ~0.6 in $[EMIM][Tf_2N]$ and ~0.5 in [2,3-DMIM][Tf_2N] (Table 3.1). This data indicates that the solute-solvent interaction is relatively stronger for MPTS-ILs systems than that for 1-PSA-ILs systems. Recently Khara and Samanta have[192] shown that rotational relaxation behaviour of mononegative solute 1-anilinonaphthalene- 8-sulfonate (ANS) lies in between stick and slip boundary of SED model in [bmim][BF_4]. The authors have suggested that since ANS has less number of hydrogen bonding sites as compared to that of MPTS, ANS is expected to rotate faster in ILs. Hence, from the present data, it can be concluded that the less number of hydrogen-bonding sites in 1-PSA as compared to that in MPTS is primarily responsible for relatively faster rotation of 1-PSA in $[EMIM][Tf_2N]$. Slightly faster rotational behaviour of 1-PSA in [2,3-DMIM][Tf_2N] as compared to the same in $[EMIM][Tf_2N]$ might arise due to the prevention of the solute-solvent specific hydrogen bonding interaction in the former one as it lacks C2-H. In a recent article Dutt and coworkers[202] have shown that rotational relaxation of N-methylated 2,5-

dimethyl-1,4-dioxo-3,6-diphenylpyrrolo[3,4-c]pyrrole (DMDPP) is faster than that of structurally similar 1,4-dioxo-3,6-diphenylpyrrolo-[3,4-c]pyrrole (DPP) in 1-alkyl-3-methylimidazolium tetrafluoroborates. The authors have suggested that N-methylation in DMDPP disrupts the solute–solvent H-bonding interaction which leads to faster rotation of DMDPP. In the present case, it is perhaps the absence of H-bonding interaction between 1-PSA and $[2,3\text{-DMIM}]^+$ that renders lesser hindrance towards rotation of 1-PSA in $[2,3\text{-DMIM}][\text{Tf}_2\text{N}]$. As a result rotational relaxation of 1-PSA is observed to be comparatively faster in $[2,3\text{-DMIM}][\text{Tf}_2\text{N}]$ than in $[\text{EMIM}][\text{Tf}_2\text{N}]$. The difference in rotational relaxation behaviour 1-PSA in the two ILs is also clear from the different slopes of the linear fit to the τ_r vs. η/T plot (equation 3.3 and 3.4).

1-PSA in $[\text{EMIM}][\text{Tf}_2\text{N}]$

$$\tau_r = (0.82 \pm 0.04)\,(\eta/T)^{(0.58\pm0.03)}\ (N=9,\ R=0.977) \tag{3.3}$$

1-PSA in $[2,3\text{-DMIM}][\text{Tf}_2\text{N}]$

$$\tau_r = (1.06 \pm 0.01)\,(\eta/T)^{(0.84\pm0.01)}\ \ (N=9,\ R=0.996) \tag{3.4}$$

It should be noted here that the absence of "superstick" behaviour during the rotation of 1-PSA in both ILs perhaps indicates that the concerned solute needs to possess sufficiently counter ion charge density (here negative) with respect to the total charge of the ionic constituents of ILs so as to demonstrate the influence of electrostatic interaction (between solute-solvent) on solute rotation. Since many earlier studies [203, 192, 193, 197, 198] in this directions were carried out by employing a nonnegative or positive solute, the effect of electrostatic interaction on solute rotation were not observed.
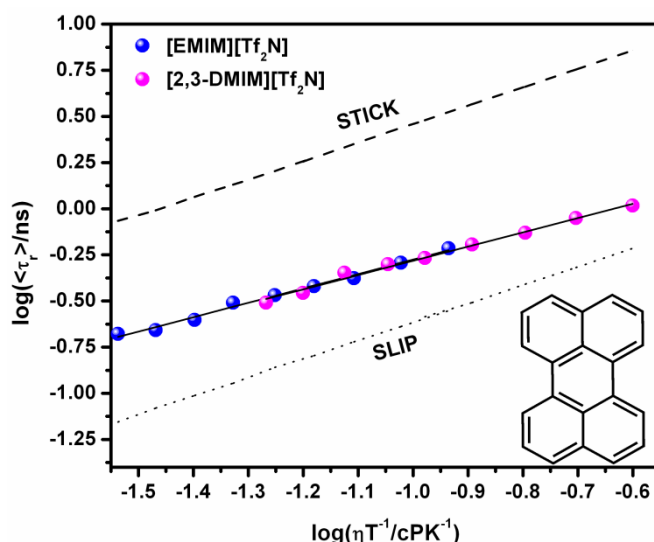
Figure 3.4. The log-log plots of τ_r vs. η/T for perylene. The solid black lines represent linear fit to the data points.

We have further studied the rotational relaxation behaviour of nonpolar perylene in the same ILs. The nonpolar and non-hydrogen bonding perylene shows similar rotational relaxation behaviour in the two ILs and found to be within the limits set by SED theory (Figure 3.4). C_{rot} values are found to be very similar in both ILs (Table 3.1). Also slopes of the linear fit to the τ_r vs η/T plot, are found to be the similar (equation 3.5 and 3.6).

Perylene in [EMIM][Tf$_2$N]

$$\tau_r = (0.31 \pm 0.03) \, (\eta/T)^{(0.70 \pm 0.02)} \quad (N = 9 \, , R = 0.990) \tag{3.5}$$

Perylene in [2,3-DMIM][Tf$_2$N]

$$\tau_r = (0.47 \pm 0.02) \, (\eta/T)^{(81 \pm 0.02)} \quad (N = 9 \, , R = 0.989) \tag{3.6}$$

The origin of such behaviour can be attributed to the similar nonpolar microenvironment experienced by perylene in both ILs. The data also indicates that perylene is located in the hydrophobic domain of the ILs. Since the length of the alkyl chain is same in both ILs rotational relaxation behaviour of perylene in both ILs are quite similar.

3.3.3. PFG-NMR Studies

To get a further understanding of the role of hydrogen-bonding and electrostatic interaction in governing the rotational dynamics in the present ILs PFG-NMR technique has also been explored. We have measured translational diffusion coefficients (D) of MPTS and 1-PSA at 298 K through PFG-NMR technique. D for MPTS and 1-PSA are found to be 1.52×10^{-10} m^2/S and 2.48×10^{-10} m^2/S respectively in deuterated dimethyl sulfoxide (DMSO-d^6). To analyse our results, Stokes-Einstein formula ($D=(kT)/(6\pi\eta a)$) for translational diffusion coefficient (*D*), is used. We have observed that with addition of the two ILs, translational diffusion of the probes slows down suggesting the solute-IL interaction. Here, we would like to mention that the concentration of ILs in the NMR samples has been maintained ~3.5×10^{-4}M so that the viscosity of the sample does not change. In case of MPTS, *D* value is found to be reduced to 1.40×10^{-10} m^2/S and 1.35×10^{-10} m^2/S with addition of [EMIM][Tf_2N] and [2,3-DMIM][Tf_2N] respectively. Similarly *D* of 1-PSA decreases to 2.23×10^{-10} m^2/S and 2.29×10^{-10} m^2/S with addition of [EMIM][Tf_2N] and [2,3-DMIM][Tf_2N] respectively. D has been observed to be reduced for both MPTS and 1-PSA with addition of [2, 3-DMIM][Tf_2N], even though hydrogen-bonding interaction is eliminated by C2-methylation. In this scenario, the only possibility that might slow down translational diffusion of the probes with addition of [2, 3-DMIM][Tf_2N] is the electrostatic interaction between the solute and the IL. These results also suggest that the electrostatic interaction plays important role in governing translational diffusion of the charged probes.

3.4. Conclusion

In this chapter rotational relaxation behaviour of two charged solutes (MPTS and 1-PSA) and one uncharged solute (perylene) have been investigated through time resolved fluorescence anisotropy measurements in two structurally similar but chemically distinguishable RTILs [EMIM][Tf_2N] and [2,3-DMIM][Tf_2N]. While [EMIM][Tf_2N] can

form intermolecular hydrogen bond via C2-H of the imidazolium moiety with the negatively charged sulfonate group of MPTS and 1-PSA, [2,3-DMIM][Tf$_2$N] cannot have such interaction as the acidic C2-H of the imidazolium moiety is replaced by the methyl group. Analysis of the fluorescence anisotropy results in light of SED hydrodynamic theory revealed superstick hydrodynamics behaviour of MPTS in both ILs. Quite interestingly, rotational coupling constant (C_{rot}), is found to be similar (~1.6) for MPTS in both ILs even though [2,3-DMIM][Tf$_2$N] cannot form stronger solute-solvent hydrogen bonding interaction owing to C2-methylation in the imidazolium moiety. This observation clearly indicates the role of electrostatic interaction on rotational relaxation of MPTS in ILs. Rotational relaxation of the mononegative solute, 1-PSA, has been observed to be faster in ILs than that has been observed for the tri-negative solute MPTS in the same ILs. This can be attributed to the weakening of solute-solvent interaction due to reduction of total charge in 1-PSA. Rotational relaxation time of neutral perylene is found to be even faster than that of 1-PSA. Similar C_{rot} values of perylene in the two ILs indicate that it locates itself in a similar nonpolar environment in both the ILs. Additionally, translational diffusion coefficients of the probes, estimated through PFG-NMR experiments, also corroborate the results obtained from anisotropy measurements. Results of the present investigations advocate the need of considering the electrostatic interaction between solute and solvent while explaining the rotational diffusion of charged solutes in ILs.

Chapter 4

Intramolecular Photoinduced Electron Transfer Reaction in Donor-Spacer-Acceptor Systems in Room-Temperature Ionic Liquids

---

The role of solvents on intramolecular photoinduced electron transfer (PET) kinetics has been investigated by employing two nitrobenzoxadiazole-based flexible donor-spacer-acceptor (DSA) derivatives in two room temperature ILs. The results obtained in ILs have been further compared with a conventional organic solvent acetonitrile. The electron transfer process has been studied by steady state and time-resolved fluorescence measurements. The reaction kinetics has been analyzed by using a two-state model. It has been observed that the dynamics of solvation of the concerned media plays important role in governing the rate of PET process.

4.1. Introduction

In recent times, ILs have shown great promise as an excellent alternative to conventional organic solvents in various electrochemical applications.[24, 63, 308] It is, therefore, important to understand the effects of ILs on electron transfer process such that these materials can be used to their fullest potential. Literature reports have shown that the rate of photoinduced intermolecular electron transfer (PIET) in room temperature ILs is slower than that in conventional solvents.[222, 223, 313] The slower rate of PIET process in ILs has been attributed to the high viscosities of ILs. However, there are reports on PIET process in ILs which have shown that significant contribution to PIET quenching may come from the electron transfer process occurring in static and transient domains in high viscous media such as ILs.[226, 249] It has also been shown in these studies that difference between diffusion controlled (viscosity dependent) and observed PIET rate can be observed.[226, 249] Moreover,

since solvation process is slow in ILs, the rate of solvation can also be an important factor in controlling the PET process in these media. Hence, studies on intramolecular PET by employing donor-spacer-acceptor (DSA) systems can provide a comprehensive comparison between conventional solvents and ILs by eliminating the differences which may arise due to transport phenomenon. Studies on intramolecular PET in conventional solvents have been carried out by various research groups.[212, 216, 217] The first example of the intramolecular PET in ILs was described by Wasielewski and coworkers.[212] The authors pointed out that the fast translational processes of constituents of the ILs contribute predominantly to the electron transfer process.[212] Some other researchers have also investigated intramolecular PET in ILs.[314-317] These investigations indicate that the PET reaction rate in ILs is broadly distributed. and solvation in ILs has profound influence on PET process.[314-317] However such studies in ILs are still limited and further investigations are necessary to fully understand the intricacies of solvation and PET process in these media.

Keeping the above facts in mind we have studied intramolecular PET process in two different DSA systems namely 4-(N,N-dimethylethylenediamino)-7-nitrobenz-2-oxa-1,3-diazole (NBDEA) and 4-(N,N-dimethylpropylenediamino)-7-nitrobenz-2-oxa-1,3-diazole (NBDPA) in two ILs (Chart 4.1). The study has been carried out with a two-fold objective; firstly to envisage the role of rate of solvation of the medium on electron transfer process and secondly to probe the role of the conformation of solute, if any, during the electron transfer process. These DSA systems differ from each other only by the length of spacer unit. We have purposefully chosen NBDEA and NBDPA as *through-space* intramolecular PET from dimethyleamino group (donor) to the nitrobenzoxadiazole (acceptor) moiety is well established.[318-322] For example, many flexible nitrobenzoxadiazole–based systems has been used as fluorescent sensor for transition metal ions due the favourable PET occurring in them.[320, 321] In the present case, electron transfer rates are determined by comparing the

fluorescence lifetimes of the DSA molecule with their parent molecule 4-aminonitrobenzoxadiazol (NBDH). We have compared the electron transfer kinetics in RTILs with closely polar conventional solvent acetonitrile (ACN).
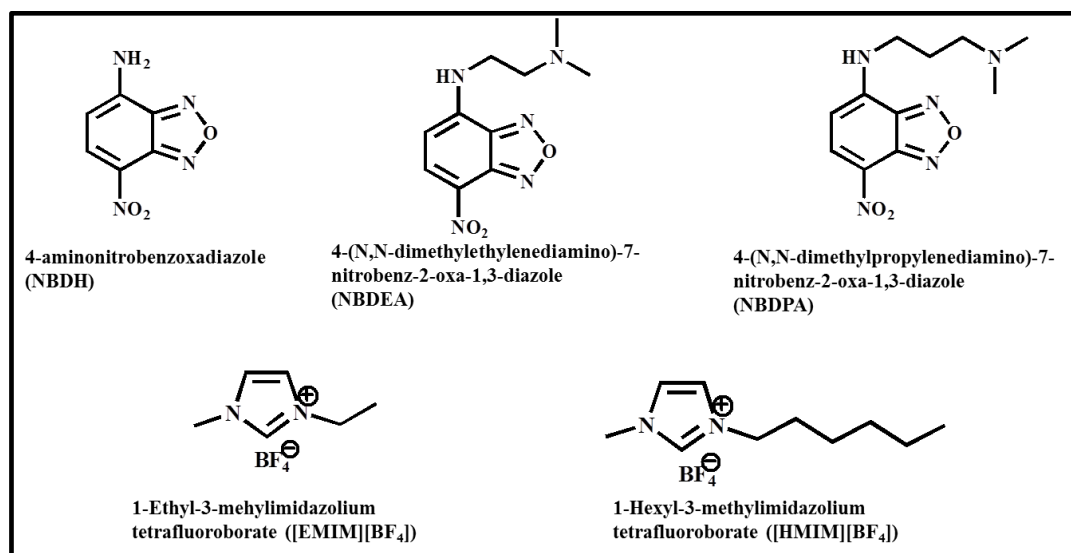
Chart 4.1: Molecular diagrams of the fluorescent probes and the RTILs.

4.2. Experiments and Methods

4.2.1. Materials

Reagents for the synthesis of different NBD compounds were purchased from Sigma-Aldrich Chemicals and were used without any further purification. The ILs (Chart 4.1) were obtained from Merck, Germany (>99% purity) and used as received. The water and halide contents of the ILs were <100 ppm.

4.2.2 Synthesis of NBDH.

NBDH was prepared from 4-chloro-7-nitrobenz-2-oxa-1,3-diazole (NBD-Cl) by following a standard procedure (Scheme 4.1)[318] The compound was characterized by ^{1}H NMR. Yield of NBDH ~ 50%.
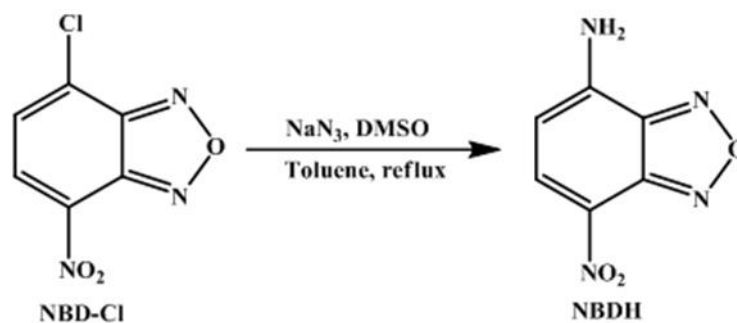
Scheme 4.1.

^{1}H NMR of NBDH (DMSO-d_6, ppm): δ 8.89 (s, 2H), 8.52 (d, 1H), 6.42 (d, 1H).

4.2.3 Synthesis of NBDEA and NBDPA.

Comp. A (NBD-Cl, 75µl, 0.75mmol) dissolved in 5ml of ethyl acetate was added drop wise to a solution of B (N,N-dimethylethylenediamine or N,N-dimethylpropylenediamine, ~50 mg, 0.5 mmol) in ethyl acetate (5ml) under ice cold condition with stirring for 4 hours to yield the desired compound. The completion of reaction was ensured by thin layer chromatography. Pure compound was obtained by column chromatography in neutral alumina (EtOAc/hexane=50%). The scheme of the reaction is given in scheme 4.2. Yield of NBDEA ~48%. Yield of NBDPA ~43%. The compounds were characterized by ^{1}H NMR.
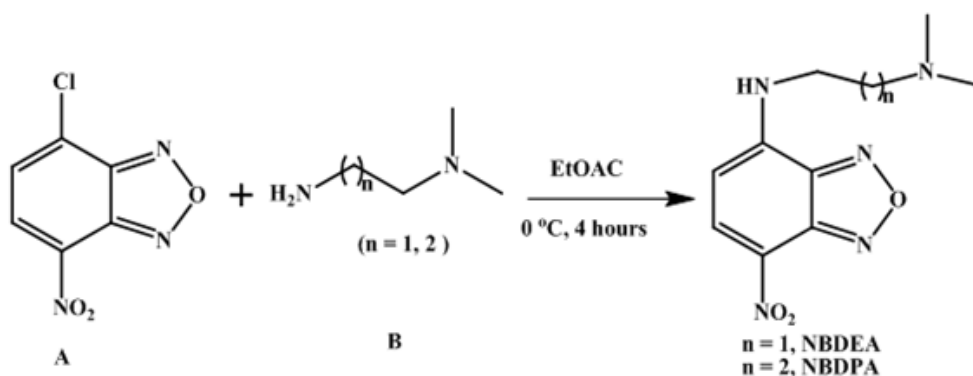
Scheme 4.2

^{1}H NMR of NBDPA (DMSO-d$_6$, ppm): δ 8.53 (d, 1H), 6.42 (d, 1H), 3.51 (t, 2H), 2.36 (t, 2H), 2.18 (S, 6H), 1.82 (m, 2H).

^{1}H NMR of NBDEA (DMSO-d$_6$, ppm): δ 8.51 (d, 1H), 6.44 (d, 1H), 3.56 (t, 2H), 2.58 (t, 2H), 2.21 (s, 6H).

4.2.4. Instrumentation

Instrumental techniques for steady state absorption, emission and time-resolved lifetime and viscosity measurements have been described in Chapter 2. The samples were excited at 405nm using picosecond laser diode (EPL) for excited state lifetime measurements. Procedures for data analysis have also been described in detail in Chapter 2.

4.3. Results and Discussion

4.3.1. Steady-state Measurements

The absorption and emission spectra of NBDH, NBDEA and NBDPA in the ILs and ACN have been measured at room temperature. The absorption and emission maxima of the compounds in the solvents are provided in Table 4.1. Representative absorption and steady-state emission spectra of NBDPA in different solvents are shown in Figure 4.1. It has been observed that the neat ILs have negligible emission (Figure 4.2). The data in Table 4.1 depicts that the peak positions corresponding to both absorption and emission for all the compounds are similar in ACN and ILs. This observation implies that the solute-solvent interactions in ILs and in ACN are very similar. Interestingly, the fluorescence quantum yield (Φ_f(%)) of the parent molecule, NBDH, in ACN is found to be 74%. However, the fluorescence quantum yields are estimated to be quite different for other two flexible compounds (NBDEA and NBDPA) in ACN as well as in RTILs (Table 4.1). For example, the ~98% lowering of fluorescence quantum yield in NBDEA and NBDPA in acetonitrile as compared to the same (74%) for NBDH in the same media indicates that the efficient *through-space* intramolecular photoinduced electron transfer (PET) (also see ΔG^0 values in

Table 4.6) from dimethyleamino (donor) group to the nitrobenzoxadiazole (acceptor) moiety is operational in flexible systems. It is well known that the fluorescence quantum yield of such flexible system drops down because of the PET communication between electron rich amine moiety and electron deficient fluorophore.[318-324] Quite interestingly, the data in Table 4.1 also reveal that reduction of fluorescence quantum yields (as compared to the parent NBDH in respective solvents) for NBDEA and NBDPA in both RTILs is not so high as is observed for them in ACN. The observation points out that the PET from dimethyl amino group to nitrobenzoxadiazole in RTILs is significantly hindered due to solvation process in these media. Wu et al.[24] while working on electron transfer in perylene compounds have observed slowing down of intermolecular electron transfer process in ionic liquids as compared to conventional solvents.

Table 4.1. Parameters of absorption and emission spectra of the synthetic compounds in different solvents

Compounds		[EMIM][BF$_4$]	[HMIM][BF$_4$]	CAN
NBDEA	λ_{abs} (nm)	457	457	461
	λ_{emi} (nm)	526	530	532
	$^a\Phi_f$ (%)	36.0	52.0	1.0
NBDPA	λ_{abs} (nm)	464	464	465
	λ_{emi} (nm)	526	530	535
	$^a\Phi_f$ (%)	10.0	50.0	0.9

^{a} quantum yield were calculated with reference to quantum yield of Coumarin 153 in acetonitrile reported in ref 325.
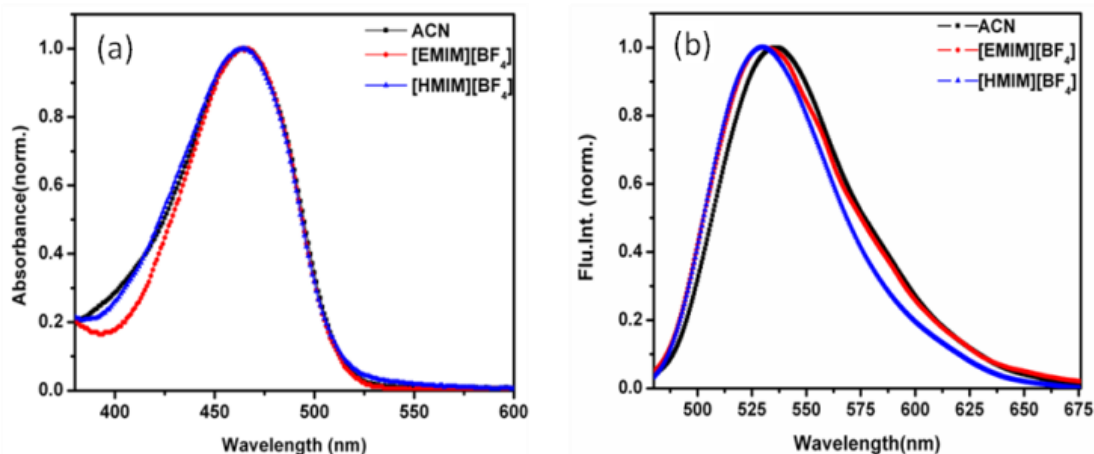
Figure. 4.1. Normalized absorption (a) and steady-state emission spectra (b) of NBDPA in ACN, [EMIM][BF$_4$] and [HMIM][BF$_4$].
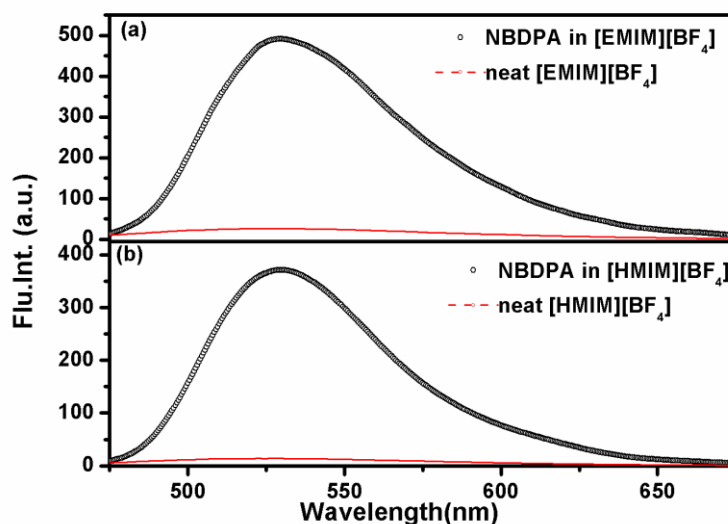
Figure. 4.2. Steady-state emission spectra of NBDPA in (a) [EMIM][BF$_4$] and (b) [HMIM][BF$_4$]. The red lines represent emission spectra of neat ionic liquids.

4.3.2. Time-resolved Measurements

The lifetimes and the rates of PET process in NBDEA and NBDPA in [EMIM][BF$_4$] and [HMIM][BF$_4$] are listed in Tables 4.2 and 4.3 respectively. Representative decay plots of NBDEA and NBDPA in [EMIM][BF$_4$] and [HMIM][BF$_4$] at different temperatures are provided in Figure 4.3. It may be mentioned that the parent molecule, NBDH, is known to exhibit single exponential decay with a lifetime of 11 ns in ACN. [320] However in ILs decay profiles of NBDH are fitted to a multiexponential decay function to calculate the average lifetime (Table 4.2 and 4.3). Samanta and coworkers[147] have also observed a similar multiexponential decay of a structurally similar molecule 4-(azetidinyl)-7-nitrobenz-2-oxa-

89

1,3-diazole (4NBD) in a series of imidazolium RTILs, and they have attributed multiexpoential decay behaviour of 4NBD to the micro-heterogeneous behaviour of ILs. It is also evident from Figure 4.3 that decay profiles for both flexible DSA systems are multi-exponential in nature. For all the DSA systems decay profile consists of shorter components (~ps-ns) and a longer component (~10 ns). Ramachandram and Samanta[321] have earlier synthesized NBDEA and observed biexponential decay behavior of the molecule in ACN with a shorter lifetime component (~0.2 ns) and a longer lifetime component (~10 ns). The authors have demonstrated that the short component represents the lifetime of quenched fluorophore due to *through-space* PET process. The longer lifetime component (~10 ns) represents the lifetime of parent fluorophore (NBDH) which is not in PET communication with the donor amino group. In the present case the bi-exponential fitting to the decay reveals the shorter and longer component as ~ 0.04 ns (~ 94%) and ~10 ns (6%) respectively for NBDEA in ACN (Table 4.4). However, the estimated average lifetime is observed to be very similar in the present and the earlier report.[321] These data essentially depicts that in majority of the molecules donor and acceptor groups are in PET communication. Similarly, for the second compound, NBDPA, a shorter ~0.07 ns (~ 98%) and a longer ~8.00 ns (~ 2%) component has been observed in ACN (Table 4.4).
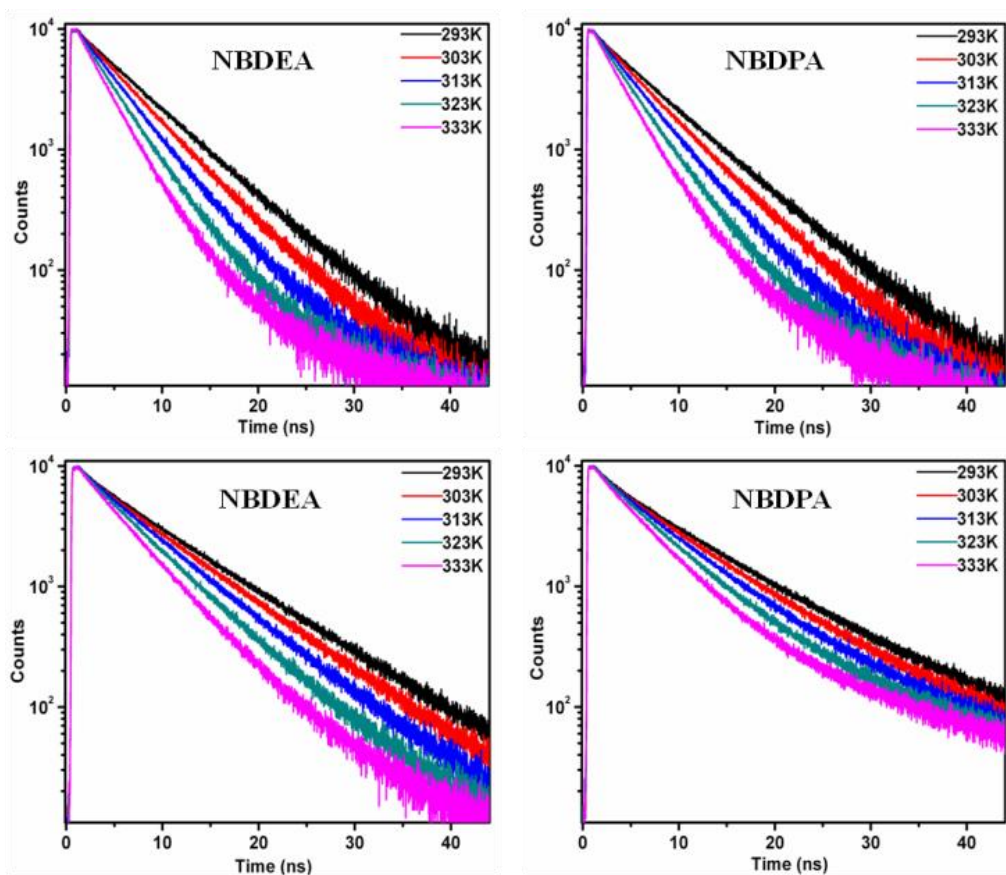
Figure. 4.3 Lifetime decay transients of NBDEA and NBDPA in [EMIM][BF$_4$] (upper panel) and [HMIM][BF$_4$] (lower panel).

Interestingly, we have observed a tri-exponential decay behaviour for both DSA (NBDEA and NBDPA) systems in ILs. Upon careful analysis of the decay components of both these systems we have found that the shortest and the longest lifetime components of these systems are very similar to the short and long decay components of the parent NBDH (Table 1 and 2). Thus the new decay component (τ_2 ~4-6 ns in Table 4.2 and 4.3) that has been observed for NBDEA and NBDPA systems essentiality represents the fluorescence decay time of the fraction of molecules that are involved in PET process. In this context it may be mentioned that flexible systems where donor acceptor group remain in PET communication are known to exhibits multiexponential decay behavior and the electron transfer rate is calculated from the reciprocal of the weighted decay component(s).[217] In the similar manner, in the present case, the electron transfer rate has been calculated from the weighted reciprocal of the lifetime component τ_2 which represents the PET process

Table 4.2. Parameters of lifetime measurements in [EMIM][BF$_4$]

[EMIM][BF$_4$]	Temp(K)	Vis. (cP)	τ_1(ns)	τ_2(ns)	τ_3(ns)	[a]$<\tau>$(ns)	[b]$k_{ET}\times10^7(s^{-1})$
NBDH	293	43.0	0.58(28%)	8.58(72%)		6.34	
	303	29.0	0.58(25%)	7.87(75%)		6.04	
	313	20.0	0.62(22%)	7.08(78%)		5.65	
	323	15.0	0.70(19%)	6.24(81%)		5.18	
	333	11.3	0.96(17%)	5.47(83%)		4.70	
NBDEA	293	43.0	0.24(20%)	5.78(77%)	11.15(3%)	4.83	13.32
	303	29.0	0.19(18%)	4.90(79%)	10.92(3%)	4.23	16.12
	313	20.0	0.12(19%)	4.10(79%)	11.20(2%)	3.48	19.27
	323	15.0	0.09(19%)	3.37(78%)	8.51(3%)	2.90	23.15
	333	11.3	0.07(22%)	2.83(76%)	9.87(2%)	2.36	26.90
NBDPA	293	43.0	0.21(30%)	5.20(45%)	7.60(25%)	4.30	8.65
	303	29.0	0.20(28%)	4.87(66%)	8.61(6%)	3.78	13.55
	313	20.0	0.17(26%)	4.09(68%)	7.81(6%)	3.30	16.63
	323	15.0	0.13(25%)	3.44(71%)	7.35(4%)	2.77	20.63
	333	11.3	0.10(27%)	2.86(70%)	7.63(3%)	2.26	24.50

[a]Experimental error ±5%. [b]PET rate constants calculated from the weighted reciprocal of the third lifetime component τ_2. Experimental error ±2%.

Table 4.3. Parameters of lifetime measurements in [HMIM][BF$_4$]

[HEMIM][BF$_4$]	Temp(K)	Vis. (cP)	τ_1(ns)	τ_2(ns)	τ_3(ns)	$^a<\tau>$(ns)	$^b k_{ET}\times10^7(s^{-1})$
NBDH	293	201.0	1.21(27%)	10.25(73%)		7.81	
	303	114.0	1.00(25%)	9.67(75%)		7.50	
	313	69.0	0.73(21%)	8.68(79%)		7.01	
	323	44.1	0.69(17%)	7.80(82%)		6.52	
	333	30.8	0.77(15%)	6.90(85%)		5.98	
NBDEA	293	201.0	0.72(13%)	3.08(14%)	8.60(73%)	6.80	4.54
	303	114.0	0.90(16%)	6.14(44%)	8.78(40%)	6.35	7.16
	313	69.0	0.63(16%)	6.04(75%)	9.98(09%)	5.54	12.41
	323	44.1	0.52(12%)	5.32(83%)	10.61(5%)	5.00	15.60
	333	30.8	0.40(11%)	4.56(85%)	11.38(4%)	4.37	18.64
NBDPA	293	201.0	0.91(18%)	4.69(25%)	9.93(57%)	7.00	5.30
	303	114.0	0.84(19%)	5.66(40%)	9.81(41%)	6.45	7.06
	313	69.0	0.65(18%)	5.79(63%)	10.88(19%)	5.83	10.88
	323	44.1	0.56(15%)	5.17(72%)	10.75(13%)	5.20	13.92
	333	30.8	0.45(15%)	4.58(78%)	12.83(07%)	4.54	17.03

^{a}Experimental error $\pm5\%$. ^{b}PET rate constants calculated from the weighted reciprocal of the third lifetime component τ_2. Experimental error $\pm2\%$.

Table 4.4. Parameters of lifetime measurements in ACN

ACN	Temp(K)	Vis. (cP)	τ_1(ns)	τ_2(ns)	[a]$<\tau>$(ns)	[b]$k_{ET}\times10^9(s^{-1})$
NBDH	293	0.362	11.07(100%)			
	303	0.329	10.53(100%)			
	313	0.30	9.77(100%)			
	323	0.278	8.90(100%)			
	333	0.258	7.90(100%)			
NBDEA	293	0.362	0.04(94%)	10.14(6%)	0.650	23.50
	303	0.329	0.04(95%)	9.89(5%)	0.533	23.75
	313	0.30	0.03(95%)	9.28(5%)	0.490	31.60
	323	0.278	0.02(95%)	8.55(5%)	0.450	47.50
	333	0.258	0.02(96%)	7.67(4%)	0.330	48.00
NBDPA	293	0.362	0.07(98%)	7.41(2%)	0.217	14.00
	303	0.329	0.06(98%)	7.55(2%)	0.210	16.30
	313	0.30	0.05(98%)	6.61(2%)	0.180	19.60
	323	0.278	0.04(98%)	5.93(2%)	0.160	24.50
	333	0.258	0.03(98%)	5.79(2%)	0.150	32.70

[a] Experimental error ±5%. [b]PET rate constants calculated from the weighted reciprocal of the second lifetime component τ_2. Experimental error ±2%.

As can be seen in ACN, ~ 95% molecules (NBDEA and NBDPA) are in PET communication (Table 4.4). However, in ILs, the observation seems to be quite different. For example, for NBDPA in [EMIM][BF$_4$], the fraction of molecules undergoing PET process is estimated to be 45% at 293K. However, with increase in temperature the molecules that remain in PET communication are found to be 70% (Table 4.2). Similarly, in the highly viscous [HMIM][BF$_4$], the fraction of molecules undergoing PET process is estimated to be ~80% for both NBDEA and NBDPA 333K (Table 4.3). These observations indicate that at lower temperature (highly viscous condition) a substantial fraction of the molecules do not undergo PET process, but with increase in temperature, fraction of these nonreactive

molecules becomes lesser. From Tables 4.2 and 4.3 one can also see that gradual increase in the temperature results in an increase in the PET rate for both the DSA systems. Such an enhancement in PET with increase in temperature can be more clearly understood by taking into consideration of the change in non-radiative decay rate constants with a change in the temperature for both systems. The non-radiative decay rate constant (k_{nr}) is calculated from the fluorescence quantum yield (Φ_f) and average lifetime ($<\tau>$) by using following relationship.

$$k_{nr} = (1 - \Phi_f)/< \tau > \qquad\qquad\qquad (4.1)$$

For NBDEA, k_{nr} increases from 1.52×10^9 s^{-1} at 293 K to 3.0×10^9 s^{-1} and for NBDPA it increases from 4.5×10^9 s^{-1} at 293 K to 6.6×10^9 s^{-1} with change in temperature from 293 K to 333 K in ACN. Similarly in [EMIM][BF$_4$], k_{nr} increases from 13.25×10^7 s^{-1} at 293 K to 27.1×10^7 s^{-1} at 333 K for NBDEA and 20.9×10^7 s^{-1} at 293 K to 39.8×10^7 s^{-1} at 333K for NBDPA. The same trend has also been observed in [HMIM][BF$_4$] where k_{nr} increases from $\sim7.1\times10^7$ s^{-1} at 293 K to $\sim11.0\times10^7$ s^{-1} at 333 K for both NBDEA and NBDPA.

It has been observed that for both NBDEA and NBDPA the electron transfer rates are relatively high in ACN (Table 4.4; order of 10^9) as compared to the rates that are estimated in present ILs. In ILs, ET rates have been reduced significantly (Tables 4.2 and 4.3). As the electron transfer in the present case is an intramolecular process, diffusion of reactants which can be affected by viscosity of the ILs during PET process in the present DSA systems is unlikely. It may be mentioned in that context that solvent reorganization in ACN completes within few ps[290] and solvation in ILs is generally much slower (ps $\sim$ ns timescale) at lower temperature (higher viscous condition).[158] Thus the significant reduction of rates of electron transfer for the present flexible DSA systems in ILs clearly suggests that the dynamics of solvation of the media playing an important role in governing rate of electron transfer

processes. The influence of solvation on rate of electron transfer in ILs has also been observed for some other systems in different ILs. [212,217, 314-316]

We have analysed the dependence of PET rate constant on solvent viscosity by plotting log-log graphs of k_{ET} vs. viscosity (Figure 4.4). The slopes of linear fits for NBDEA in three solvents are -2.56 ± 0.38 (ACN), -0.53 ± 0.01 ([EMIM][BF$_4$]) and -0.77 ± 0.06 ([HMIM][BF$_4$]). Similarly slopes of linear fits of NBDPA are -2.44 ± 0.28 (ACN), -0.75 ± 0.06 ([EMIM][BF$_4$]) and -0.64 ± 0.03 ([HMIM][BF$_4$]). Figure 4.4 demonstrates that solvation plays a role in influencing rate of PET as dynamics of solvation is directly proportional to medium viscosity. We have calculated average solvation time in these ILs through a semiempirical relationship developed by Maroncelli and coworkers.[165] It has been found that average solvation time is 373 ps and 3.68 ns in [EMIM][BF$_4$] and [HMIM][BF$_4$] respectively at 293K. It seems that very fast solvation time in [EMIM][BF$_4$] might have a lesser influence on PET rate. However, it should also be mentioned that solvation dynamics in ILs is broadly distributed.[158,165, 326, 327] Hence, some slow component of solvation can influence PET process substantially. At higher temperatures the slow component of solvation becomes much faster thus its effect on PET process becomes negligible. This is clearly observable in case of lower viscous [EMIM][BF$_4$] where at higher temperature PET rates of both the probes become very close (Table 4.2). It indicates that at lower viscous condition the rate of solvation cannot influence electron transfer rate appreciably owing to the faster solvation process. However, since the viscosity of [HMIM][BF$_4$] is appreciably higher than that of [EMIM][BF$_4$], it is expected that at lower temperature, overlap between solvation rate and PET rate becomes more probable in case of [HMIM][BF$_4$]. Such an overlap has similar effect on the PET rates of NBDEA and NBDPA which is evident from the very close values of PET rates of both the probes (Table 4.3). This is in contrast to the observation in [EMIM][BF$_4$] where PET rates for the DSA systems are found to be close only at higher temperature (low viscous condition). In

view of this observation, we have tried to investigate the role of the conformation of solute, if any, during the electron transfer process. Here we want to mention that at higher temperature, rates of PET for both DSA systems remain very close to each other in a particular medium. For example at 333 K k_{ET} for NBDEA and NBDPA in [HMIM][BF$_4$] is found to be 18.60×10^7 s^{-1} and 17.03×10^7 s^{-1} respectively.
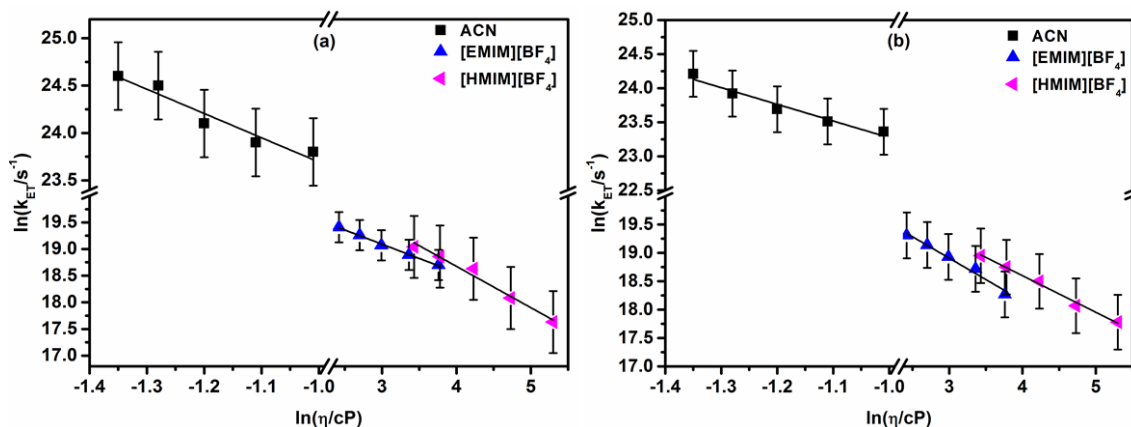
Figure. 4.4. Variation of k_{ET} with viscosity for NBDEA (a) and NBDPA (b) in ACN, [EMIM][BF$_4$] and [HMIM][BF$_4$].
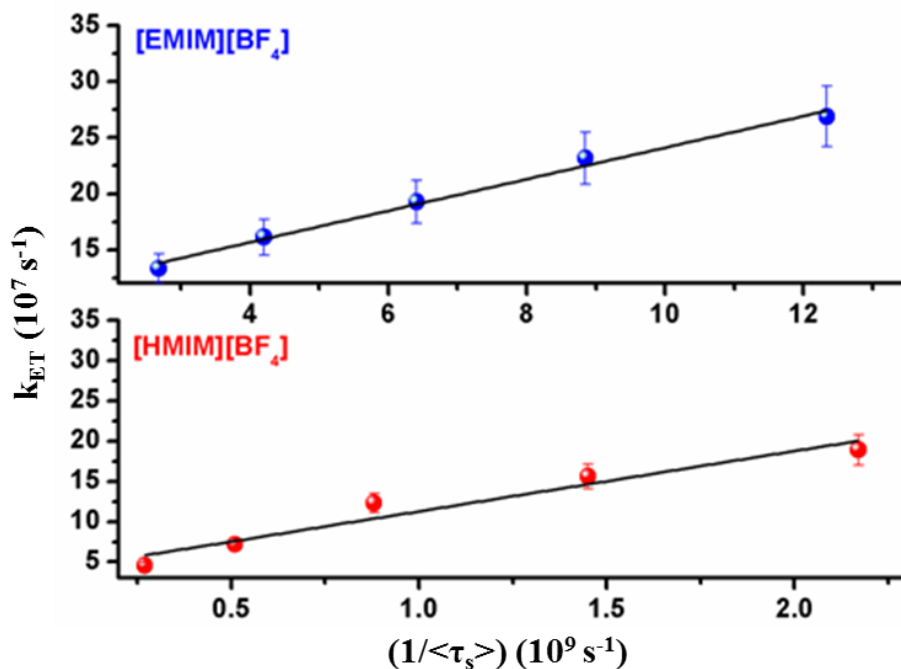
Figure 4.5. Variation of k_{ET} with average solvation time $<\tau_s>$ for NBDEA in [EMIM][BF$_4$] and [HMIM][BF$_4$]. Solid lines represent linear fit to the data points.

In this context it may be mentioned that Schryver and co-workers [328, 329] while working on the electron transfer kinetics by using flexible pyrene derivatives in alkanes have demonstrated that the formation of an exciplex between a dimethyl amino group and pyrene is much easier when they are linked by $-CH_2-CH_2-CH_2-$, where the lone pair of nitrogen can overlap effectively with the aromatic core. The process is less efficient when dimethyl amino group and pyrene moiety are linked through $-CH_2-CH_2-$ bridge. The exciplex formation occurs quickly in the conformation where $-CH_2-CH_2-CH_2-$ linker is present. Similar argument was given by Wu et al.[216] to explain their PET results observed in two pyrene-based DSA compounds which differ by the linker chain between the dimethyl and pyrene moiety. However we have not observed a faster PET rate in case of NBDPA in any of the medium.

As mentioned earlier, solvation has a profound role in controlling PET process. [212, 216, 314-316] A representative plot of k_{ET} as a function of inverse of average solvation time ($1/<\tau_s>$) for NBDEA in both ILs is shown in Figure 4.5. The data corresponding to PET rate constants and $<\tau_s>$ in both ILs are presented in Table 4.5. From Figure 4.5, one can observe a linear dependence of PET rate with solvation time in both the ILs with change in temperature. It is important to mention here that solvation in ILs comprises components ranging from subpicosecond to nanosecond time range. [158, 165, 326, 327] Generally, it is the slowest component of solvation in ps~ns timescale that influence the rate of PET in ILs.[313] We would also like to take a note that in a system where the timescale of solvation and timescale of PET are coupled, determining the actual rate of PET becomes difficult. In that scenario multi-dimensional spectroscopy is expected to provide more accurate results.[330]

Table 4.5. PET rate constants and average solvation times in the RTILs for the DSA systems

Temp(K)	[EMIM][BF$_4$]			[HMIM][BF$_4$]		
	[a]k_{ET} (×10^7 s^{-1})		<τ_s>(ps)	[a]k_{ET} (×10^7 s^{-1})		<τ_s>(ps)
	NBDEA	NBDPA		NBDEA	NBDPA	
293	13.32	8.65	373	4.54	5.30	3680
303	16.12	13.55	238	7.16	7.06	1980
313	19.27	16.63	156	12.41	10.88	1130
323	23.15	20.63	113	15.60	13.92	686
333	26.90	24.50	81	18.64	17.03	460

[a] Experimental error ±2%.

We have also estimated the driving force for the PET process in the DSA systems from the expression

$$\Delta G^0 = N_A \{ e[E^0(D^{+\bullet}/D) - E^0(A/A^{-\bullet})] + w_D{}^{+\bullet}{}_A{}^{-\bullet} - w_{DA} \} - \Delta E_{0,0} \tag{4.2}$$

where N_A is Avogadro's number, $E^0(D^{+\bullet}/D) - E^0(A/A^{-\bullet})$ is the difference between the donor oxidation and acceptor reduction potentials, and the $\Delta E_{0,0}$ term represents the electronic transition energy from the ground state to the excited state and is estimated from the average energy of the absorption and fluorescence maxima. The terms $w_{xy} = e^2 z_x z_y/(4\pi\varepsilon_0\varepsilon_s R_{DA})$ is electrostatic work which account for the Coulombic interactions between the donor and the acceptor in their original and charge-separated states, where z_x and z_y are the respective charges, ε_0 is the vacuum permittivity, and R_{DA} is the donor-acceptor distance. Here, $w_{DA} = 0$, since the donor and acceptor are originally uncharged. The dielectric constants ε_s for [EMIM][BF$_4$] and [HMIM][BF$_4$] are 14.8 and 11.3 respectively[331] and for CH$_3$CN is 36[332] at 298K. R_{DA} for NBDEA (7.0 Å) and NBDPA (7.42 Å) is obtained from ground state geometry optimization of the probes using DFT-B3LYP/6-311+G (d,p) level of optimization in gas phase. Literature values of $E^0(D^{+\bullet}/D)$ (0.49V) and $E^0(A/A^{-\bullet})$ (-0.91V)[319, 320] were used to calculate ΔG^0.
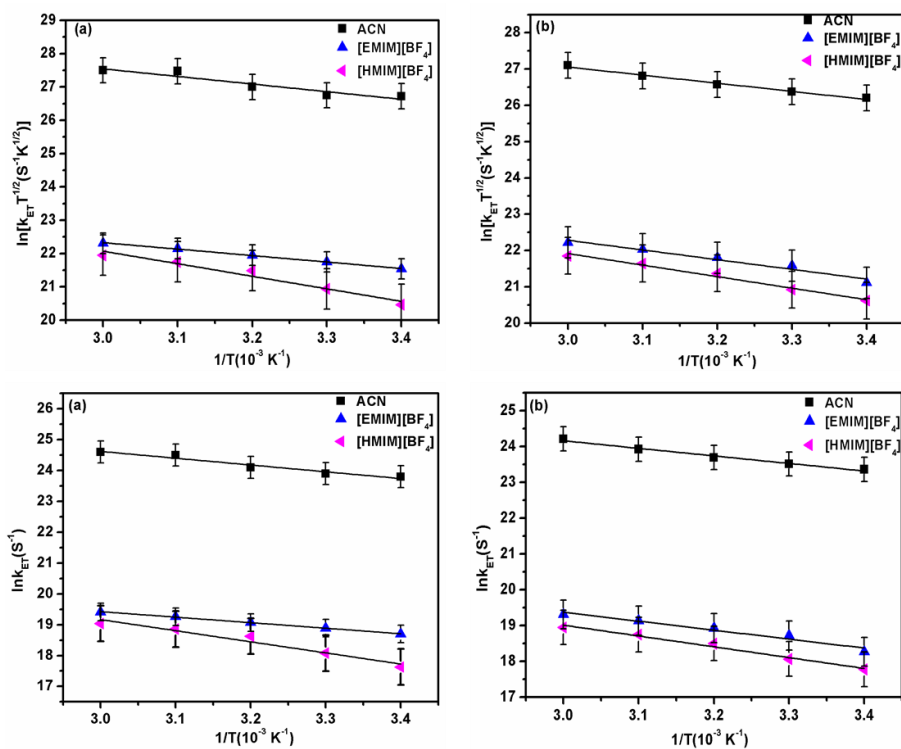
Figure 4.6. Plot of $\ln(k_{ET}T^{1/2})$ vs. (1/T) for NBDEA (a) and NBDPA (b) in three different solvents (upper panel) and plot of $\ln(k_{ET})$ vs. (1/T) for NBDEA (a) and NBDPA (b) in three different solvents (lower panel).

We have calculated activation free energy (ΔG^*) for the PET process for each probe in each medium from adiabatic or solvent controlled Marcus equation[333] given as

$$k_{ET} = \frac{1}{\tau_S}\sqrt{\frac{\lambda}{16\pi k_B T}}\,exp\left(\frac{-\Delta G^*}{k_B T}\right) \qquad (4.3)$$

from the plot of $\ln(k_{ET}T^{1/2})$ vs. (1/T) for various probes (Figure 4.6, upper apnel)). λ is the reorganization energy and τ_s is the solvation relaxation time of the photoexcited probe. ΔG^* an ΔG^0 are related through the expression.[54]

$$\Delta G^* = \frac{(\lambda + \Delta G^0)^2}{4\lambda} \qquad (4.4)$$

The reorganization energy is the sum of two terms: $\lambda = \lambda_i + \lambda_o$, where λ_i is the reorganization energy of the inner sphere, the DSA molecule, and λ_o is the outer sphere or the solvent reorganization energy.

Activation energy for the PET process ($E_{a,ET}$) is evaluated from Arrhenius analysis of the variation of k_{ET} with T (Figure 4.6, lower panel). Arrhenius and Marcus equation parameters for the DSA molecules in different solvents are tabulated in Table 4.6. One can see from Table 4.6 that both ΔG^* and $E_{a,ET}$ are about 2 to 5 times higher in RTILs than that in molecular solvent ACN. Lee and coworkers[27] have also observed higher values of ΔG^* and $E_{a,ET}$ in ILs than conventional solvents CH_3OH and ACN. We have observed that in all the solvents, $-\Delta G^0 > \lambda$ which is an indicative of the PET process occurring in the inverted region. We have also calculated ΔH^* (enthalpy of activation) and ΔS^* (entropy of activation) (Table 4.6) by fitting k_{ET} to the following equation.[52-54]

$$k_{ET} = \frac{k_B T}{h} \exp\left(\frac{-\Delta H^* + T\Delta S^*}{RT}\right) \tag{4.5}$$

Table 4.6. Arrhenius and Marcus equation parameters for different DSA systems in different medium

Medium	DSA systems	ΔG^0 (eV)	$^a\Delta G^*$ (eV)	$^aE_{a,ET}$ (eV)	$\Delta E_{0,0}$ (eV)	$w_D^{+\bullet}{}_A^{-\bullet}$ (eV)	λ (eV)	ΔH^* (eV)	ΔS^* (eV)
ACN	NBDEA	-1.17	0.18	0.07	2.51	-0.056	0.54	0.36	0.0009
	NBDPA	-1.14	0.18	0.11	2.49	-0.053	0.53	0.19	0.0008
[EMIM][BF$_4$]	NBDEA	-1.28	0.15	0.45	2.54	-0.138	0.66	0.17	0.0004
	NBDPA	-1.24	0.22	0.29	2.51	-0.130	0.45	0.23	0.0005
[HMIM][BF$_4$]	NBDEA	-1.30	0.31	0.26	2.52	-0.181	0.51	0.32	0.0008
	NBDPA	-1.27	0.26	0.28	2.50	-0.172	0.52	0.27	0.0007

^{a} Experimental error $\pm 2\%$

The ΔG^* calculated from ΔH^* and ΔS^* differs from the ΔG^* value calculated from equation 4.3 at any temperature. For example at 293 K, ΔG^* is calculated to be 0.05 eV for NBDEA in [EMIM][BF$_4$] where as ΔG^* from equation 4.3 is found out to be 0.15 eV. This difference indicates that the excited state PET in our DSA systems is not purely a thermally

controlled process; rather it indicates that dynamics of solvation of the medium plays important role during the process.

4.4. Conclusion

In this chapter, study on intramolecular PET on two flexible DSA systems in two ILs and ACN has been discussed. The results have indicated that PET rates are hindered in the ILs compared to that in ACN. Present study has clearly demonstrated the consequences of rate of solvation in respective media in influencing the rate of electron transfer process. It may be mentioned here that solvation dynamics in ILs is quite complex and broadly distributed in time.[158] In this context investigation on PET process by employing multidimensional spectroscopic techniques would be helpful to provide deeper understanding of the role of solvation on electron transfer processes in ILs.

Chapter 5

Solute-Solvent and Solvent-Solvent Interaction in A Borate-Based Room Temperature Ionic Liquid and Its Binary Mixtures ith Various Cosolvents Through Fluorescence and NMR Study

The high viscosity, high manufacturing cost and difficulties in purification impose limitations to the effective use of ILs. In this context binary mixtures of ILs with various cosolvents can be envisioned to be an alternative solvent system which may help in widening the applicability of ILs.[276] This chapter describes our effort in understanding IL-cosolvent systems by investigating the solute-solvent and solvent-solvent intermolecular interactions through fluorescence and NMR spectroscopy.

5.1. Introduction

The evolution of ILs from laboratory chemical to the materials of industrial importance has been possible by virtue of their interesting physicochemical properties such as low vapour pressure, wide liquidus range, high thermal conductivity, etc.[4-8] However, sometimes too high viscosity, high manufacturing cost and difficulties involved in their purification limits the use of neat ionic liquids. In this context, binary mixtures of ionic liquids with various cosolvents can thought of to be a better alternative as these mixtures are easy to prepare, easy to handle and are cost effective in their use.[262] Therefore, the use of binary mixtures of ILs with various cosolvents is expected to widen the applicability of ILs.[276] It is known that the intermolecular interactions among solute and solvent molecules have profound role in determining the physicochemical properties of solvent and its solution.[298] It may be noted here that studies carried out on IL-cosolvent mixtures have depicted that the physicochemical properties undergo perceptible changes in presence of cosolvents.[262] Moreover, ILs are micro-heterogeneous in nature and it is reasonable to expect that

cosolvents can induce significant variation in their physicochemical properties.[147, 336, 337] In fact, it has been reported that the organized structure of neat ILs is perturbed by the addition of various additives into it.[338-340] Thus, it is extremely important to understand the structural organisation and various intermolecular interactions prevailing in IL-molecular solvent mixtures so that they can be used in newer avenues.

Since solute reactivity is intricately related to solvation dynamics, studies on dynamics of solvation by monitoring the time-dependent fluorescence Stokes shift (TDFSS) of a dipolar solute in the given medium have been carried out by several researchers to understand the dynamical features of IL-cosolvent mixtures.[262, 298, 336] Time resolved fluorescence anisotropy measurement is also an extremely important tool to gather useful information on both solute-solvent and solvent-solvent interactions.[146, 183, 185, 204,] These studies have demonstrated that addition of cosolvents in RTILs affects both the solvent relaxation as well as solute rotation. Apart from the time-resolved studies, fluorescent correlation spectroscopy has also emerged as an excellent technique in probing the microenviornment of ionic liquids.[150, 342]

In recent times, vibrational,[343, 344] and NMR,[345-348] spectroscopic techniques have been extensively used to understand the behaviour of IL-cosolvent binary mixtures. Neutron/X-ray diffraction studies and molecular dynamics simulation has also been performed to address the heterogeinity of IL/molecular liquid mixtures.[349, 350] These studies essentially point out that the microheterogenity and intermolecular interactions in the ILs are significantly perturbed by addition of cosolvents.

Among the IL-cosolvent binary mixtures, IL-water system has been explored extensively so far.[342,343, 348, 350-352] However, the studies on the binary mixtures of ionic liquids with other molecular solvents are rather limited.[11, 183, 339, 352] We would also like to mention that most of the reports discussed above are on the conventional imidazolium-based

ionic liquids with varying anions. However, borate imidazolium-based ionic liquids have not been explored for such purposes. Very recently it has been demonstrated that the borate-based ionic liquids can be used as electrolyte in lithium ion battery.[353, 354] Therefore, it would be interesting to have a molecular level understanding on the behaviour of the said ionic liquid, and also its mixtures with other common organic solvents.

In this chapter, an attempt has been made to understand the behaviour of a borate-based IL, [BIMIMDBA][TF$_2$N] (Chart 5.1) and its binary mixture with various non-aqueous solvents by investigating the solute-solvent and solvent-solvent intermolecular interactions through 1D and 2D NMR spectroscopy, FCS and time-resolved fluorescent anisotropy measurements. The non-aqueous solvents dimethylsulfoxide (DMSO), methanol (MeOH), dimethylformamide (DMF) and toluene are chosen in such a way that there is a systematic variation in their dipole moment values and the strength of their H-bond formation abilities. We have further investigated solvent and solute dynamics in neat IL and IL-DMF binary mixtures through time-resolved fluorescence studies with coumarin 153 (C153) as a fluorescent probe. Additionally, DMF has been purposefully chosen as it has been used to dissolve a wide range of organic and inorganic compounds which in turn has also made this solvent to be used in variety of industrial processes.[355, 356]

The results of the present study are expected to provide valuable insight which may be helpful in designing a new borate IL-cosolvent system for newer applications.
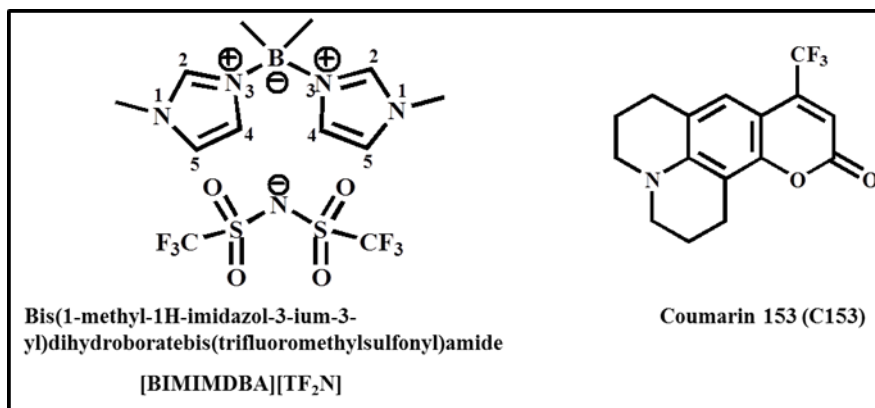
Chart 5.1. Molecular diagrams of the IL and C153.

5.2. Experiments and Methods

5.2.1 Materials

C153 (laser grade, Exciton) was used as received. The ionic liquid [BIMIMDBA][TF$_2$N] was obtained from Frontier Scientific Chemicals, USA (95% purity). The IL is further purified by activated charcoal treatment to remove any coloured impurity and characterised by ^{1}H NMR (Figure 5.1). After purification IL was found to be ~98% pure. The water content of the IL was found to be <100ppm respectively. Anhydrous methanol, DMSO, DMF and toluene were obtained from Sigma-Aldrich. All anhydrous solvents were >98% pure. The IL was taken in a long-necked quartz cuvette and requisite amount of fluorophore was added to prepare the solution. Proper precaution was taken to avoid moisture absorption by the media while transferring the sample to into the cuvette and NMR tubes. Cuvettes and NMR tubes were properly sealed with parafilm. D$_2$O is taken in a separate capillary and inserted into the NMR tube to serve as lock for NMR experiments. All the IL-cosolvent binary mixtures have been prepared in 1:1 mole fraction.
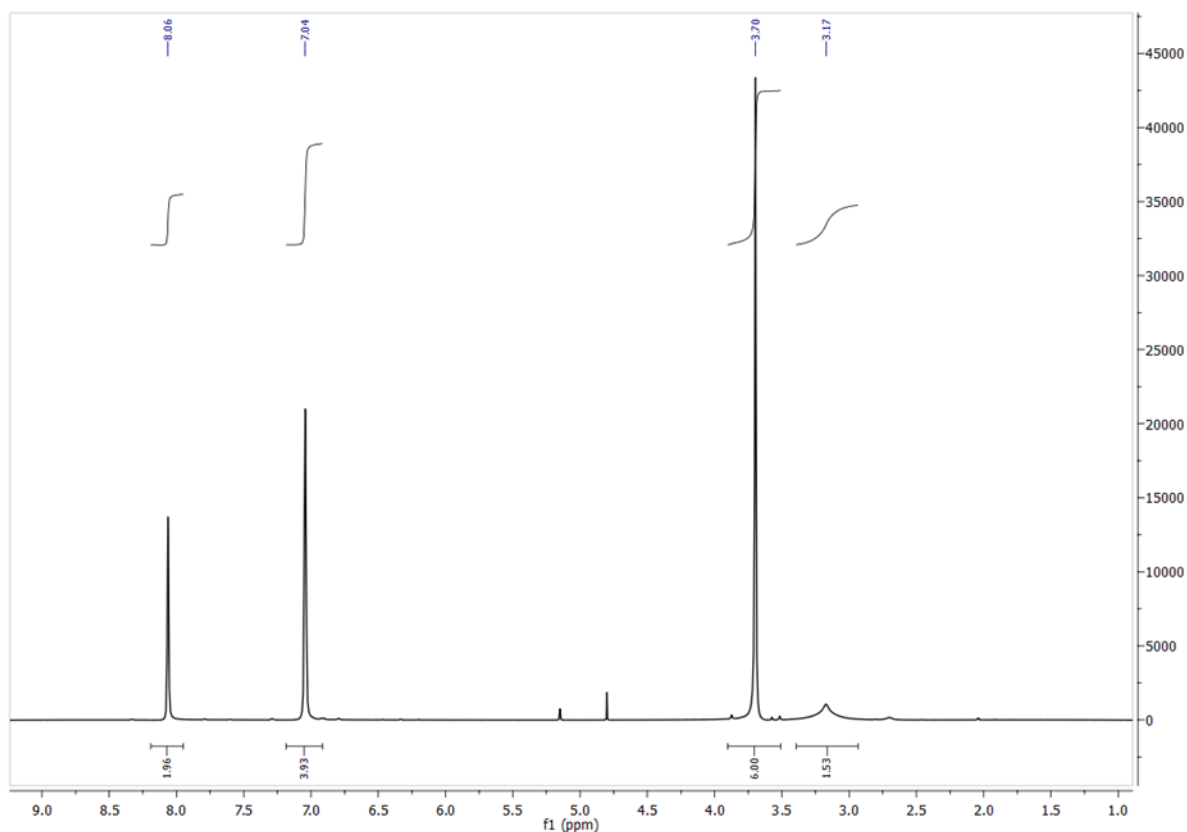
Figure 5.1. ^{1}H NMR spectrum of neat [BIMIMDBA][TF$_2$N].

5.2.2. Instrumentation.

Instrumental techniques for steady-state and time-resolved fluorescence as well as NMR experiments were have been described in Chapter 2. Details of procedures for data analysis have also been discussed in Chapter 2.

FCS measurements were carried out using a time-resolved confocal fluorescence microscope, Micro-Time 200 (PicoQuant) equipped with an inverted microscope (Olympus IX 71) containing a water immersion objective (Olympus UPlans Apo, 60 ×/1.2 NA). An excitation light of 405 nm was applied to excite the samples through a pulsed diode laser (Pico Quant) with a stable repetition rate of 40 MHz and excitation power of 1μW. The sample fluorescence collected by the water immersion objective was passed through a filter and pinhole before entering the two single-photon avalanche photodiodes (SPADs) detectors.

The correlation curves were generated by cross-correlating the signal from the two SPAD detectors.

5.3. Results and Discussion

5.3.1. ^{1}H NMR

Among various techniques employed to study the intermolecular interactions, NMR spectroscopy has been found to be very useful as it does not require any external probe.[348] Moreover, it should be noted that the chemical shifts of different nuclei of the IL in absence and presence of cosolvent can be helpful in understanding the intermolecular interactions in the binary mixtures.[262] The chemical shifts of relevant protons of the cation in neat IL and in the IL-cosolvent binary mixtures employed in the present study are shown in Figure 5.2 and the corresponding chemical shift values are collected in Table 5.1. It can be seen from Figure 5.2 and Table 5.1 that all the imidazolium ring protons and N-CH$_3$ protons of ionic liquid show a high frequency shift in presence of all the molecular solvents used in the present study except toluene where a low frequency shift is observed. This indicates that there is a change in the structural organisation of the IL in presence of molecular solvents. Here, we would like to mention that the observed chemical shift of the proton signals in the present study cannot be accounted for merely dilution effect as the shift is observed to be different in IL-cosolvent mixtures even after addition of same mole fraction of cosolvent to neat IL. Upon careful observation one can also find out that the proton chemical shifts (δ/ppm) are in the order of IL-toluene < neat IL < IL-MeOH< IL-DMSO < IL-DMF (Figure 5.2 and Table 5.1). Interestingly this trend of chemical shifts in IL-cosolvents binary mixtures can be correlated with the dipole moment values of the molecular solvents which increases in the order of toluene (0.36 D) < MeOH (1.69 D) < DMF (3.86 D) < DMSO (3.96 D). This correlation indicates that the ion-dipole interaction between the cation of the IL and the dipole of the molecular solvent plays an important role in influencing the chemical environment of the

protons in the binary mixtures. However, a reversal in the order of chemical shift of the protons of the IL and dipole moment values of DMF and DMSO in IL-DMSO and IL-DMF mixtures has also been observed. In this context it may be noted here that along with ion-dipole interaction, hydrogen bonding interaction between the IL and added solvent is also known to be an important factor for disrupting the structural organisation of ILs.[262, 345, 346, 348] The interionic hydrogen bonding network between the constituents of the IL can be disrupted, and that might facilitate the IL-cosolvent intermolecular H-bonding interaction. On the contrary to ion-dipole interaction, hydrogen-bonding interaction between cation and added cosolvent usually contributes in deshielding of the protons of the cation.[262] Hence, a combined but opposing effect of ion-dipole and hydrogen bonding interaction between the cation and added molecular solvent can be considered to be the responsible factor for the observed chemical shift values of IL in IL-DMF and IL-DMSO mixtures.
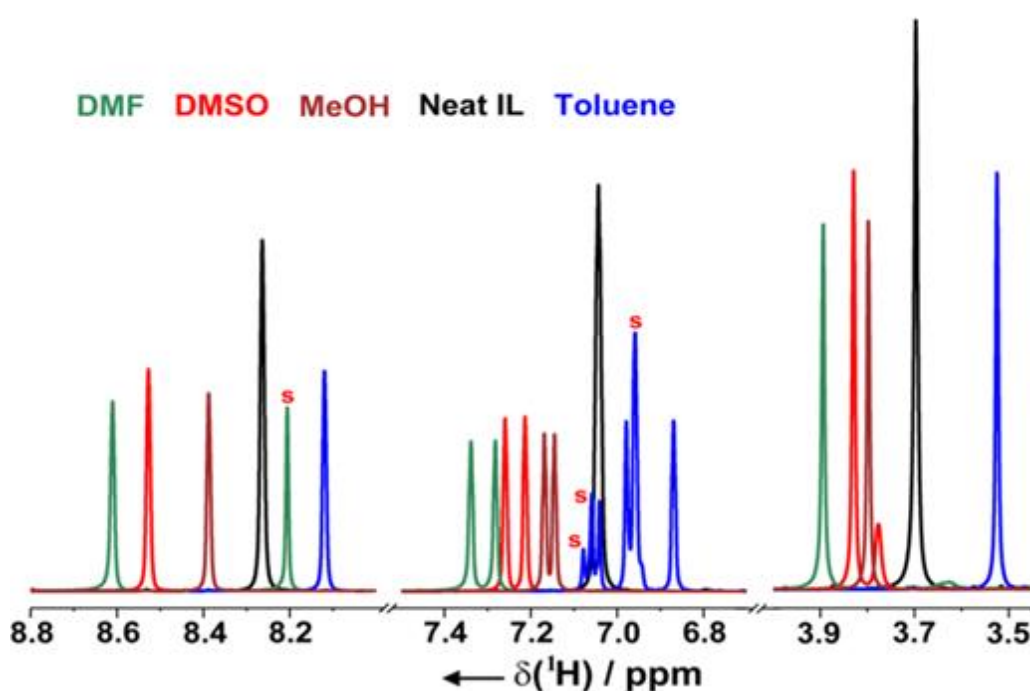
Figure 5.2. ^{1}H Chemical shifts of C2 (8.7-8.1 ppm), C4 and C5 (7.4-6.8 ppm) and N-CH$_3$ (3.9-3.5 ppm) protons of the cation. The solvent peaks are denoted by 'S' marks.

Table 5.1.[1]H and ^{19}F chemical shifts (δ)/ppm of the cation and anion of the IL in neat and IL-molecular solvent binary mixtures

System	[1]H Chemical shift (δ)/ppm			[19]F chemical shift (δ)/ppm
	C2H	C4H, C5H	N-CH$_3$	
Neat IL	8.06	7.04	3.70	-81.18
IL + DMF	8.41	7.34, 7.28	3.89	-80.93
IL + DMSO	8.33	7.26, 7.21	3.83	-80.80
IL + MeOH	8.19	7.17, 7.15	3.80	-81.14
IL + Toluene	7.92	6.98, 6.87	3.53	-80.78

The low frequency shift of C2, C4 and C5 proton signals of the IL in IL-toluene mixture is another interesting observation in the present study. In a recent report Deetlefs *et. al.*[357] through X-ray diffraction and NMR spectroscopy study have demonstrated that addition of benzene to the IL, 1,3-dimethylimidazolium hexafluorophosphate leads to an expansion of the cation-cation distance. They have shown that the anion interacts with ring hydrogen and the cation interacts with the ring electrons of benzene. Similar interaction of the cation with other aromatic systems was also reported in some other recent literature reports.[358, 359] Such interactions may lead to low frequency shift of proton signals of the imidazolium cation. In light of these observations, the low frequency shift of the proton signals of the cation in IL-toluene mixture as compared to those in neat IL in the present case can be rationalised through cation-π (electrons) interaction. The cation-cosolvent interactions in IL-cosolvent mixtures are also supported by the corresponding ROESY (Rotating frame Overhauser Effect Spectroscopy) spectra which are discussed below.

5.3.2 ROESY spectrum

The ROESY spectra of the IL-molecular solvent binary mixtures have been investigated to support our observation of cation-solvent interaction in these systems. The corresponding ROESY spectra for different IL-cosolvent systems are shown in in Figure 5.3. One can clearly see the cross peaks between all the protons of the cation and solvent peaks (marked as "s") which indicate strong interaction between the cation and the added solvent.
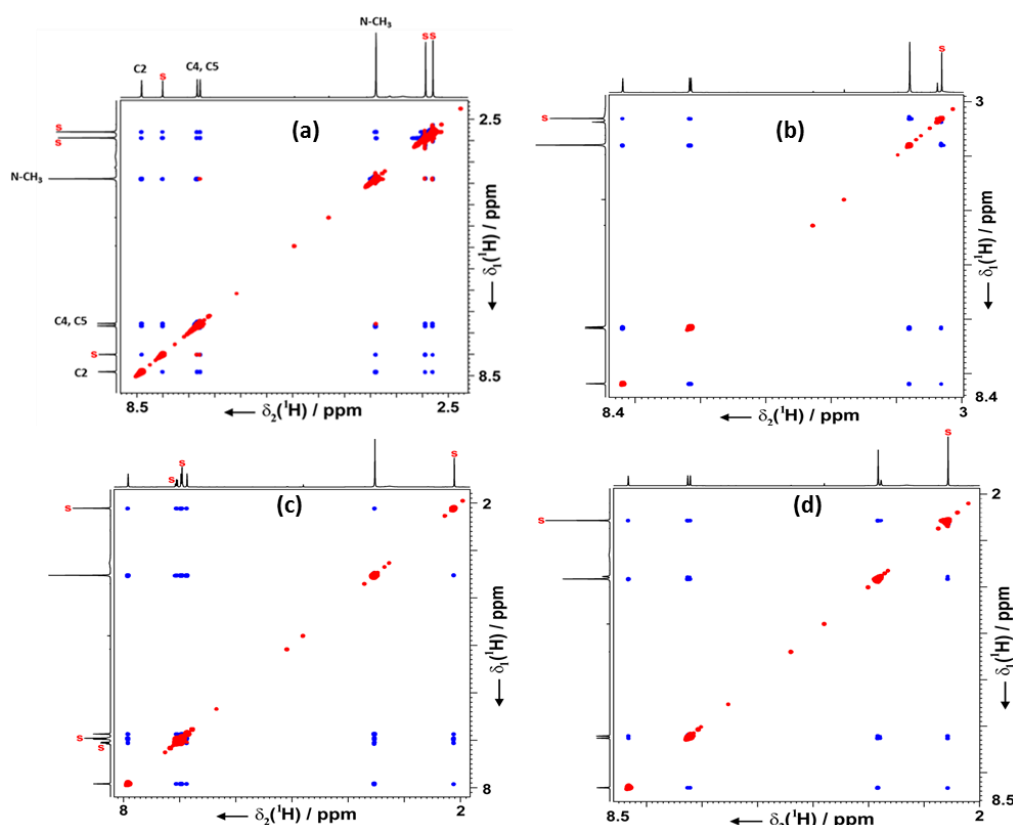
Figure 5.3. ROESY spectrum of IL-cosolvent binary mixture ((a) IL-DMF, (b) IL_MeOH, (c) IL-tolune, (d) IL-DMSO) showing cation-solvent cross peaks. Solvent peaks are marked as 'S'.

5.3.3 ^{19}F NMR

Intermolecular interaction between the anion of the IL and the added co-solvents in the IL-cosolvent binary mixtures, has also been investigated through ^{19}F 1D NMR studies. The chemical shifts of the fluorine atoms of the anion of the IL in neat as well as in the binary mixtures are represented in Table 5.1. The stacked plot of the 1D spectra is shown in Figure 5.4. We have observed a high frequency shift of the ^{19}F signals in the order of neat IL < IL-

MeOH< IL-DMF < IL-DMSO < IL-toluene (Figure 5.4 and Table 5.1). Except in IL-toluene mixture, the change in the order of chemical shift values of anion can be correlated to the dipole moment values of the added molecular solvent. To explain the result in IL-toluene mixture we would like to note the work of Deetlefs *et al.*[357] where they have shown that the hexafluorophosphate anion interacts with the ring hydrogen of benzene molecule. Therefore, similar interaction between the [NTf$_2$]$^-$ anion and toluene ring protons is also expected to lead to high frequency shift of the ^{19}F signals in IL-toluene mixture in the present case.
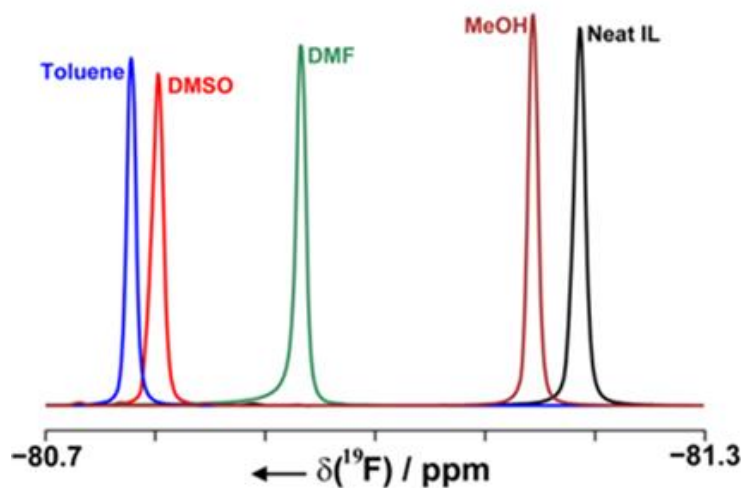
Figure 5.4. ^{19}F Chemical shifts of the anion of the IL.

5.3.4 Translational Diffusion Coefficient (*D*)

In order to get insight into the effect of added solvent on diffusion of cation of the IL, the diffusion coefficient of the cation in neat as well as in the binary mixtures of the IL has been estimated by employing PFG-NMR technique. The data has been analysed by employing Stokes−Einstein (SE) model. The SE model relates translational diffusion coefficient (*D*) of spherical particle with its radius (a) and medium viscosity η as *D* = *kT/(6πηa)*, where k is the Boltzmann constant, T is absolute temperature. Viscosities of all the binary mixtures of the IL have been calculated through following relation

$$\ln \eta_{mix} = x_{IL} \ln \eta_{IL} + x_s \ln \eta_s \tag{5.1}$$

where η_{mix}, η_{IL} and η_s are the viscosities of the binary mixture, IL and the molecular solvent respectively. x_{IL} and x_s represent mole fractions of the IL and solvent respectively. It has been shown by Seddon et.al.[3] that the viscosities of the mixtures of the IL with various cosolvents can be estimated from the mole fractions of the IL and the added cosolvent. While studying the solute and solvation dynamics in ILs, Sarkar and coworkers[177] have also used the logarithmic mixing relationship (equation 5.1) to estimate the viscosities of IL-cosolvent binary systems. Diffusion coefficients of the cation and the viscosities of the neat IL and the binary mixtures are provided in Table 5.2. Plot of D vs. $1/\eta$ for neat IL and the binary mixtures is shown in Figure 5.5. A relatively faster diffusion of the cation of the IL in different IL-cosolvent mixtures as compared to the in neat IL has been observed. This observation can be attributed to the decrease in viscosity of the medium by addition of molecular solvent. However, upon more careful look, one can also clearly observe from Figure 5.5 that the variation of D with medium viscosity (η) is not linear. This observation indicates different structural organisation for different IL-cosolvent systems. Had the viscosity been the only factor in influencing diffusion of the cation, then the $D \times \eta$ values would have been same for both neat IL as well as its mixtures with other solvents. However, this has not been observed in the present case as is also evident from the $D \times \eta$ values in Table 5.2. These observations indicate that the size of the diffusing species varies in different systems due to different type of association between the IL and cosolvents.[360] The observation can be attributed to the varying nature of cation-solvent interactions such as ion-dipole and hydrogen bonding interactions etc. in different IL-cosolvent systems.

Table 5.2. Diffusion coefficients (D) of the cation and viscosities of the medium in neat IL and IL-molecular solvent binary mixtures

System	η (cP) at 298 K	D ($\times 10^{-11}$ m^2/sec)	$D\eta$ ($\times 10^{-11}$ m^{2}cP/sec)
Neat IL	160.00	1.00	160.00
IL + DMF	1.32	5.83	66.00
IL + DMSO	17.81	3.90	69.50
IL + MeOH	9.26	5.07	46.97
IL + Toluene	9.46	4.48	42.38
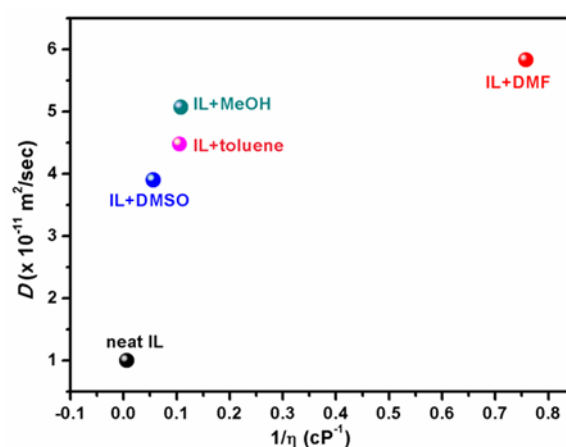
Figure 5.5. Diffusion coefficients (D) of the cation in neat IL and IL-cosolvent binary mixtures.

Apart from NMR measurements, fluorescence techniques such as fluorescence correlation spectroscopy (FCS) and time-resolved fluorescence anisotropy measurements have also been exploited to gain insight into the translational and rotational diffusion of the cation in the neat IL and IL-cosolvent binary mixtures. The results are discussed in the following section.

5.3.5 FCS Studies

FCS is capable of measuring the diffusion time of the molecules through the open detection volume.[361] Since diffusion is intricately related to the shape and molecular mass of the diffusing fluorescent species, it would be possible to study the association of fluorescent solute molecule with the solvent molecules by exploiting FCS technique.[361] In the present

case, the role of polar and nonpolar cosolvents on translational diffusion of the cation of the neat IL and in IL-cosolvent systems has been investigated by using FCS technique. For this purpose we have measured translational diffusion coefficient (D) in IL-DMF and IL-toluene mixtures along with the neat IL. The observed correlation curves for these systems are provided in Figure 5.6. Relevant data pertaining to the FCS measurements are provided in Table 5.3. One can clearly see from Table 5.3 that the variation in D obtained from FCS measurement are in the order IL-DMF > IL-toluene> neat IL. Interestingly, this trend is similar to that has been observed for D in those mixtures from NMR measurements. Magnitudes of D obtained from FCS as well as NMR studies are found to be in the same order (10^{-11}) (Tables 5.2 and 5.3). Therefore, the results obtained from FCS studies, corroborate our earlier inference that the nature of IL-solvent interaction is different in different IL-cosolvent systems.

Table 5.3. Translational diffusion coefficient (*D*) obtained from FCS Measurement for neat IL and IL-cosolvent systems

System	η (cP)	D ($\times 10^{-11}$ m^2/sec)	Conc. (nM)
Neat IL	160.00	0.96±0.09	4620 ± 40
IL + DMF	1.32	4.63±0.41	1750 ± 70
IL + Toluene	9.46	2.66±0.29	2700 ± 70
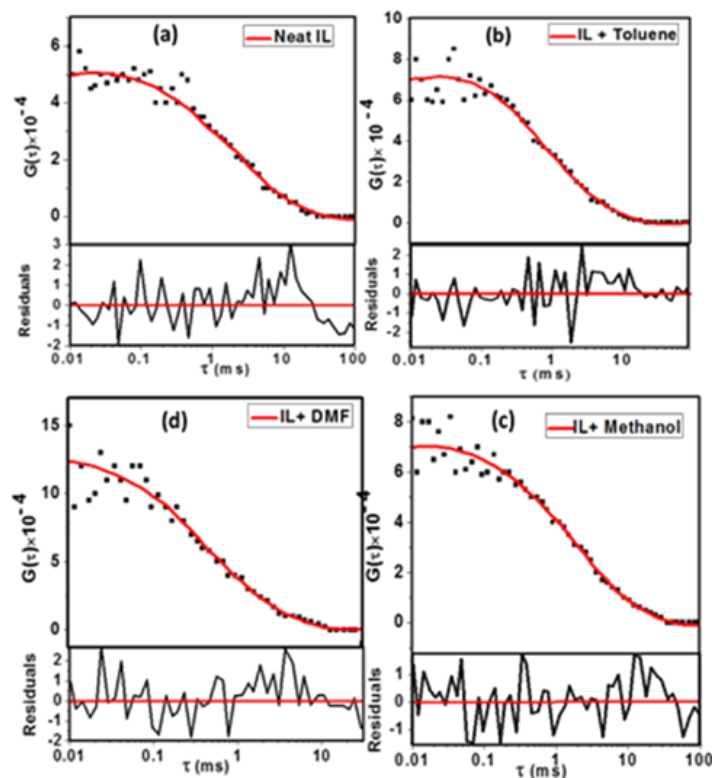
Figure 5.6. Fluorescence correlation curves for neat IL and IL-cosolvent systems. The solid red line indicates fit to the data points.

5.3.6 Time Resolved Fluorescence Studies

5.3.6.1. Solvation Dynamics

To understand the dynamical behavior of IL-cosolvent binary mixtures, solvation dynamics has been carried out in the neat IL and IL-DMF binary mixtures with different weight percentage of DMF have investigated at 298 K. DMF has been purposefully chosen as it has been used to dissolve a wide range of organic and inorganic compounds which in turn has also made this solvent to be used in variety of industrial processes.[355, 356] The time-resolved emission spectra (TRES) of the system, constructed from the fitted decay profiles, have been observed to be show progressive red shifted with time. Representative TRES of C153 is shown in Figure 5.7. A time-dependent shift of the emission maximum to lower energy has observed in all cases. This indicates that the excited state of dipolar molecule is stabilized by solvent molecules with time. The relaxation parameters of solvation of C153 for the systems have been collected in Table 5.4. The time constants of the observable dynamics

are determined from the plots of the spectral shift correlation function, *C(t)*, versus time. Average solvation time has been calculated by using both bi-exponential function as well as stretched exponential function. But while describing results we have resorted to the biexponential function as it gives better fit. Decay of solvation correlation function, *C(t)* of C153 in neat IL and IL-DMF binary mixtures has been shown in the Figure 5.8.
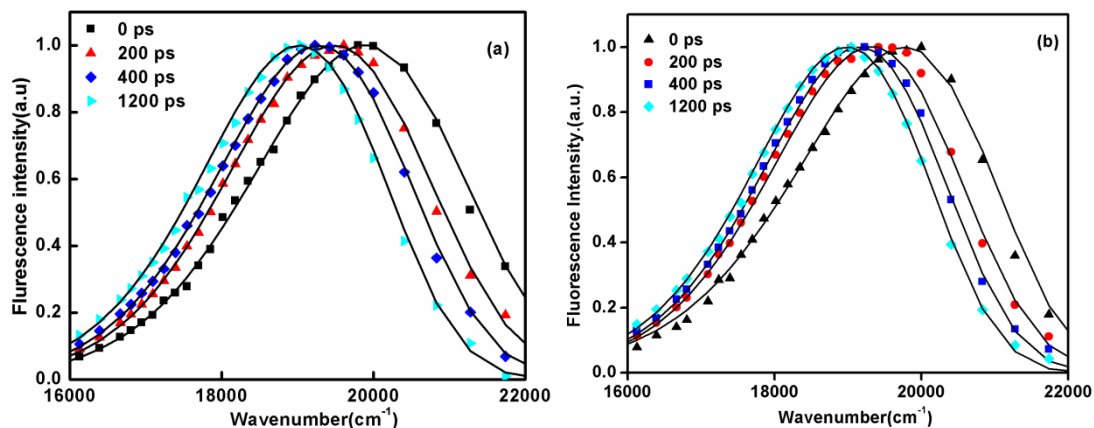
Figure 5.7. TRES plots C153 in (a) neat IL and in (b) IL+6wt% DMF mixture.

Table 5.4. Solvation relaxation parameters of C153 in IL-DMF binary mixtures

Wt% DMF	Viscosity(cP) at 298 K	[a]Biexponential Fit					[b]Stretched Exponential Fit			[c]Observed Shift (cm^{-1})
		a_1	$\tau_1(ns)$	a_2	$\tau_2(ns)$	$\tau_{avg}(ns)$	β	τ_{solv}	$\langle\tau_{st}\rangle(ns)$	
0	160	0.57	0.23	0.42	1.11	0.6	0.74	0.47	0.57	1016
6	78	0.64	0.17	0.36	0.84	0.41	0.738	0.317	0.38	855
12	40.7	0.83	0.14	0.18	0.67	0.24	0.841	0.194	0.21	910

[a] by equation 2.14 and 2.15, [b] by equation 2.16, [c] calculated by from $[\bar{v}_0 - \bar{v}_\infty]$
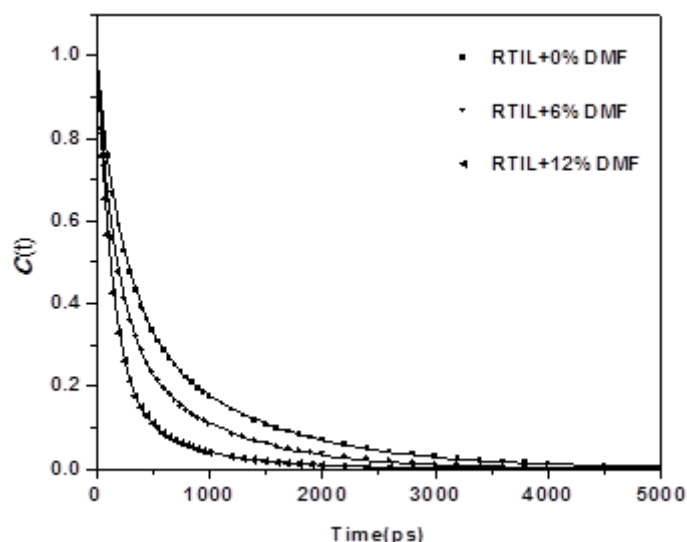
Figure 5.8. Decay of the spectral shift correlation function, *C(t)* of C153 in neat IL, IL+6wt% DMF and IL+12wt% DMF ($\lambda_{exc.}$ = 405 nm). In all cases, solid lines denote the bi-exponential fit to the data.

From Table 5.4, it is evident that the average solvation time of C153 decreases with the increase in wt. percentage of DMF in the IL. For example, the average solvation time decreases from 600 ps in neat IL to 240 ps upon addition of 12 wt% DMF (Table 5.4). This lowering of average solvation time with gradual addition of DMF to neat ionic liquid can be attributed to gradual lowering of bulk viscosity of the media. To get a better understanding on the dependence of bulk viscosity on average solvation time of the probe molecule in the different IL-DMF composition, we have plotted the average solvation time of C153 against the bulk viscosity values of IL-DMF mixtures (Figure 5.9). Almost a linear decrease in average solvation time with bulk viscosity has been observed. In DMF the average solvation time and average rotational time are reported to be 2 ps and 47 ps respectively [290, 310] which can be attributed to the low viscosity of DMF.
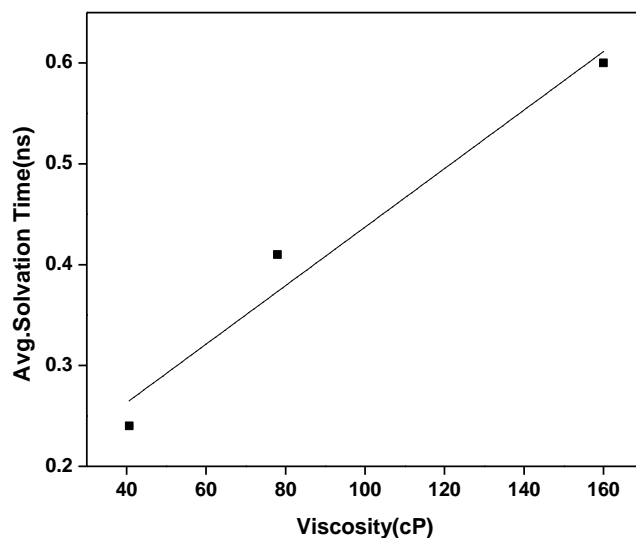
Figure 5.9. Average solvation time against bulk viscosity at 293 K.

5.3.6.1. Rotational Relaxation Dynamics

Since rotational diffusion of a fluorescent rotating species can also be influenced by its association with the surroundings[239] florescence anisotropy measurements have been carried out in neat IL as we as IL-cosolvent systems in order to investigate the interaction of cosolvents with neat IL. We have further investigated the excitation wavelength dependent fluorescent anisotropy behaviour of the rotating species in mixtures so that the micro-heterogeneous behaviour of the binary systems is also captured. It has been demonstrated that excitation wavelength fluorescence measurements can provide idea about the micro-hetrogeneoius behaviour of ionic liquids.[105] A representative anisotropy decay plot of IL-MeOH system at different excitation wavelengths is shown in Figure 5.10.

The rotational relaxation times (τ_r) obtained for each system are provided in Table 5.5. As can be seen, τ_r is found to decrease in IL-cosolvent systems as compared to the neat IL. This has happened due the lowering of viscosity of medium upon cosolvent addition to neat IL. However, upon careful look, the decrease in τ_r upon decrease in the medium viscosity are observed to be different for different IL-cosolvent systems (Table 5.5). For example, τ_r is

found to be faster by ~ 2- 3ns in IL-DMSO mixture despite the fact that the bulk viscosity of IL-DMSO is higher than those of IL-MeOH and IL-toluene (Table 5.5). Such observation indicates that the nature of interaction in various IL-cosolvent systems is different which corroborates the results obtained from translational diffusion measurements.

An interesting observation in the rotational dynamics study in the present systems is the excitation wavelength dependent rotational relaxation behaviour of the rotating solute in the given medium. Excitation at longer wavelength leads to preferential excitation of molecules that are located in the polar region of the medium, and are highly solvated.[155] Hence, the rotational relaxations of these molecules are more hindered and a longer reorientation time is observed.[155, 186] On the other hand, excitation at shorter wavelengths preferentially excite those molecules that are located in the nonpolar region of the medium and are relatively less solvated. Rotational relaxation of these molecules are observed to be faster as they experience lesser hinderance.[186] As can be seen from Table 5.5, upon changing the excitation wavelength from 375nm to 445nm, ~1.5 times change in the τ_r values has been obtained for neat IL. For conventional low viscous solvents one should not expect different rotational relaxation times at different excitation wavelength. Therefore, the present observation indicates the micro-heterogeneous nature of the IL. Variation of τ_r with excitation wavelength for all IL-cosolvent systems is shown in Figure 5.11. In the present study, the longer rotational relaxation time at higher excitation wavelength (λ_{exc} = 445nm) in all the system can be attributed to highly solvated rotating entity. Among the IL-cosolvent systems, least variation of τ_r is observed in case of IL-DMF system (~0.4ns) and largest variation is observed in IL-MeOH system (~4ns), IL-DMSO and IL-Toluene show a change of ~1.6 ns and ~2.7 ns in τ_r values respectively (Table 5.5) when excitation wavelength is varied from 375 nm to 445 nm. The present data on excitation wavelength dependent fluorescence measurements indicate that the cosolvent can play significant role in altering the structural

organisation of the neat IL. These data also points out that change in the structural organisation behaviour of a specific ionic liquid will depend on the nature of cosolvents that are added to it. The present observation can be attributed to the varying nature of IL-cosolvent interaction (ion-dipole and hydrogen bonding etc.) in various IL-cosolvent binary mixtures.

Table 5.5. Rotational relaxation time (τ_r) at different excitation wavelength in neat IL and IL-cosolvent systems

System	η (cP) at 298 K	Rotational relaxation time (τ_r/ns)		
		λ_{exc}= 375nm	λ_{exc}= 405nm	λ_{exc}= 445nm
Neat IL	160.00	8.05	9.38	12.53
IL + DMF	1.32	1.74	1.98	2.12
IL + DMSO	17.81	2.57	4.22	4.19
IL + MeOH	9.26	7.15	9.27	11.14
IL + Toluene	9.46	5.09	6.15	7.76
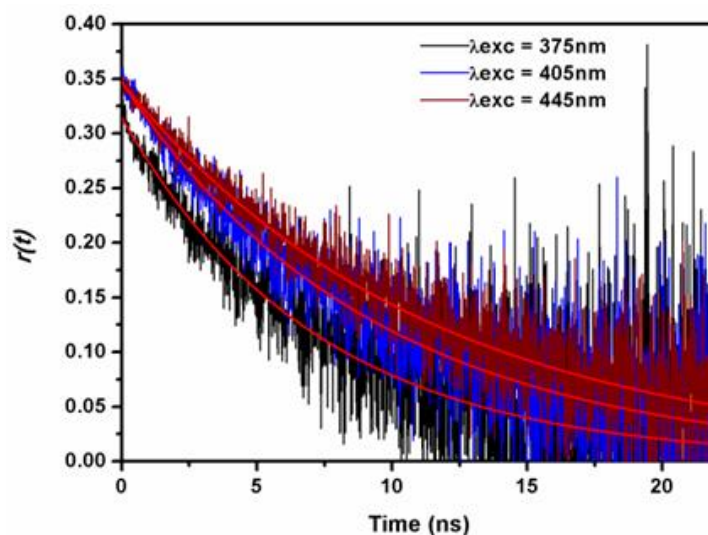
Figure 5.10. Rotational anisotropy decay profiles of IL-MeOH system at different excitation wavelengths. Solid red lines represent single exponential fit to the data points.
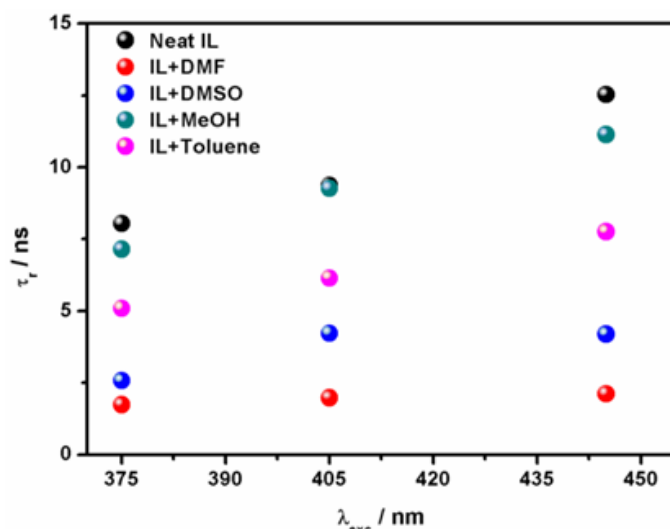
Figure 5.11. Variation of rotational relaxation time (τ_r) with excitation wavelength for different IL-cosolvent systems.

To understand the effect of change in the microenvironment (with addition of cosolvent) on solute rotation, we have further investigated the rotational relaxation dynamics of C153 in neat IL and IL-DMF binary mixtures. The rotational relaxation parameters of C153 in neat IL and in IL-DMF binary mixtures at different temperatures have been provided in Table 5.6. The anisotropy decay profiles have been fitted to a bi-exponential function. Decay of time-resolved anisotropy ($r(t)$) of C153 in IL+6%(wt.) DMF at various temperatures have been shown in Figure 5.12.
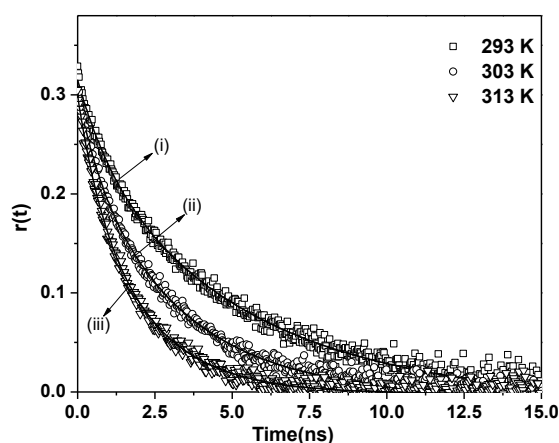
Figure 5.12. Decay of time-resolved anisotropy ($r(t)$) of C153 in RTIL+6%(wt.) DMF at $\lambda_{exc.}$ = 405 nm at temperatures (i) 293 K, (ii) 303 K and (iii) 313 K respectively. Solid line represents the fitting curve.

Table 5.6. Rotational relaxation parameters of C153 in RTIL-DMF binary mixtures at different temperatures (λ_{exc}=405 nm).

Wt% of DMF in IL	Temp.(K)	Viscosity(cP)	[a]r_0	a_1	τ_1 (ns)	a_2	τ_2 (ns)	$<\tau_r>/$ (ns)	[b]C_{rot} (avg.)
0	293	160	0.35	0.17	0.75	0.83	7.69	6.52	0.48
	298	117.4	0.36	0.19	0.47	0.81	5.72	4.74	
	303	88.5	0.35	0.17	0.53	0.82	4.50	3.82	
	308	68.3	0.35	0.18	0.48	0.82	3.52	2.95	
	313	53.5	0.35	0.18	0.31	0.82	2.72	2.29	
6	293	78	0.32	0.22	1.11	0.77	5.37	4.41	0.59
	298	62.3	0.32	0.19	0.83	0.80	3.95	3.35	
	303	50.7	0.30	0.20	0.74	0.80	3.19	2.70	
	308	42.2	0.30	0.18	0.52	0.82	2.40	2.06	
	313	35.8	0.30	0.23	0.72	0.77	2.07	1.75	
12	293	40.7	0.32	0.23	0.85	0.76	3.14	2.6	0.62
	298	32.3	0.32	0.20	0.57	0.80	2.36	2.00	
	303	26	0.38	0.27	0.09	0.72	1.68	1.24	
	308	23.5	0.35	0.20	0.13	0.80	1.41	1.15	
	313	19.7	0.36	0.20	0.13	0.80	1.17	0.95	

[a] r_0 is the initial anisotropy.

C_{rot} values have been calculated by following the procedure described in Chapter 2. Temperature averaged C_{rot} values have been provided in Table 5.6.

As can be seen from Table 5.6, the average rotational time of C153 which is higher in neat ionic liquid gradually decreases with gradual addition of DMF to RTIL. For example, at 293 K, the average rotational time of C153 decreases from 6.52 ns in neat ionic liquid to 2.60 ns in IL-DMF (12wt %) mixture. The faster rotation of C153 with decrease in viscosity of the IL–DMF mixture is also evident when the average rotational time of C153 is plotted against the viscosity of the media. The log-log plot of average rotational relaxation time (τ_r) against viscosity with respect to temperature is shown in Figure 5.13. It is clear from the plot

that rotational relaxation dynamics of C153 can be well explained within the broad limits of SED hydrodynamic theory. It is also evident from the plot that the average rotational relaxation time decreases with lowering of the bulk viscosity of the media. We have also fitted the $\langle\tau_r\rangle$ and η/T data for C153 to the function, $\tau_r = A(\eta/T)^P$. In these expressions N and R denote the number of data points and regression coefficient, respectively. Prominent nonlinear composition dependence has not been observed in the present case (equations 5.2-5.4).

C153 in IL+ 0(wt%) DMF

$$\langle\tau_r\rangle = (11.203 \pm 0.2913)\,(\eta/T)^{0.887\pm0.02584} \quad (N=5,\ R=0.9988) \tag{5.2}$$

C153 in IL+ 6(wt%) DMF

$$\langle\tau_r\rangle = (18.704 \pm 0.7959)\,(\eta/T)^{1.069\pm0.026} \quad (N=5,\ R=0.9991) \tag{5.3}$$

C153 in IL+ 12(wt%)DMF

$$\langle\tau_r\rangle = (32.9689 \pm 13.62)\,(\eta/T)^{1.28\pm0.185} \quad (N=5,\ R=0.9712) \tag{5.4}$$
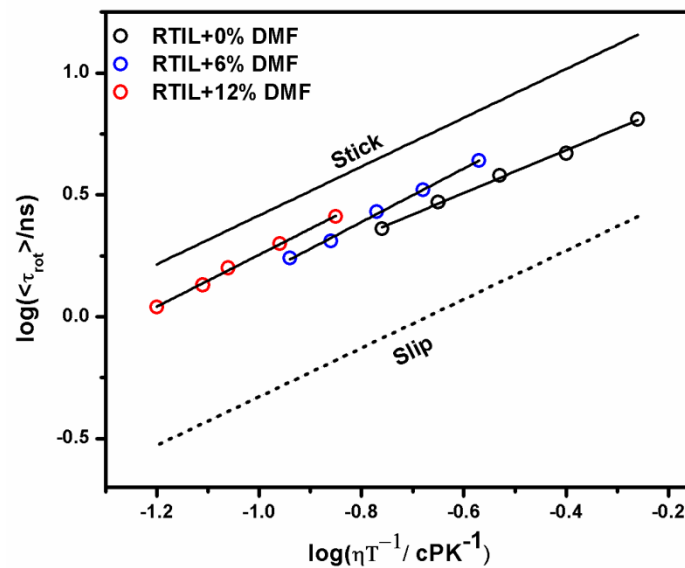
Figure 5.13. The log-log plots of $\langle\tau_r\rangle$ vs. (η/T) showing the stick and slip boundary conditions with solid and dashed line respectively.

We have also estimated the rotational coupling constants (C_{rot}) of C153 at different IL-DMF composition by employing SED hydrodynamic theory. As can be seen from Table 5.6, the C_{rot} value varies from 0.48-0.62 with increasing weight percentage of DMF. The C_{rot} values, which are measure of the extent of departure from normal hydrodynamic behavior of a solute due to specific interaction, are found to be very similar to that obtained for C153 in conventional solvents.[310] The C_{rot} values also indicate no involvement of specific solute-solvent interaction in the present case. The observation demonstrates that other than the lowering of viscosity of the medium, DMF does not seem to play any role towards the rotational dynamics of C153 in RTIL-DMF mixtures.

5.4. Conclusion

The present chapter describes a combined NMR, FCS and time-resolved fluorescence study on the borate-based IL and its mixture with various common organic cosolvents demonstrates some interesting outcomes in relation to intermolecular interaction in IL-cosolvent binary mixtures. A linear correlation between the ^{1}H NMR chemical shift (δ/ppm) of the imidazolium protons with the dipole moment of the added cosolvent suggests the role ofion-dipole interactions in binary systems. However, analysis of proton chemical shift values of IL in IL-DMF and IL-DMSO also reveals that hydrogen bonding interaction can also play important role along with ion-dipole interaction in those binary mixtures.^{1}H and ^{19}F chemical shift values of the IL in IL-toluene mixture has been rationalised through cation-π and anion-πinteractions respectively. The cation-cosolvent interactions in the binary mixtures are also supported by the corresponding ROESY spectra. Interestingly, present data demonstrates a nonlinear variation of the translational diffusion coefficient (D) with medium viscosity for different IL-cosolvent systems. This observation indicates the presence of different intermolecular interactions in different IL-cosolvent systems. Translational diffusion coefficient values obtained from FCS measurements also substantiates the outcome of the

NMR studies. Excitation wavelength dependent fluorescence anisotropy measurements have depicted that change in the rotational relaxation time with a change in the excitation wavelength is different for different IL-cosolvent binary mixture. This data also points out that structural organisation within IL-cosolvent binary mixtures could be very different due to the presence of different intermolecular interactions in different IL-cosolvent system. Further solvation and rotational relaxation dynamics of C153 in neat IL and IL-DMF binary mixtures have been investigated. The decrease in both average solvation and rotational time of probe molecule upon gradual addition of DMF has been attributed to the lowering of bulk viscosity of the medium.

The outcome of the present study is expected to provide useful insight in designing a new borate IL-cosolvents system for various applications such as electrolytes for lithium ion batteries and solvent systems for synthesis of inorganic and organic materials especially when solubility of the reactants is less in neat IL.

Chapter 6

Solute and Solvent Relaxation Dynamics in Mono and Dicationic Room-Temperature Ionic Liquids: A Combined Fluorescence and NMR Study

With an aim to understand the structure-property relationship in dicationic ionic liquids, steady state, time resolved fluorescence and NMR experiments have been carried out by employing structurally similar imidazolium-based mono and dicationic ILs. Analysis of the rotational relaxation dynamics data by Stokes-Einstein-Debye hydrodynamic theory has unveiled distinctive features of solute-solvent interaction in the mono and dicationic ILs. The present fluorescence and NMR data have revealed that the ultrafast component of solvation can be related to the dipolar rotation of imidazolium cation.

6.1. Introduction

During the last decade, monocation-based ILs (MILs) have been used for several purposes because of their interesting physicochemical properties.[4-8] However ILs based on dications (DILs) have not gained considerable attention until recently, when DILs comprising imidazolium,[47,126-129] ammonium and pyridinium[130-135] dication and mono negative inorganic or organic anions have been designed and developed. Interestingly, it has been observed that DILs exhibit physicochemical properties those are superior to the traditional MILs in terms of higher thermal stability, higher shear viscosity, higher surface tensions and larger liquid density.[47, 126-135] Keeping in mind the structural variation in both DILs and MILs, it can also be realized that more number of cation and anion combinations is possible in DILs than that in MILs.[47] The greater structural variability in DILs is expected to result in diverse physiochemical properties of DILs, compared to MILs, making them even more tunable and versatile.[10] Since DILs show great promise for future applications, at this stage, it is now

extremely important to have proper understanding of the structure-property correlation in DILs so that they can be effectively utilized for several industrial and academic purposes.

It is widely known that intra and inter molecular interactions among solute and solvent molecules play significant role in shaping physicochemical properties of liquids and solutions.[239] Hence, investigation on these aspects with variation in structures of the concerned molecules would help in gaining deeper insights into the structure-property-dynamics correlations among such systems. It may be also noted here that solute reactivity in a particular solvent is intricately related to dynamical behavior of the solvent.[235] Moreover, solute-solvent interaction is known to influence the rotational behavior of solute molecules.[185, 190, 193, 201-206] Due to these reasons, studies on solute and solvent dynamics by exploiting time-resolved fluorescence spectroscopy have been extensively exploited over the past few years to successfully understand the behavior of medium such as ILs. However, all these studies are carried out by taking MILs as target. In recent times some theoretical[362-366] and experimental[367, 368] studies have been carried out on DILs. Shirota and Ishida[368] have investigated the interionic vibrations among ILs by using femtosecond optical-heterodyne-detected Raman-induced Kerr effect spectroscopy (OHD-RIKES). This study has revealed difference in the low-frequency Kerr spectra between the monocationic 1-methyl-3-propylimidazolium bis-(trifluoromethylsulfonyl)amide ($[C_3MIm][NTf_2]$) and the dicationic IL, 1,6-bis-(3-methylimidazolium-1-yl)hexane bis-(trifluoromethylsulfonyl)amide ($[C_6(MIm)_2][NTf_2]_2$). Segregation in the microstructures of DILs having longer alkyl chain is believed to be responsible for this behavior. The authors have also pointed out that the difference of Kerr spectra of the ILs arises due to the distinct angular momentum and relaxation behavior of the two cationic species $[C_6(MIm)_2]^{2+}$ and $[C_3MIm]^{+}$.[363] Molecular dynamics (MD) simulation studies on a series of germinal DILs by Bodo *et al.*[365] have demonstrated many common characteristics with corresponding MILs. Cummings and

coworkers[366] have compared the structural nano-organization and heterogeneity in various mono and dicationic ILs through MD simulation. They have observed that for short alkyl chain, the cations in DILs and MILs exhibit very similar structural nano-organization and heterogeneity, whereas significant difference in structural heterogeneity is observed for medium and long-chain DILs and MILs.

As is realized at this stage, the studies on DILs are very limited and no experimental studies by exploiting fluorescence on DILs have been carried out. In view of the above facts, the present investigation on structurally similar MILs and DIL, by employinf fluorescene and NMR techniques have been undertaken. Specifically, rotational relaxation dynamics of organic solutes (C153, MPTS and perylene) in the MILs 1-methy-3-propyllimidazolium bis-(trifluoromethylsulfonyl)amide $[C_3MIm][NTf_2]$ and 1-hexyl-3-methylimidazolium bis(trifluoromethylsulfonyl)amide $[C_6MIm][NTf_2]$ and in the DIL 1,6-bis-(3-methylimidazolium-1-yl)hexane bis-(trifluoromethylsulfonyl)amide $[C_6(MIm)_2][NTf_2]_2$ have been studied. Additionally dynamics of solvation of the above mentioned MILs and DIL have been investigated by employing C153 as probe molecule. The translational diffusion and reorientational dynamics of the cations and anions of the neat ILs, by employing PFG-NMR technique, have also been investigated in detail in the present work. The molecular structures of the ILs and the probes are shown in Chart 6.1.
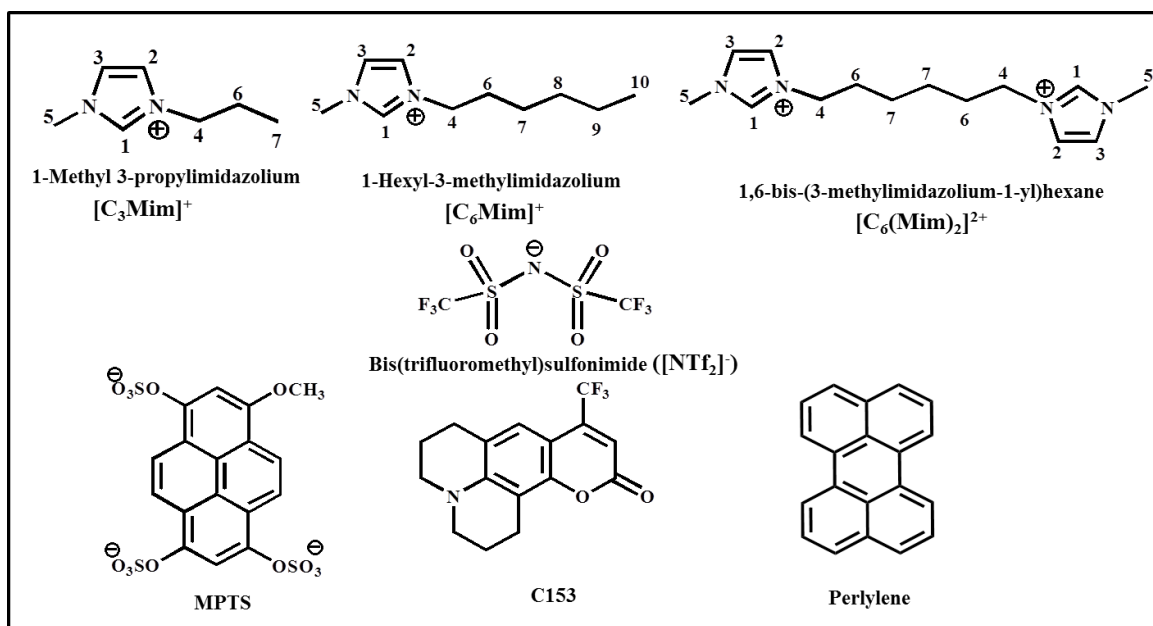
Chart 6.1: Molecular structures of ILs and probes.

6.2 Experiments and Methods

6.2.1. Materials.

C153 (laser grade, Exciton), MPTS (Fluka, Sigma-Aldrich), and perylene (Fluka, Sigma-Aldrich) were used as received. The DIL $[C_6(MIm)_2][NTf_2]_2$ was synthesized by following previously reported procedure.[47]

6.2.2. Synthesis of DIL $[C_6(MIm)_2][NTf_2]_2$

6.2.2.1. *1,6-Bis(3-methylimidazolium-1-yl)hexane bromide, $[C_6(Mim)_2][Br]_2$ (precursor for target DIL)*

1, 6-Dibromohexane (25 gm, 102.5 mmol) was gradually added to an acetonitrile solution(50 mL) of 1-methylimidazole(22 gm, 267.9 mmol) in a round-bottom flask equipped with a reflux condenser and a magnetic stirrer under nitrogen atmosphere, and the solution was stirred at 343 K for 3 days. The solution was then condensed by evaporation, and was washed by diethyl ether. The salt was precipitated as a brown powder. Then the salt was recrystallized from diethyl ether for several times and the purified product was finally obtained as a white solid after it was dried under vacuum at 308 K. The yield was 88%.[1]H-

NMR (DMSO-d$_6$, 400 MHz): δ (ppm) = 9.28 (s, 2H), 7.83 (s, 2H), 7.74 (s, 2H), 4.20(t, 4H), 3.86(s, 6H), 1.80(m, 4H), 1.28(m, 4H).

6.2.2.2.   *1,6-Bis(3-methylimidazolium-1-yl)hexanebis(trifluoromethylsulfonyl)amide, [C$_6$(Mim)$_2$][NTf$_2$]$_2$*

[C$_6$(Mim)$_2$][Br]$_2$ (5.74 gm, 14.1 mmol) was dissolved in water (50 mL), and aqueous lithium bis(trifluoromethylsulfonyl)amide solution (8.5 gm, 29.6 mmol in 30 mL water) was gradually added to the solution. After the mixture was stirred at room temperature for 1 day, the aqueous solution was decanted. The ionic liquid layer was dissolved in ethyl acetate (30 mL) and was washed with water (30 mL × 5). The organic layer was dried with anhydrous NaSO$_4$ filtered to remove the dry agent. After the solvent was evaporated, the residue was mixed with activated charcoal in acetonitrile. The activated charcoal was removed by filtration, and the solvent was evaporated. This decolorizing charcoal step was repeated twice. The ionic liquid was then dried under vacuum at 308 K for 3 days. The product was a colourless liquid. The yield was 88%. ^{1}H NMR (DMSO, 400MHz): δ(ppm)= 9.07(s, 2H), 7.73(s, 2H), 7.69(s, 2H), 4.15(t, 4H), 3.84(s, 6H), 1.79(m, 4H), 1.26(m, 4H). ESI-MS (+ve): 528.1217 m/z [C$_6$(MIm)$_2$ NTf$_2$]$^+$

The ILs were taken in different long-necked quartz cuvettes with proper precaution to avoid moisture absorption. Requisite amount of different probes were added to the ILs to prepare the solution. The cuvettes were properly sealed with septum and parafilm to maintain dry condition.

6.2.3. Instrumentation

Details of the instruments and techniques employed to record steady-state absorption and fluorescence spectra as well as time-resolved measurements have been described in Chapter 2. Techniques employed for NMR investigations and methodologies to analyse experimental data have also been described in Chapter 2.

6.3. Results and Discussions

6.3.1. Steady state spectral behavior of C153 and 2-amino-7-nitrofluorene (ANF) in ILs

Figure 6.1 displays the absorption and emission spectra of C153 dissolved in $[C_3MIm][NTf_2]$ and $[C_6(MIm)_2][NTf_2]_2$. Very close emission maximum for C153 in $[C_3MIm][NTf_2]$ and $[C_6(MIm)_2][NTf_2]_2$ indicates that the polarity of the ionic liquids are very similar. The polarity of $[C_6(MIm)_2][NTf_2]_2$ has been found to be close to that of dichloromethane.[190] The absorption and emission maxima of C153 are found not be affected by temperature from 293K to 333K.
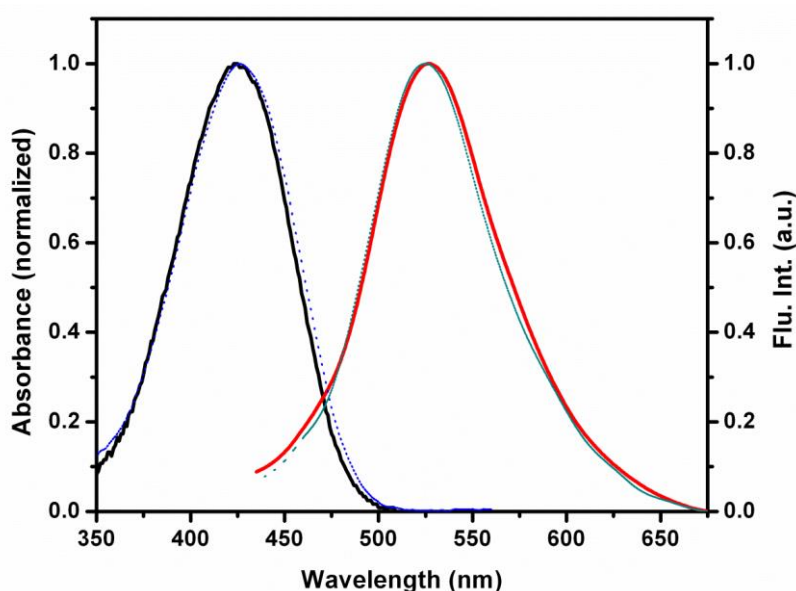
Figure 6.1.Combined normalized absorption (solid black line) and emission spectrum (solid red line) of C153 in $[C_3MIm][NTf_2]$. Absorption and emission spectra of C153 in $[C_6(MIm)_2][NTf_2]_2]$ are shown with dotted blue and dotted green line respectively. The spectra were normalized with respect to the corresponding peak maxima. λ_{exc}=405 nm.

Further, we have carried out excitation wavelength dependent fluorescence measurements to explore the spatial heterogeneity of the ILs. It may be noted here that ILs are micro-heterogeneous in nature.[105,155, 158] The micro-heterogeneous behaviour of ILs [105,155, 158] can be investigated by exploiting the excitation wavelength ($\lambda_{exc.}$) dependent fluorescence measurements. If there is a distribution of energetically different solvated species in the ground state, and energy transfer between them is slow, then instead of obeying Kasha's rule

a gradual shift (red) of fluorescence maximum with a change in the excitation wavelength is expected. The phenomenon is also known as "red-edge effect" (REE). The magnitude of the total fluorescence shift in the given medium can provide qualitative idea about the microheterogeniety of the medium. Therefore, this study can provide at least qualitative idea about the micro-heterogeneous nature of the medium. In the present study we have monitored the excitation wavelength dependent fluorescence behaviour in the ILs by employing of 2-amino-7-nitrofluorene (ANF) as a fluorescent probe. ANF has a shorter excited state lifetime (τ) ~100 ps, and thus it is expected that spectral behavior of ANF in the ILs would be more sensitive towards the micro-heterogeneous nature of the ILs.
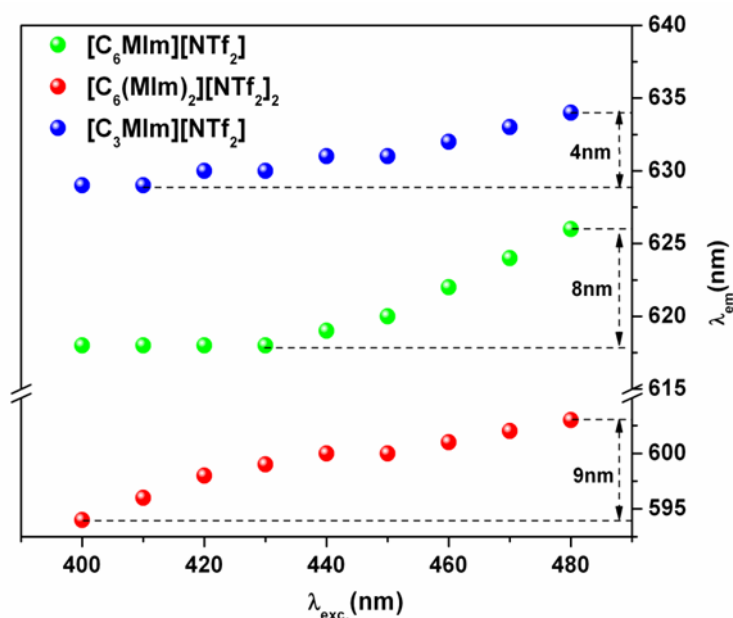
Figure 6.2. Excitation wavelength dependent fluorescence response of ANF in [C_3MIm][NTf_2], [C_6MIm][NTf_2] and [$C_6(MIm)_2$][$NTf_2]_2$ at 298K.

A steady red-shift in the fluorescence maximum of ANF has been observed with a change in the excitation wavelength in both MILs and the DIL. However, a significant difference in the magnitude of the total shift between the MIL, [C_3MIm][NTf_2] and the DIL, [$C_6(MIm)_2$][$NTf_2]_2$ has been observed. The shift in fluorescence maxima in [C_3MIm][NTf_2] is found to be about half (~4 nm) of the shift observed in [$C_6(MIm)_2$][$NTf_2]_2$ (~9 nm) (Figure 6.2). Our observation indicates that [$C_6(MIm)_2$][$NTf_2]_2$ is more micro-heterogeneous than its

monocationic counterpart [C$_3$MIm][NTf$_2$]. Interestingly, when we compare the excitation wavelength ($\lambda_{exc.}$) dependent fluorescence behavior of ANF in the present DIL [C$_6$(MIm)$_2$][NTf$_2$]$_2$, with a structurally similar IL, [C$_6$MIm][NTf$_2$], maximum shift of the fluorescence maxima is also found to be similar (Figure 6.2). The present observation is interesting in a sense that quite different results were obtained in terms of heterogeneity for monocationic and dication ILs. Cummings and coworkers,[366] through molecular dynamics (MD) simulation, have shown that monocationic ILs have a higher heterogeneity order parameter (HOP) than their dicationic counter parts. They have found that dicationic and monocationic ILs with short-range alkyl chain (such as [C$_6$(Mim)$_2$][BF$_4$]$_2$ and monocationic [C$_3$Mim][BF$_4$]) exhibit very similar structural nano-organization. Another MD simulation study by Ishida and Shiorta,[363] on dicationic and monocationic ILs having different alkyl chain lengths, reveals that the length of the apolar alkyl side chain has strong influence on the heterogeneous behavior. From the above discussion it is clear that the effect of alkyl chain length on structural organization of mono and dicationic ILs is different. Hence further investigation exploiting both experimental and theoretical techniques is required to have an in-depth understanding of the subtle difference in the micro-heterogeneous behavior of the mono and dicationic ILs.

6.3.2. Translational Dynamics

To get a better understanding of the structural organisation of mono and dicationic ILs, measurement of self-diffusion coefficient has been carried out on neat ILs using PFG-NMR technique. The famous Stokes-Einstein formula for translational diffusion coefficient (D) is employed to analyse the experimental data. This relation correlates D with radius of solute molecule (a) of spherical solute molecules that are large compared to the solvent molecules as, $D=(kT)/(6\pi\eta a)$. In this expression k is the Boltzmann constant, T is absolute temperature, η is the coefficient of viscosity of the diffusion medium. The radius a, in turn relates to the

mass, M, of a spherical solute molecule as $M = 4\pi a^3 \rho/3$, ρ being the density. This makes D dependent on M as $D \propto M^{-(1/3)}$. Here we would like to mention that diffusion of ions in ILs and other confined media has been investigated through many experimental and simulation studies.[371-377] It has been shown that motion of ions in ILs are jumplike.[371-377] Apart from mass, shape and size of the cation/anion, strength of cation-anion interaction and the nanostructural organization in the ILs are some of the factors which influence the diffusion of ions in the ILs.[377] Very recently relaxation and diffusion properties of anions and cations in the neat IL, 1-butyl-3-methylimidazolium bis(trifluoromethylsulfonyl)imid ([Bmim][Tf$_2$N]) has been investigated by Mattea and coworkers[374] through PFG-NMR experiments. The authors have shown that the rotational and translational correlation times show different dependences on temperature which indicates the decoupling of translational and rotational dynamics of the ions. In the present case we have investigated the translational diffusion of cations in the ILs [C$_3$Mim][NTf$_2$], [C$_6$Mim][NTf$_2$] and [C$_6$(MIm)$_2$][NTf$_2$]$_2$ as there is variation in the shape and size of the cations in these ILs in terms of alkyl chain length and alkyl bridge. Figure 6.3(a) shows the temperature dependence of translational diffusion coefficients of the [C$_6$(MIm)$_2$]$^{2+}$, [C$_6$MIm]$^+$ and [C$_3$MIm]$^+$ in neat ILs. Diffusion coefficient of [C$_6$(MIm)$_2$]$^{2+}$ has been found to be smallest while that of [C$_3$(MIm)]$^+$ has been found to be the largest at all temperatures. This is expected as per their relative masses. Figure 6.3(b) shows D as a function of T/η and as expected from the Stokes-Einstein formula shows linear relationships for all the three molecules. The slope of D-T/η curve is given by $k/(6\pi a)$ and hence a steeper slope indicates smaller hydrodynamic radius. It is interesting to note that the slope has been found to be the steepest for [C$_6$(MIm)$_2$]$^{2+}$ (0.70 JK^{-1}m^{-1}), in spite of the fact that it is the bulkiest cation. A possible explanation for the small hydrodynamic radius for [C$_6$(MIm)$_2$]$^{2+}$ could be that it remains in the experimental condition in a folded form.
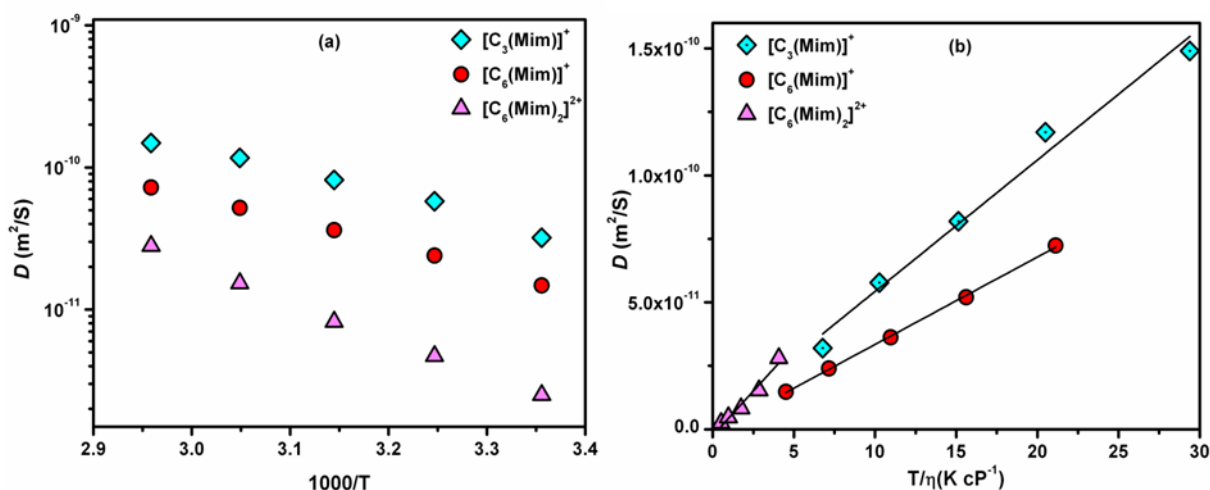
Figure 6.3. (a) Temperature dependence of diffusion coefficient of cations of the ILs. (b) Diffusion coefficient plotted against T/η. The dotted lines are linear fits of the data points.

6.3.3 Time-resolved Fluorescence Anisotropy Study

Solute-solvent and solvent-solvent interactions is known to play an important role in determining physicochemical properties of liquid and solution.[239] Since study of molecular rotation in liquids helps us to understand intermolecular interaction, in the present work we have carried out the time-resolved fluorescence anisotropy study in both monocationic and dicationic ILs basically to understand how the structural variation within mono and dicationic systems influence the intermolecular interactions. This is important as the outcome of this study would be helpful to understand structure-property correlation within ILs. We have analysed the rotational diffusion behavior of nonpolar perylene, dipolar C153 and anionic MPTS, in the MILs and also compared the data with the dicationic counterpart. Representative time resolved fluorescence anisotropy decay profile of C153 in [C$_3$Mim][NTf$_2$] is shown in Figure 6.4. Table 6.1 lists the probe properties of all the three probes that are used in this study. Rotational relaxation parameters of the three probes in both dicationic and monocationic ILs are collected in Table 6.2. As can be seen from Table 6.2, the average rotational relaxation time ($<\tau_r>$) decreases with increase in temperature. The lowering of average rotational time upon increasing the temperature is caused due to the lowering of the medium viscosity upon increase in temperature.
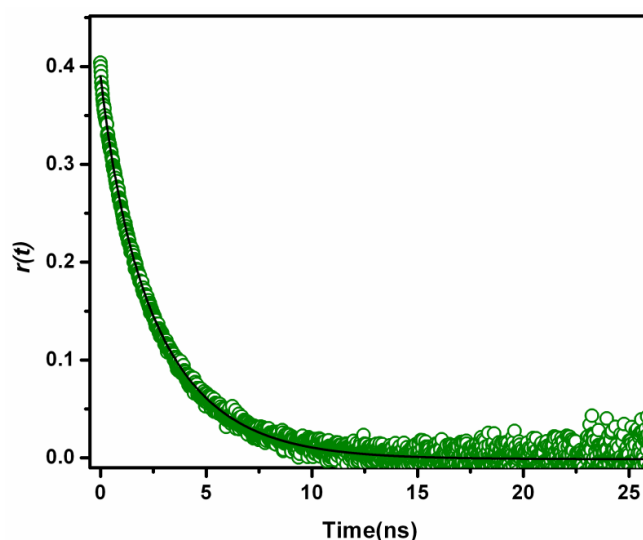
Figure 6.4. Time resolved fluorescence anisotropy decay for C153 in [C$_3$Mim] [NTf$_2$] at 293K. Solid line in the figure represents the biexponential fit to the data points.

Table 6.1.van der Waals volumes, shape factor, and slip boundary condition parameters for different solute molecules

Systems	van der Waals volume($\mathring{A}^3$)	f	C_{slip}
Perylene	225	1.76	0.085
C153	243	1.5	0.18
MPTS	343	1.33	0.11

Further, the viscosity dependence of average rotational relaxation time have been rigorously analyzed in light of Stokes-Einstein-Debye (SED) equation.[240] The data is analyzed by plotting $\log<\tau_r>$ vs. $\log(\eta/T)$ along with the stick and slip boundary condition (Figure 6.5 and 6.6).

137
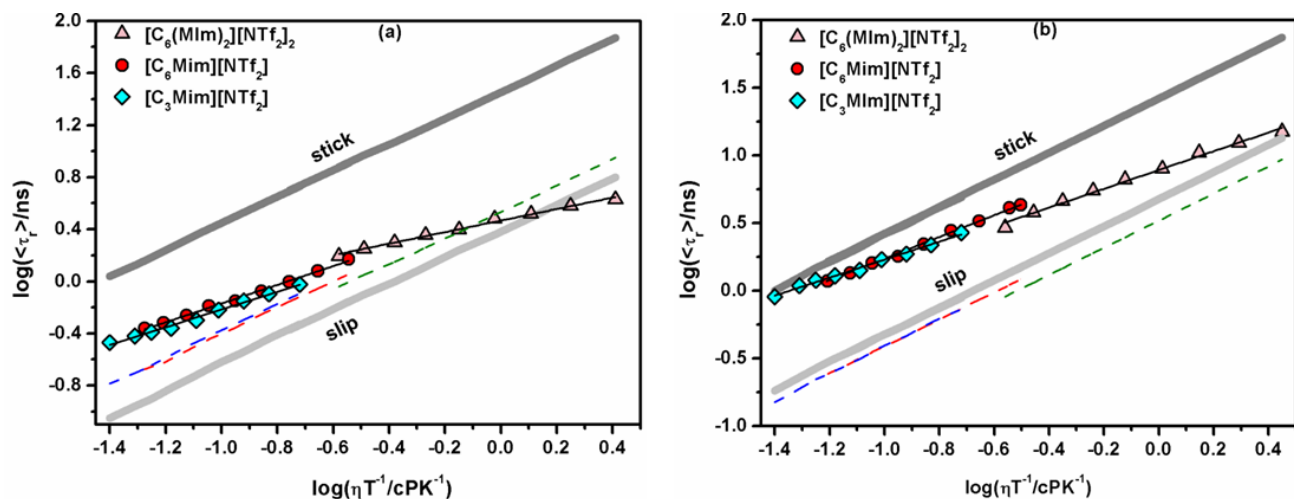
Figure 6.5. The log-log plots of $<\tau_r>$ vs. η/T for (a) perylene and (b) C153. The solid black line is the linear fit to the data points. Blue, red and green dotted lines represent the boundary condition obtained from Gierer-Wirtz (GW) quasihydrodynamic theory (ref 241) in $[C_3Mim][NTf_2]$, $[C_6Mim][NTf_2]$ and $[C_6(MIm)_2][NTf_2]_2$ respectively.
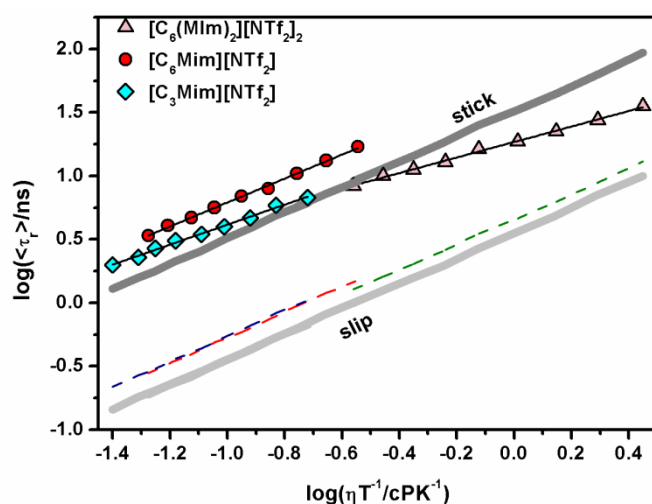
Figure 6.6. The log-log plots of $<\tau_r>$ vs. η/T for MPTS. The solid black line is the linear fit to the data points. Blue, red and green dotted lines represent the boundary condition obtained from Gierer-Wirtz (GW) quasihydrodynamic theory (ref 241) in $[C_3Mim][NTf_2]$, $[C_6Mim][NTf_2]$ and $[C_6(MIm)_2][NTf_2]_2$ respectively.

Table 6.2. Rotational relaxation parameters of MPTS, Perylene, and C153 in $[C_6(MIm)_2][NTf_2]_2$, $[C_6Mim][NTf_2]$ and $[C_3Mim][NTf_2]$ at different temperatures

System	Temp.(K)	$[C_6(MIm)_2][NTf_2]_2$			$[C_6Mim][NTf_2]$			$[C_3Mim][NTf_2]$		
		Vis. (cP)	$<\tau_r>$(ns)	C_{rot}(av.)	Vis. (cP)	$<\tau_r>$(ns)	C_{rot}(av.)	Vis. (cP)	$<\tau_r>$(ns)	C_{rot}(av.)
Perylene	293	827	4.3	0.13	84	1.5	0.22	55	0.95	0.23
	298	585	3.8		66	1.2		44	0.80	
	303	425	3.3		53	0.99		36	0.70	
	308	317	3.0		43	0.84		30	0.58	
	313	235	2.5		35	0.74		25	0.50	
	318	183	2.4		29	0.65		21	0.45	
	323	144	2.0		24	0.54		18	0.41	
	328	115	1.87		21	0.47		16	0.38	
	333	92	1.57		18	0.4		13	0.34	
C153	293	827	14.9	0.32	84	4.09	0.63	55	2.65	0.31
	298	585	12.32		66	3.27		44	2.24	
	303	425	10.49		53	2.79		36	1.92	
	308	317	7.99		43	2.21		30	1.70	
	313	235	6.64		35	1.80		25	1.46	
	318	183	5.48		29	1.60		21	1.33	
	323	144	4.61		24	1.35		18	1.23	
	328	115	3.79		21	1.18		16	1.10	
	333	92	2.93		18	1.10		13	0.91	
[b]MPTS	293	827	36.0	0.64	84	17.7	1.87	55	6.85	1.33
	298	585	27.4		66	13.4		44	5.93	
	303	425	22.2		53	10.6		36	4.69	
	308	317	18.7		43	8.0		30	4.08	
	313	235	16.5		35	7.0		25	3.56	
	318	183	13.0		29	5.6		21	3.12	
	323	144	11.4		24	4.7		18	2.66	
	328	115	10.0		21	4.1		16	2.33	
	333	92	8.4		18	3.4		13	2.03	

Experimental error ±5%. [b]C_{rot}(av.) is temperature averaged rotational coupling constant. For [b]MPTS rotational relaxation time is calculated from single-exponential decay function.

From Figure 6.2(a) and 6.2(b) it seems that the rotational diffusion behavior of perylene and C153 is more or less similar in all three ionic liquids and lie between stick and slip boundary condition. However, Figure 6.2(a) demonstrates that the rotational relaxation behavior of perylene is quite different in the DIL as compared to the MILs and shows departure from normal hydrodynamic behavior at higher η/T values in the DIL. The relatively faster rotational relaxation behavior of perylene in dicationic IL has also been analyzed by invoking quasi-hydrodynamic theory (Gierer-Wirtz theory).[241] GW theory takes into account both solute and solvent size. The theory considers solvent as concentric shells of spheres around the solute molecule. The friction coefficient in GW theory is expressed as

$$C_{GW}=\sigma C_0 \tag{6.1}$$

where σ is the sticking factor.

For a solvent volume V_s and probe volume V_p,

$$\sigma = \left[1 + 6\left(\frac{V_s}{V_p}\right)^{1/3} C_0\right]^{-1} \tag{6.2}$$

$$C_0 = \left[\frac{6\left(\frac{V_s}{V_p}\right)^{1/3}}{\left[1+2\left(\frac{V_s}{V_p}\right)^{1/3}\right]^4} + \frac{1}{\left[1+4\left(\frac{V_s}{V_p}\right)^{1/3}\right]^3}\right]^{-1} \tag{6.3}$$

In these equations, and V_p are the van der Waals volume of the solvent and solute, respectively. V_s for $[C_6(MIm)_2][NTf_2]_2$, $[C_6Mim][NTf_2]$ and $[C_3Mim][NTf_2]$ are 335.5 cm^3/mol, 201.9 cm3/ mol and 171.2 cm^3/mol respectively.[47] C_{GW} is found to be 0.12 for perylene in the DIL, which is close to the experimentally determined average C_{rot} value (Table 6.2). From Figure 9(a) we can clearly observe that the rotational relaxation behaviour of perylene follows different hydrodynamics at different η/T in DIL. At lower η/T rotational dynamics of perylene is well within GW quasi-hydrodynamics boundary and SED slip

boundary. At higher η/T (>0.2) it departs from both SED and GW boundary, and in the range 0.1-0.2 of η/T, rotational dynamics of perylene lies within GW and SED slip boundary. This indicates that none of the hydrodynamics theory (SED and GW) is successful in explaining the rotational dynamics of perylene in DIL. This decoupling of rotational motion of perylene with medium viscosity can be rationalized in terms of micro-heterogeneous behaviour of the IL.[378] This data also demonstrates that solute-solvent interaction is similar in MILs but is different in DIL.

It can be observed from Figure 6(b) that the rotational diffusion behavior of C153, like perylene, lies well within the boundary conditions set by SED theory in both dicationic and monocationic ILs. However, unlike perylene, no subslip behavior has been observed for C153 within the same experimental conditions. Average rotational relaxation times measured at comparable viscosity condition (Table 6.2) demonstrated that the rotational motion of C153 is somewhat faster in the DIL than that in the MILs. The observed faster rotational behavior of C153 can be explained on the basis of increase in the size of the solvent (DIL) which offers lower friction to the rotating solute.[185] A void space is created around the solute molecule because of the larger size of the DIL and the molecule can rotate with minimal hindrance. We have observed that at a particular temperature, the average rotational relaxation times for C153 in both ILs are found to lie in between perylene and MPTS (Table 6.2). Interestingly, the rotational coupling constant (C_{rot}) for C153 also exhibits intermediate value as compared to that of other two probes perylene and MPTS (Table 6.2). These results indicate that location of C153 is quite different than locations of the other two probes in ILs. A recent study shows that a similar dipolar probe PRODAN has been found itself to be distributed between polar and nonpolar domians in various morpholinium ILs.[204]

Interestingly, for MPTS, rotational relaxation dynamics shows a different behaviour in MILs than the DIL (Figure 6.3). We have observed superstick behavior for MPTS in the MILs. However, the C_{rot} value, which measures the solute-solvent interaction,[47] is observed to be slightly less (1.33) for [C$_3$Mim][NTf$_2$] than that has been observed in [C$_6$Mim][NTf$_2$] (1.87). This shows that solute-solvent association is stronger in [C$_6$Mim][NTf$_2$] than in [C$_3$Mim][NTf$_2$]. Similar results have also been observed by Fruchey and Fayer[193] earlier in different ILs with varying alkyl chain length. The reason behind such observation can be explained by considering the difference in rotator volume in [C$_6$Mim][NTf$_2$] and [C$_3$Mim][NTf$_2$]. This inference originates from the outcome of "solventberg" model[243] which assumes attachment of solvent molecules of non-negligible size to the rotating solute, causing increase in effective rotator volume. It has also been inferred that the solute-solvent association takes place due to specific solute-solvent hydrogen bonding interaction between to three sulfonate groups of MPTS and C2-H moiety of the imidazolium cation of the ILs. Based on this result one would also expect a similar stronger association between MPTS and the DIL [C$_6$(MIm)$_2$][NTf$_2$]$_2$ where two imidazolium cationic moieties bearing acidic hydrogen (C2-H) are present. But, Figure 6.3 clearly shows that rotational relaxation behavior of MPTS in the DIL is relatively faster than in the two MILs despite the fact that at any given temperature bulk viscosity of the DIL is higher than those of the MILs. At comparable viscosity condition (333K for [C$_6$(MIm)$_2$][NTf$_2$]$_2$ and 293K for [C$_6$Mim][NTf$_2$]) the rotational relaxation time in DIL has been observed to be about less than half (8.4 ns) of the value (17.7ns) that has been observed in [C$_6$Mim][NTf$_2$] (Table 6.2). Thus both average rotational relaxation times and C_{rot} values of MPTS in MILs and the DIL (Table 6.2) clearly indicates that solute-solvent interaction is relatively less in DIL than that in MILs. This observation leads us to believe that imidazolium cation in the DIL perhaps attain a folded structure where the counter anion NTf$_2^-$ makes H-bonding interaction with the acidic C2-H of

the two imidazolium moieties. And because of this, imidazolium cation cannot form stronger H-bonding interaction with bulkier MPTS which causes relatively faster rotation of MPTS in DIL.[190] We would like to note that we have earlier demonstrated the folded structure of of the DIL through translational diffusion measurements by NMR studies. Essentially rotational relaxation behaviour of the three solutes in the three ILs under investigation, demonstrates that the solutes locate themselves in distinct environment of the media. This data also depicts that the behaviour of the DIL is quite different from that of the MILs having equal or half-hydrocarbon chain with respect to the spacer chain length of the DIL.

6.3.4. Solvation Dynamics Study

Since reactivity of solute is closely related to solvation process[235], studies on dynamics of solvation would be helpful to understand and distinguish (if any) the dynamical behavior of both mono and dicationic ILs. To study this phenomenon, the emission decay profiles of C153 at magic angle (54.70) are collected at several wavelengths (5–10 nm intervals) across the emission spectra by exciting the sample at $\lambda_{exc} = 405$ nm at different temperatures. The occurrence of solvation process is indicated by the observation of faster decay at shorter monitoring wavelengths and a rise with usual decay at longer monitoring wavelength.[379] The detail procedure to obtain time-resolved emission spectra (TRES), solvent correlation function ($C(t)$) and solvation time (τ_s) have been provided in Chapter 2.

Representative TRES for C153 in the DIL $[C_6(MIm)_2][NTf_2]_2$ has been shown in Figure 6.7. In all the cases time dependent shifts of the emission maximum of the TRES to lower energy have been observed. This indicates that with time the excited state of dipolar molecule is stabilized by solvent molecules. The variation of full width at half maxima (FWHM) of TRES with time for both $[C_3Mim][NTf_2]$ and $[C_6(MIm)_2][NTf_2]_2$ has been shown in Figure 6.8. It is noticeable from Figure 6.8 that FWHM decreases with time in both cases. It indicates the stabilization of excited state of the solute by the solvent. However, the variation

in the rate of decrease of FWHM with time (Figure 6.8.) for the MIL and DIL can be ascribed to the difference in the local solvation environment of the MIL and DIL. Local solvation environment are known to have significant influence on the FWHM of time resolved emission spectrum.[290, 380]
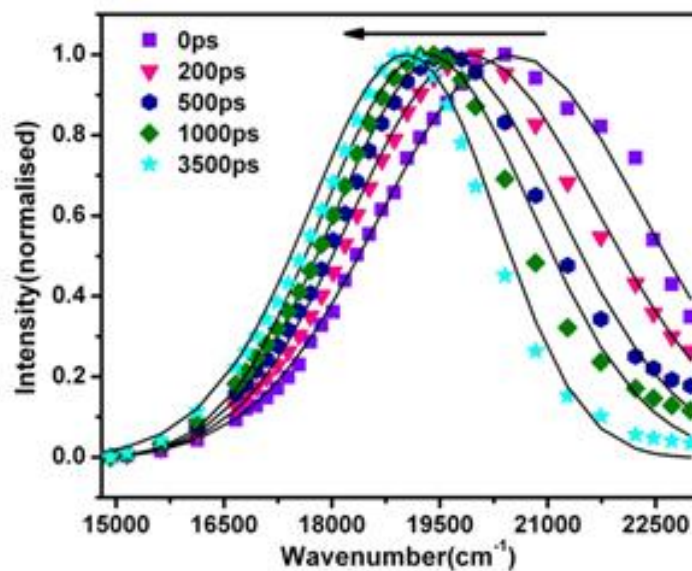
Figure 6.7. TRES of C153 in $[C_6(MIm)_2][NTf_2]_2$ at different time at 293K (λ_{exc}=405nm). All spectra are normalized at their corresponding peak maxima.
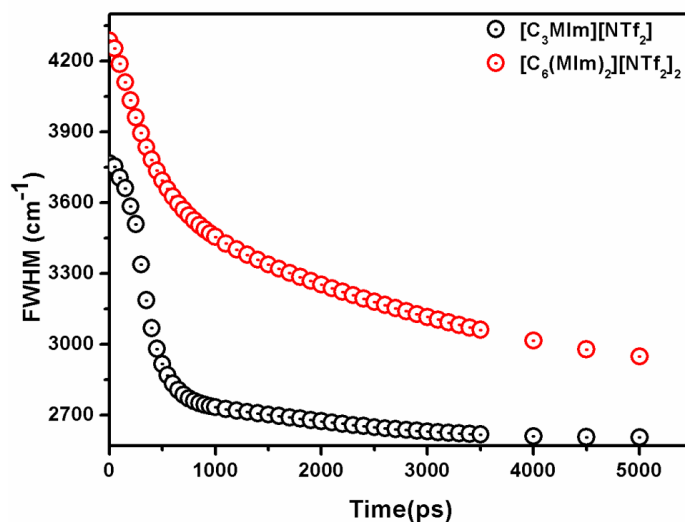
Figure 6.8. Variation of FWHM (full width at half maxima) of TRES with time for $[C_3Mim][NTf_2]$ and $[C_6(MIm)_2][NTf_2]_2$.

The detailed solvation parameters at different temperatures are collected in Table 6.3. It is noticeable from Table 6.3 that with the increase in temperature the average solvation time ($<\tau_s>$) decreases. The observation can be attributed to the gradual lowering of bulk viscosity of the medium with rise in temperature.[158] Moreover, when weighted components of average solvation time are plotted against the bulk viscosity values of the DIL (Figure 6.9), long weighted slow components have been found to correlate linearly with the bulk viscosity of the medium, whereas the fast components show much less changes with increase in the viscosity of the medium. The observation indicates that the average solvation rate is dominated by viscosity change. The similar behavior has also been observed for monocationic imidazolium-based ionic liquids.[158]
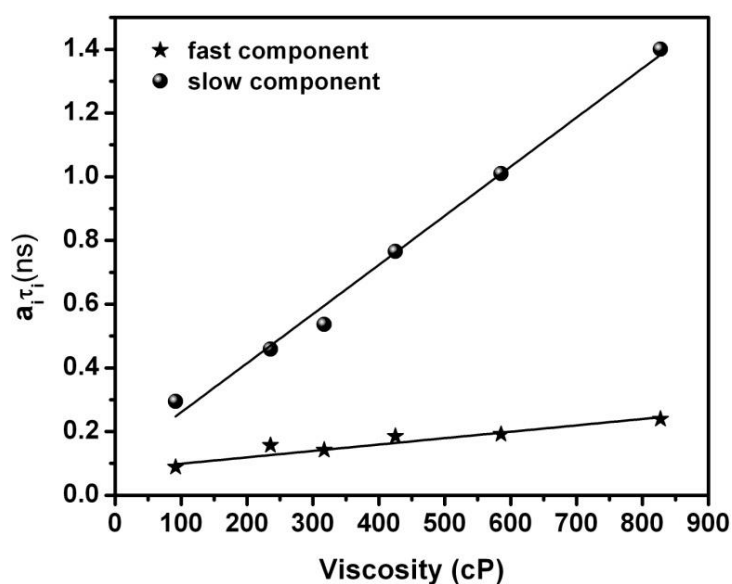
Figure 6.9. Plot of weighted components of solvation time vs. viscosity for [C$_6$(MIm)$_2$][NTf$_2$]$_2$.

Table 6.3. Solvation relaxation parameters of C153 in $[C_3MIm][NTf_2]$, $[C_6MIm][NTf_2]$ and $[C_6(MIm)_2][NTf_2]_2$ at $\lambda_{exc.} = 405nm$ at different temperatures

	Vis.(cP)/ Temp.(K)	Biexponential Fit[a]							Stretched exponential Fit[b]			
		a_1	τ_1(ns)	a_2	τ_2(ns)	$<\tau_s>$(ns)	$\Delta\nu_{obs}$ (10^3cm^{-1})	$\Delta\nu_{est}$ (10^3cm^{-1})	f_{obs}	β	τ_{sol}(ns)	$\langle\tau_{st}\rangle$(ns)
$[C_3MIm]$ $[NTf_2]$	55/293	0.93	0.45	0.07	2.15	0.46	1.11	1.38	0.80	0.95	0.37	0.38
	44/298	0.92	0.32	0.08	1.48	0.41	1.19	1.37	0.86	0.96	0.36	0.37
	36/303	0.95	0.31	0.05	1.58	0.37	1.08	1.36	0.79	0.95	0.33	0.34
	30/308	0.95	0.25	0.05	1.30	0.30	1.13	1.36	0.83	0.96	0.27	0.28
	25/313	0.98	0.22	0.02	2.55	0.26	1.04	1.33	0.78	1.01	0.25	0.24
	13/333	0.51	0.21	0.49	0.21	0.21	0.94	1.33	0.71	1.05	0.22	0.21
$[C_6MIm]$ $[NTf_2]$	92/291.3	0.73	0.33	0.27	1.85	0.74	1.10	1.32	0.83	0.71	0.527	0.66
	84/293	0.77	0.34	0.23	2.06	0.73	1.07	1.32	0.81	0.72	0.51	0.62
	66/298	0.80	0.29	0.20	1.73	0.58	1.06	1.31	0.81	0.74	0.41	0.49
	53/303	0.81	0.27	0.19	1.39	0.48	0.98	1.30	0.75	0.78	0.37	0.43
	43/308	0.84	0.241	0.16	1.28	0.40	0.97	1.30	0.75	0.84	0.35	0.38
	35/313	0.69	0.188	0.31	0.655	0.33	0.84	1.29	0.65	0.84	0.30	0.34
$[C_6(MIm)_2]$ $[NTf_2]_2$	827/293	0.64	0.37	0.36	3.89	1.64	1.64	1.43	1.15	0.57	0.94	1.53
	585/298	0.63	0.30	0.37	2.73	1.20	1.65	1.42	1.16	0.57	0.74	1.19
	425/303	0.67	0.28	0.33	2.32	0.95	1.61	1.40	1.15	0.58	0.59	0.92
	317/308	0.69	0.21	0.31	1.73	0.68	1.71	1.43	1.19	0.59	0.42	0.64
	235/313	0.72	0.22	0.28	1.64	0.60	1.53	1.43	1.07	0.64	0.40	0.57
	92/333	0.64	0.12	0.36	0.82	0.38	0.95	1.40	0.67	0.65	0.28	0.38

[a,b]Details of biexponential and stretched exponential fitting procedure have been provide in Chapter 2. $\Delta\nu_{obs}$ is the observed dynamic shift calculated time resolved solvation data. $\Delta\nu_{est}$ is the difference between $\nu(\infty)$ from the fits of TRES and the time-zero frequency estimated according to the methods of ref 379 and $f_{obs} = \Delta\nu_{obs}/\Delta\nu_{est}$. Experimental error $\pm 5\%$.

We would like to note here that one of the interesting outcomes from the time-dependent fluorescence Stokes shift measurements is the observation of missing solvation component. The ultrafast component of solvation is generally missed due to finite time-resolution of the experimental set up.[158] It has been observed that generally imidazolium-based MILs exhibit significant amount of missing solvation component.[163] Interestingly, in the present case, one can clearly see (Table 6.3) that there is no ultrafast component of solvation in case of imidazolium-based dicationic ionic liquid, whereas an ultrafast solvation component of ~20% is observed in the MILs. More interestingly, at higher temperature (~333 K), ~32% missing solvation component was also observed for dicationic IL. This study clearly points out that the dynamical behavior of the MILs and the DIL is quite different. The present observation is also interesting in a sense that the absence of missing component in solvation dynamics has only been observed in case of some phosphonium IL and ammonium ILs.[163] Hence, the observation of ultrafast component in case of imidazolium-based DIL is quite interesting. Initially it had been proposed that the small-amplitude motions of the planar and polarizable imidazolium cations in the close proximity of the probe molecule, might be responsible for origin of ultrafast component of solvation as the same could not be observed in case of ammonium and phosphonium ILs. However, ultrafast component of solvation has also been observed in a pyrrolidinium IL, which is a nonplanar cyclic analogue of the ammonium salts.[163] Later, Maroncelli and co-workers have found that inertial characteristics of the ions can be correlated to the amplitude and time constant of the ultrafast component.[169] This discussion points out that though absence of ultrafast solvation component has been encountered in some ILs, no proper explanation has been provided till date.

In recent reports, Biswas and coworkers[181, 182] have pointed out that ionic liquids are fairly large and polarizable and hence significant portion of solvent stabilization of dipolar solutes may also come from reorientational motion of imidazolium cation. They have shown

that for imidazolium IL, contribution of dipole-dipole interaction to the total dynamic Stokes shift can be ~ 40% suggesting that a significant portion of solvent dynamics can come from reorientational motion of imidazolium ion.[61] In a recent study on solvation dynamics in ILs through dielectric spectra, Petrich and coworkers'[381] have suggested that the translational motion of ions may not be the only predominant factor in solvation dynamics in ILs in subnanosecond time-range. Outcome of all these studies helped us to conjecture that perhaps there is a strong connection between the nature of cation and ultrafast component of solvation dynamics in ILs. It is expected that knowledge about the molecular rotational behavior of both monocationic and dicationic imidazolium moiety would be helpful to understand the correlation between ultrafast solvation component and dipolar rotation of the imidazolium cation in much better fashion. Note that recently PFG-NMR[265-268, 274] and quasi-elastic neutron scattering (QENS)[371] techniques are found to be very useful in providing insight into the reorientational motion of cations and anions in ILs. In view of this, in the present study, we have also investigated reorientational dynamics of the cations and anions of the ILs by exploiting ^{1}H and ^{19}F spin-lattice relaxation time (T_1) through NMR spectroscopy.

6.3.5. Reorientational Behaviour of the Cations and Anions of the ILs.

6.3.5.1. ^{1}H T_1 Measurements

^{1}H T_1 data have been acquired using inversion recovery method[292] and fitted to the Bloembergen−Purcell−Pound (BPP) relationship[293] (Chapter 2, equation 2.25) to obtain rotational correlation time, τ_c, for the protons of the ILs. BPP relationship is derived assuming isotropic motion, a condition satisfied only by spherically shaped molecules and they are completely characterized by a single correlation time. But the actual movement of molecules in solution can be quite complex. Moreover, shapes of many organic molecules show significant departures from spherical shape. Along with molecular reorientation, molecules may have various modes of internal motion such as rotation of methyl group, segmental

motion of the alkyl side chain, isomerism and conformational ring inversions etc. These motions influence the dipole–dipole interaction between coupled sites and thereby spin–lattice relaxation. Hence, τ_c in equation 6.4 is understood as an effective correlation time representing both overall reorientation and local internal motions.

Figures 6.10, 6.11 and 6.12 represent the temperature dependence of measured ^{1}H spin –lattice relaxation times (T_1) and effective rotational correlation time (τ_c) calculated there from, for individual protons of [C$_3$Mim][NTf$_2$], [C$_6$Mim][NTf$_2$] and [C$_6$(MIm)$_2$][NTf$_2$]$_2$ respectively. The calculated τ_c represents overall correlation time of certain part of the molecule and is contributed by not only global rotation but also by additional relaxation inducing processes like fast local motions such as internal rotation around a three symmetrical axis in CH$_3$, segmental motions of alkyl chains and conformational change of imidazolium ring. Hence τ_c can be represented as

$$\frac{1}{\tau_c} = \frac{1}{\tau_0} + \frac{1}{\tau_s} \tag{6.4}$$

where τ_0 and τ_s are the correlation times for the isotropic reorientation and local intramolecular motions, respectively.
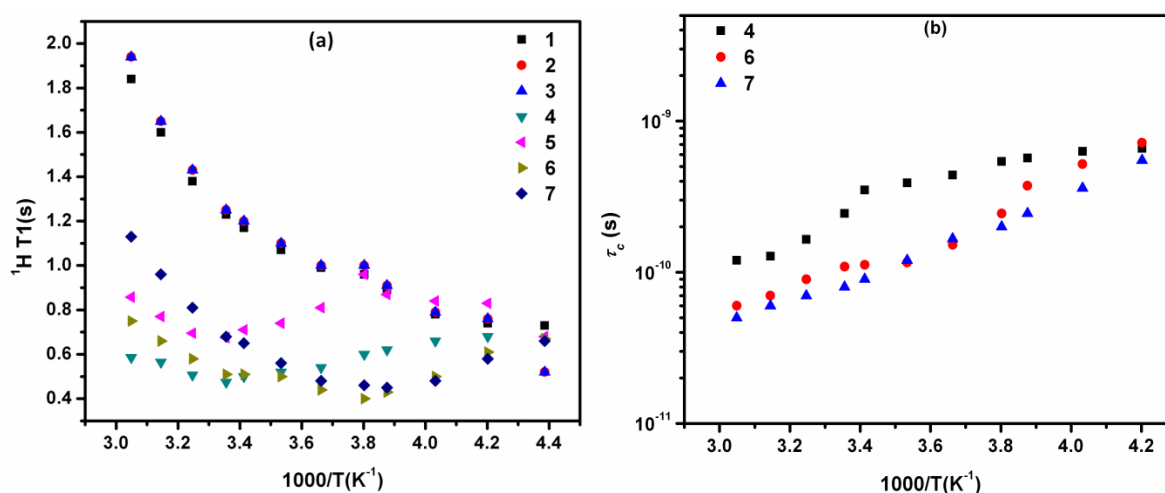
Figure 6.10. Temperature dependence of ^{1}H T_1 (a) and correlation time (τ_c) (b) of protons of the cation [C$_3$Mim]$^+$.
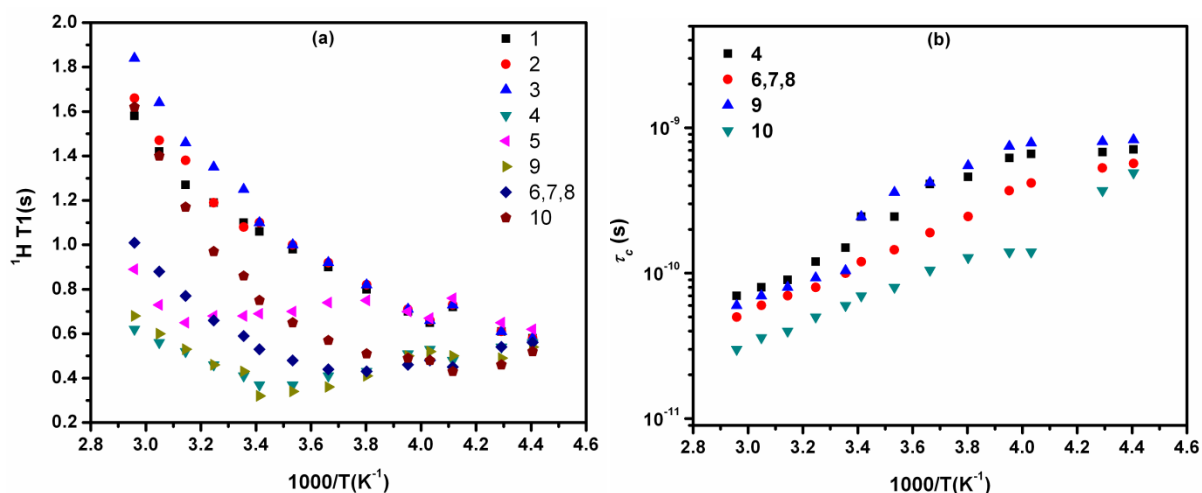
Figure 6.11. Temperature dependence of measured ^{1}H T_1 (a) and correlation time (τ_c) (b) of protons of the cation $[C_6Mim]^+$.
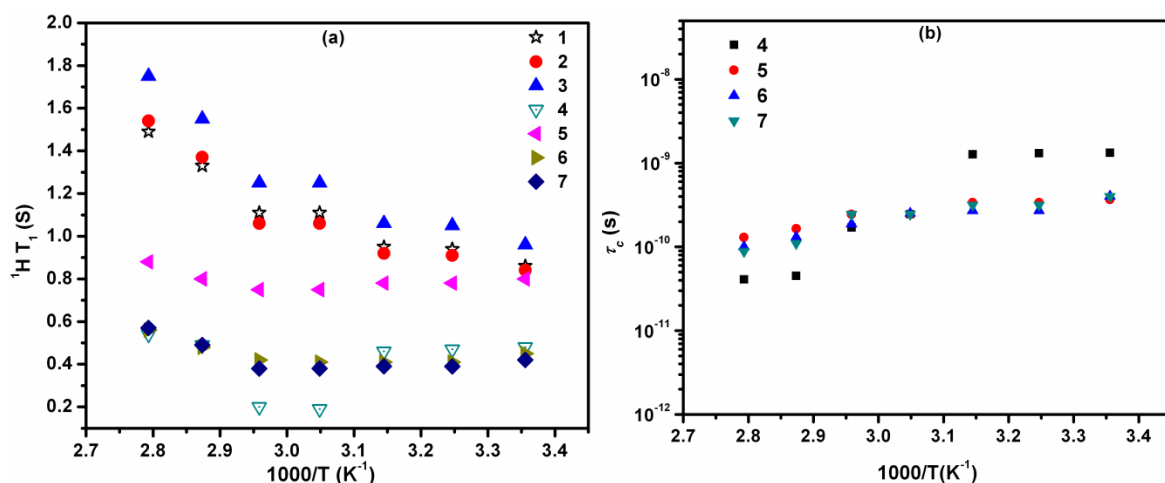
Figure 6.12. Temperature dependence of ^{1}H T_1 (a) and correlation time (τ_c) (b) of protons of the cation $[C_6(Mim)_2]^{2+}$.

It can be seen from Figure 6.10-6.12 that the imidazolium ring protons show two distinct characteristics across the molecules. First they do not show a T_1 minimum in the chosen temperature range (227 K- 358 K) and second, their T_1 values are the largest among all protons in the molecule. Such behavior has been previously observed for other imidazolium ILs.[265-268, 274] The fact that the imidazolium protons do not show a minimum indicates fast motion of the ring causing very small correlation time. A ring flipping might be a possibility. With decrease in temperature the overall correlation time increases as all motions, global and local, become slower. However, if certain portions of the molecule

exhibit fast motion (hence small correlation time) relative to other parts of the molecule, the correlation time does not increase enough to reach the condition $\omega_0 \tau_c = 0.616$, so that a minimum in T_1 is observed. Higher the temperature (lower the value of 1000/T) a proton show a minimum in T_1, more rigid is the portion of the molecule where the proton is located. For all other protons showing T_1 minimum, it is the molecular reorientational motion which contributes predominantly for the corresponding portion of the molecule. It is clear from Figure 6.10(a) and 6.11(a) that as we go towards terminal of the alkyl chain, τ_c becomes faster. For example τ_c of terminal CH_3 protons of $[C_3Mim]^+$(0.05 ns) and $[C_6Mim]^+$ (0.03 ns) are the fastest among all. This can be explained by the flapping motion of the end of a free chain. On the other hand N-CH_2 protons show slower τ_c (0.66 ns in $[C_3Mim]^+$ and 0.71 ns in $[C_6Mim]^+$) as they are adjacent to the bulky imidazolium unit. Also in the dication $[C_6(Mim)_2]^{2+}$, τ_c for N-CH_2 protons is the slowest at lower temperature (1.33 ns at 298 K). However with increase in temperature τ_c for N-CH_2 protons changes more as compared to the bridging alkyl protons (Figure 6.12(b)). At 358 K τ_c for N-CH_2 protons becomes faster (0.041ns) compared to the bridging alkyl protons (0.1 ns for proton 6 and 0.09 ns for proton 7) (Figure 6.12(b)). This is because the two imidazolium units in $[C_6(Mim)_2]^{2+}$ restrict the flapping motion of alkyl bridge protons unlike the protons of the free alkyl chain in $[C_3Mim]^+$ and $[C_6(Mim)_2]^{2+}$. At higher temperature probably the molecule exhibit a rapid interconversion between the folded form and an unfolded linear shape and the again a folded form in the opposite direction. Such motion is possible as the bulky imidazolium rings are connected through a flexible alkyl bridge. Figures 6.10(a), 6.11(a) and 6.12(a) show an overall pattern that at lower temperature all protons have similar T_1 and with increase in temperature the T_1 values of protons in different portion of the molecules exhibit different relaxation times. This clearly indicates presence of local motions. At lower temperatures, the

local motions are not dominant and all protons show similar relaxation times contributed primarily by global rotation of the molecules. As temperature rises, different local motions set in and cause different T_1 for different protons. We can say that the overall molecular reorientational motion of the heavy dication $[C_6(Mim)_2]^{2+}$ is slower than those of comparatively lighter monocationic $[C_3Mim]^+$ and $[C_6(Mim)_2]^{2+}$, which is expected. In a recent study through molecular dynamic (MD) simulations by Pal and Biswas,[327] it has been shown that the the slow nanosecond solvation component in ILs originates from the dynamic heterogeneity (DH) of these media. Maximum cation jump length was shown to be around ~50% of the ion diameter. The authors have shown that the DH timescale correlates well with the slow solvation rate. In this connection we would like to mention that the fact that we have not observed any missing component of solvation in the DIL can be due to the slower molecular reorientation of the DIL.

6.3.5.2. ^{19}F T_1 Measurements

We have also tried to observe the change in reorientational motion of the anions in the ILs through ^{19}F relaxation experiment. Here it should be noted that the anion is the same $[NTf_2]^-$ in all the ILs. We have measured T_1 at two different temperatures 298K and 308K. The reason for measuring T_1 at a temperature higher than 298K is because at higher temperature viscosity decreases which allow free reorientation of the anion, hence any change in reorientational motion of the anions in different ILs can be better observed at higher temperature. We have tried to compare the T_1 values with those of the protons of two different positions of the cations of the ILs, one is the imidazolium ring proton (proton no. 2) and other is N-CH$_2$ protons (proton no. 4). The results are presented in Table 6.4.

Table 6.4. Spin-lattice relaxation time (T_1) for cations and anions of ILs

IL	Temp. (K)	T_1 (s) of Cation		T_1 (s) of Anion
		Proton 2	Proton 4	
$[C_3MIm][NTf_2]$	298	1.25	0.48	0.60
	308	1.43	0.50	0.65
$[C_6MIm][NTf_2]$	298	1.08	0.41	0.64
	308	1.19	0.46	0.71
$[C_6(MIm)_2][NTf_2]_2$	298	0.84	0.48	0.55
	308	0.91	0.46	0.60

A closer look on Table 6.4 reveals a significant difference in the variation of T_1 of the protons of the cations and anions of the mono and dicationic IL as well as within monocationic ILs. For example between $[C_3MIm][NTf_2]$ and $[C_6(MIm)_2][NTf_2]_2$, T_1 for imidazolium ring proton (proton 2) varies by ~33% (at 298K) and ~40% (at 308K) whereas T_1 for anions varies only by ~8% at both temperature. Similarly between $[C_6MIm][NTf_2]$ and $[C_6(MIm)_2][NTf_2]_2$, T_1 for proton 2 varies by ~23% whereas T_1 for anions varies by ~15% at both temperatures. This shows that the reorientational motion of the cations is affected significantly, as compared to the anions on going from monocationic to dicationic IL. This is expected as the structural variation between the mono and dicationic ILs is only in the cation of the ILs and not in the anion. Even among MILs, variation in T_1 for proton 2 is more (15-17%) as compared to that of the anion (6-8%) at two temperatures. Variation in the T_1 for N-CH_2 protons (proton 4) among the ILs is very small (within 15%). This can be attributed to the negligible change in the environment (in particular dipolar coupling) of the N-CH_2 protons in the ILs. In general we have observed a significant difference in reorientational motion among the cation of the ILs whereas the same is not observed in case of anions. The

above discussion points out that the difference in solvation dynamics between the MILs and the DIL can be attributed to the difference in rerientational motion of the cation rather than the anions.

6.4. Conclusions

In this chapter, we have employed steady state and time-resolved fluorescence as well as NMR techniques to understand the structure-property correlation in MILs and one DIL. The study unravels several fascinating distinctions between dicationic and monocationic ionic liquids. Excitation wavelength dependent steady-state fluorescence response of ANF reveals a significant difference in the magnitude of the total shift in the fluorescence maximum for three-membered monocationic and six-membered dicationic IL which is indicative of the difference in microheterogeneous behavior of the concerned ILs. The present excitation wavelength dependent fluorescence study also demonstrates that the effect of alkyl chain length on structural organization of mono and dicationic ILs is different. PFG-NMR experiments have revealed distinctive features of translational diffusion of cations in the ionic liquids. Further, rotational dynamics of C153 and perylene was found to be similar for $[C_3MIm][NTf_2]$ and $[C_6MIm][NTf_2]$. However rotational dynamics of MPTS shows a stronger interaction of MPTS with $[C_6MIm][NTf_2]$ than with $[C_3MIm][NTf_2]$. The charged solute MPTS experiences the most polar environment in all the ILs. Relatively faster rotational behavior (near stick) of MPTS in DIL has been attributed to the stronger cation-anion interaction within the DIL which in turn makes it difficult for imidazolium cation to have stronger hydrogen bonding interaction with bulkier negatively charged molecule MPTS. The absence of ultrafast component of solvation in the DIL is another interesting outcome of the present study. NMR experiments have been carried out in order to examine correlation between the reorientational motion of the imidazolium cation and dynamics of solvation. ^{1}H spin-lattice relaxation experiments have demonstrated a dissimilar reorientational dynamics

of the cations of monocationic and dicationic ILs. Thus from the outcomes of the NMR experiments it can be inferred that the role of reorientational motion of the imidazolium cation and consequently the contribution from dipole-dipole interaction influencing the ultrafast component of solvation in particular and solvation dynamics in general in ILs deserves serious consideration. These investigations show that the structure-property correlation in MILs and DIL is quite different. The present work entails a significant step forward in understanding the structure-property relationship in mono and dicationic ILs.

Summary and Future Prospects

Steady-state, time-resolved fluorescence and NMR spectroscopic measurements have been carried out in several mono and dicationic ILs in order to obtain deeper insights into the structure-property correlation in these media. Several interesting features in relation to understanding the fundamentals of solute and solvent dynamics have been emerged from the present studies which are summarised as follows. (1) Electrostatic (ion-ion) interaction is observed to significantly hinder the rotational relaxation of charged solutes. (2) It has been observed that the rate of solvation dynamics can influence the rate of intramolecular PET process in a significant manner. (3) Nature of intermolecular interaction for different IL-cosolvent systems has been observed to be different. (4) It has been demonstrated that the chain length of alkyl group (terminal/bridge) plays important role in determining nanostructural organization in mono and dicationic ILs. (5) As far as rotational motion of solute is concerned, the behaviour of the DIL is observed to be quite different than the structurally similar MILs. (6) Dipolar rotation of the imidazolium cation is found to be responsible for ultrafast component of solvation.

The present work provides valuable information with regard to understanding of structure, intermolecular interaction and dynamics of various mono and dicationic ILs. However, studies on solute and solvent dynamics in DILs (symmetric and asymmetric) are very limited. We would like to investigate these aspects in various symmetric and assymetric DILs. As DILs can also be used as an electrolyte in lithium-ion batteries, it would be interesting to investigate the influence of lithium ion on the structural organisation of DILs by carrying out studies on solute and solvent dynamics in various DILs. We would also like to investigate electron transfer and energy transfer processes in various ILs by employing quatum dots (QDs).

Though ILs have been exploited for various applications, their high manufacturing cost[10] and toxicity towards environment[278,279] are the major concerns. Deep Eutectic Solvents (DESs) which have similar physicochemical properties like ILs, can be thought as alternatives to ILs.[280] DESs are cheaper, easy to prepare and non-toxic.[280] It would be interesting to study different photophysical processes in these systems so that information about the dynamical behavior of these systems are obtained.

REFERENCES

1. Wilkes, J. S.; A short history of ionic liquids-from molten salts to neoteric solvents. Green Chem., **2002**, *4*, 73.

2. Wasserscheid, P.; Keim, W. *Angew. Chem. Int. Ed.* **2000**, *39*, 3772.

3. Seddon, K. R.; Stark, A.; Torres, M. J. *Pure Appl. Chem.* **2000**, *72*, 2275.

4. Welton, T. *Chem. Rev.* **1999**, *99*, 2071.

5. Xue, H.; Verma, R.; Shreeve, J. M. *J. Fluorine Chem.* **2006**, *127*, 159.

6. Pandey, S. *Anal. Chim. Acta* **2006**, *556*, 38.

7. Zhang, J.; Bond, A. M. *Analyst* **2005**, *130*, 1132.

8. Buzzeo, M. C.; Evans, R. G.; Compton, R. G. *Chemphyschem* **2004**, *5*, 1106.

9. Rogers, R. D.; Seddon, K. R. *Science* **2003**, *302*, 792.

10. Sheldon, R. *Chem. Commun.* **2001**, 2399.

11. Seddon, K. R. *Ionic Liquids, Industrial Applications for Green Chemistry, American Chemical Society, Washington DC*, **2002**.

12. Hayashi, S.; Ozawa, R. Hamaguchi, H. *Chem. Lett.* **2004**, *33*, 1590.

13. Dupont, J.; de Suza, R. F.; Suarez, P. A. Z. *Chem. Rev.* **2002**, *102*, 3667.

14. Wasserscheid, P.; Keim, W. *Angew. Chem. Int. Ed.* **2000**, *39*, 3772.

15. Hough, W. L.; Rogers, R. D. *Bull. Chem. Soc. Jpn.* **2007**, *80*, 2262.

16. Plechkova, N. V.; Seddon, K. R. *Chem. Soc. Rev.* **2008**, *37*, 123.

17. Rogers, R. D.; Voth, G. A. *Acc.Chem. Res.* **2007**, *40*, 1077.

18. Chiappe, C.; Pieraccini, D. *J. Phys. Org. Chem.* **2005**, *18*, 275.

19. Weingartner, H. *Angew. Chem. Int. Ed.* **2008**, *47*, 654.

20. Chiappe, C.; Konig, B.; Impareto, G. *Eur. J. Org. Chem.* **2007**, 1049.

21. Rantwijk, F. V.; Sheldon, R. *Chem. Rev.* **2007**, *107*, 2757.

22. Dubreuil, J. F.; Bourahla, K.; Rahmouni, M.; Bazureau, J. P.; Hamelin, J. *Catal. Commun.* **2002**, *3*, 185.

23. Hallett, J. P.; Welton, T. *Chem. Rev.* **2011**, *111*, 3508.

24. J. F. Wishart, *Energy Environ. Sci.* **2009**, *2*, 956.

25. D. B. Kuang, P. Wang, S. Ito, S. M. Zakeeruddin, M. Gra¨tzel, *J. Am. Chem. Soc.* 2006, *128*, 7732.

26. Mazille, F.; Fei, Z. F.; Kuang, D. B.; Zhao, D. B.; Zakeeruddin, S. M.; Gratzel, M.; Dyson, P. J. *Inorg. Chem.* **2006**, *45*, 1585.

27. Walden, P. *Bull. Acad. Imper. Sci.St. Petersberg* **1914**, 1800.

28. Wasserscheid, P.; Welton, T. *Ionic Liquids in Synthesis, Wiley-VCH, Weinheim* **2003.**

29. Golding, J. J.; MacFarlane, D. R.; Spiccia, L.; Forsyth, G. B.; Skelton, B. W.; White, A. H. *Chem. Commun.* **1998**, *18*, 1593.

30. Polyakov, O. G.; Ivanova, S. M.; Gaudinski, C. M.; Miller, S. M.; Anderson, O. P.; Strauss, S. H. *Organometallics* **1999**, *18*, 3769.

31. Larsen, A. S.; Holbrey, J. D.; Tham, F. S.; Reed, C. A. *J. Am. Chem. Soc.* **2000**, *122*, 7264.

32. Xu, W.; Wang, L.-M.; Nieman, R. A.; Angell, C. A. *J. Phys. Chem. B* **2003**, *107*,11749.

33. Rogers, R. D.; Seddon, K. R.; Volkov, S. *Green Industrial Applications of Ionic Liquids*; Kluwer Academic: Dordrecht, Netherlands, **2002**.

34. Enomoto, T.; Nakamori, Y.; Matsumoto, K.; Hagiwara, R. *J. Phys. Chem. C* **2011**, *115*, 4324.

35. Ngo, H. L.; LeCompte, K.; Hargens, L.; McEwen, A. *Thermochim. Acta* **2000**, *357*, 97.

36. Lewandowski, A.; Swiderska-Mocek, A. *J. Power Sources* **2009**, *194*, 601.

37. Bonhôte, P.; Dias, A.; Papageorgiou, N.; Kalyanasundaram, K.; Gratzel, M. *Inorg. Chem.* **1996**, *35*, 1168.

38. Karmakar, R.; Samanta, A. *J. Phys. Chem. A* **2002**, *106*, 6670.

39. Nishida, T.; Tashiro, Y.; Yamamoto, M. *J. Fluorine Chem.* **2003**, *120*, 135.

40. MacFarlane, D. R.; Meakin, P.; Sun, J.; Amini, N.; Forsyth, M. *J. Phys. Chem. B* **1999**, *103*, 4164.

41. Fuller, J.; Carlin, R. T.; Long, H. C. D.; Haworth, D. *Chem. Commun.* **1994**, 299.

42. Carda-Broch, S.; Berthold, A.; Armstrong, D. W. *Anal. Bioanal. Chem.* **2003**, *375*, 191.

43. Law, G.; Watson, P. R. *Langmuir* **2001**, *17*, 6138.

44. Reichardt, C. *Green Chem.* **2005**, *7*, 339.

45. Buzzeo, M. C.; Evans, R. G.; Compton, R. G. *ChemPhysChem* **2004**, *5*, 1106.

46. Aki, S. N. V. K.; Brennecke, J. F.; Samanta, A. *Chem. Commun.* **2001**, 413.

47. Shirota, H.; Mandai, T.; Fukazawa, H.; Kato, T. *J. Chem. Eng. Data* **2011**, *56*, 2453.

48. Dzyuba, S.; Bartsch, R. A. *ChemPhysChem* **2002**, *3*, 161.

49. Zhang, S.; Sun, N.; He, X.; Lu, X.; Zhang, X. *J. Phys. Chem. Ref. Data.* **2006**, *35*, 1475.

50. Xu, W.; Cooper, E. I.; Angell, C. A. *J. Phys. Chem. B* **2003**, *107*, 6170.

51. Hirao, M.; Sugimoto, H.; Ohno, H. *J. Electrochem. Soc.* **2000**, *147*, 4168.

52. Zhou, Z. B.; Matsumoto, H.; Tatsumi, K. *Chem. Eur. J.* **2005**, *11*,752.

53. Zhou, Z. B.; Matsumoto, H.; Tatsumi, K. *Chem. Lett.* **2004**, *33*, 1636.

54. Du, Z. Y.; Li, Z. P.; Guo, S.; Zhang, J.; Zhu, L. Y.; Deng, Y. Q. *J. Phys. Chem. B* **2005**, *109*, 19542.

55. Holbrey, J. D.; Turner, M. B.; Reichert, W. M.; Rogers, R. D. *Green Chem.* **2003**, *5*, 731.

56. Branco, L. C.; Rosa, J. N.; Ramos, J. J. M.; Afonso, C. A. M. *Chem. Eur. J.* **2002**, *8*, 3671.

57. Bagno, A.; Butts, C.; Chiappe, C.; D'amico, F.; Lord, J. C. D.; Pieraccini, D.; Rastrelli, F. *Org. Biomol. Chem.* **2005**, *3*, 1624.

58. Santhosh, K.; Banerjee, S.; Rangaraj, N.; Samanta, A. *J. Phys. Chem. B* **2010**, *114*, 1967.

59. Greaves, T. L.; Weerawardena, A.; Fong, C.; Krodkiewska, I.; Drummond, C. J. *J. Phys. Chem. B* **2006**, *110*, 22479.

60. Hirao, M.; Sugimoto, H.; Ohno, H. *J. Electrochem. Soc.* **2000**, *147*, 4168.

61. Tokuda, H. Baek S. J.; Watanable, M. *Electrochemistry* **2005**; *73*, 620.

62. Jarosik, A.; Krajewski, S. R.; Lewandowski, A.; Radzimski, P. *J Mol Liq* **2006**; *123*, 43.

63. Hapiot, P.; Lagrost, C. *Chem. Rev.* **2008**, *108*, 2238.

64. Carmichael, A. J.; Seddon, K. R. *J. Phys.Org. Chem.* **2000**, *13*, 591.

65. Reichardt, C. *Green Chem.* **2005**, *7*, 339.

66. Aki, S. N. V. K.; Brennecke J. F.; Samanta, A. *Chem. Commun.* **2001**, 413.

67. Mandal, P. K.; Samnta, A. *J. Phys. Chem. B* **2005**, *109*, 15172.

68. Kawai, A.; Hidemori, T.; Shibuya, K. *Chem. Lett.* **2004**, *33*, 1464.

69. Wakai, C.; Oleinikova, A.; Ott, M.; Weingartner, H. *J. Phys. Chem. B* **2005**, *109*, 17028.

70. Tao, G.-H. Zou, M. Wang, X.-H. Chen, Z.-y; Evans, D. G.; Kou, Y. *Aus. J. Chem.* **2005**, *58*, 327.

71. Köddermann, T.; Wertz, C.; Heintz, A.; Ludwig, R. *Angew. Chem. Int. Ed.*, **2006**, *45*, 3697.

72. Dyson, P. J.; Laurenczy, G.; Ohlin, C. A.; Vallance, J.; Welton, T. *Chem. Comm.* **2003**, 2418.

73. Ohlin, C. A.; Dyson, P. J.; Laurenczy, G. *Chem. Comm.* **2004**, 1070.

74. Liu, H.; Tao, G.-H.; Evans, D. G.; Kou, Y. *Carbon*, **2005**, *43*, 1782.

75. Greaves, T. L.; Weerawardena, A.; Fong, C.; Krodkiewska, I.; Drummond, C. J. *J. Phys. Chem. B* **2006**, *110*, 22479.

76. Bernal, J. D. *Proc. R. Soc. London, Ser. A* **1964**, *280*, 299.

77. Weingärtner, H.; Merkel, T.; Käshammer, S.; Schröer, W.; Wiegand, S. *Ber. Bunsen-Ges. Phys. Chem.* **1993**, *97*, 970.

78. Avent, A. G.; Chaloner, P. A.; Day, M. P.; Seddon, K. R.; Welton, T. *J. Chem. Soc., Dalton Trans.* **1994**, *0*, 3405.

79. Every, H. A.; Bishop, A. G.; MacFarlane, D. R.; Oradd, G.; Forsyth, M. *Phys. Chem. Chem. Phys.* **2004**, *6*, 1758.

80. Gebbie, M. A.; Valtiner, M.; Banquy, X.; Fox, E. T.; Henderson, W. A.; Israelachvili, J. N. *Proc. Natl. Acad. Sci. U.S.A.* **2013**, *110*, 9674.

81. Daguenet, C.; Dyson, P. J.; Krossing, I.; Oleinikova, A.; Slattery, J. M.; Wakai, C.; Weingärtner, H. *J. Phys. Chem. B* **2006**, *110*, 12782.

82. Weingärtner, H. S.; Sasisanker, P.; Daguenet, C.; Dyson, P. J.; Krossing, I.; Slattery, J. M.; Shubert, T. *J. Phys. Chem. B* **2007**, *111*, 4775.

83. Schrödle, S.; Annat, G.; MacFarlane, D. R.; Forsyth, M.; Buchner, R.; Hefter, G. *Chem. Commun.* **2006**, 1748.

84. Turton, D. A.; Sonnleitner, T.; Ortnew, A.; Walther, M.; Hefter, G.; Seddon, K. R.; Stana, S.; Plechkova, N.; Buchner, R.; Wynne, K. *Faraday Discuss.* **2012**, *154*, 145.

85. Weingärtner, H. *Curr. Opin. Colloid Interface Sci.* **2013**, *18*, 183.

86. Zhao, W.; Leroy, F.; Heggen, B.; Zahn, S.; Kirchner, B.; Balasubramanian, S.; Müller-Plathe, F. *J. Am. Chem. Soc.* **2009**, *131*,15825.

87. Kohagen, M.; Brehm, M.; Thar, J.; Zhao, W.; Müller-Plathe, F.; Kirchner, B. *J. Phys. Chem. B* **2010**, *115*, 693.

88. Lynden-Bell, R. M. *Phys. Chem. Chem. Phys.* **2010**, *12*, 1733.

89. http://www.ccdc.cam.ac.ok/(accessed Jan 2006).

90. Dupont, J. *J. Braz. Chem. Soc.* **2004**, *15*, 341.

91. Hardacre, C.; Holbrey, J. D.; McMath, S. E. J.; Bowron, D. T.; Soper, A. K. *J. Chem. Phys*. **2003**, *118*, 273.

92. Dieter, K. M.; Dymek, C. J., Jr.; Heimer, N. E.; Rovang, J. W.; Wilkes, J. S. *J. Am. Chem. Soc.* **1988**, *110*, 2722.

93. Ozawa, R.; Hayashi, S.; Saha, S.; Kobayashi, A.; o Hamaguchi, H. *Chem. Lett.* **2003**, *32*, 948.

94. Fannin, A. A., Jr.; King, L. A.; Levisky, J. A.; Wilkes, J. S. *J. Phys. Chem.* **1984**, *88*, 2609.

95. Abdul-Sada, A. K.; Elaiwi, A. E.; Greenaway, A. M.; Seddon, K. R. *Eur. J. Mass Spectrom.* **1997**, *3*, 245.

96. Gozzo, F. C.; Santos, L. S.; Augusti, R.; Consorti, C. S.; Dupont, J.; Eberlin, M. N. *Chem. Eur. J.* **2004**, *10*, 6187.

97. Margulis, C. J. *Mol. Phys.* **2004**, *102*, 829.

98. Triolo, A.; Russina, O.; Fazio, B.; Triolo, R.; Di Cola, E. *Chem. Phys. Lett.* **2008**, *457*, 362.

99. Schröder, U.; Wadhawan, J. D.; Compton, R. G.; Marken, F.; Suarez, P. A. Z.; Consorti, C. S.; de Souza, R. F.; Dupont, J. *New J. Chem.* **2000**, *24*, 1009.

100. Wang, Y.; Voth, G. A. *J. Phys. Chem. B* **2006**, *110*, 18601.

101. Urahata, S. M.; Ribeiro, M. C. C. *J. Chem. Phys.* **2004**, *120*, 1855.

102. Canongia Lopes, J. N.; Costa Gomes, M. F.; Padua, A. A. H. *J. Phys. Chem. B* **2006**, *110*, 16818.

103. Santos, L. M. N. B. F.; Canongia Lopes, J. N.; Coutinho, J. A. P.; Esperanç a, J. M. S. S.; Gomes, L. R.; Marrucho, I. M.; Rebelo, L. P. N. *J. Am. Chem. Soc.* **2006**, *129*, 284.

104. Xiao, D.; Rajian, J. R.; Cady, A.; Li, S.; Bartsch, R.A.; Quitevis, E.L. *J. Phys. Chem. B* **2007**, *111*, 4669.

105. Mandal, P. K.; Sarkar, M.; Samanta, A. *J. Phys. Chem. A* **2004**, *108*, 9048.

106. Hu, Z.; Margulis, C. J. *Proc. Natl. Acad. Sci. U.S.A.* **2006**, *103*, 831.

107. Jin, H.; Li, X.; Maroncelli, M. *J. Phys. Chem. B* **2007**, *111*, 13473.

108. Adhikari, A.; Sahu, K.; Dey, S.; Ghosh, S.; Mandal, U.; Bhattacharyya, K. *J. Phys. Chem. B* **2007**, *111*, 12809.

109. Zheng, Z.-P.; Fan, W.-H.; Roy, S.; Mazur, K.; Nazet, A.; Buchner, R.; Bonn, M.; Hunger, *J. Angew. Chem., Int. Ed.* **2014**, *54*, 687.

110. Tanaka, K.; Toda, F. *Chem. Rev*. **2000**, *100*, 1025.

111. Kajimoto, O. *Chem. Rev.* **1999**, *99*, 35H.

112. Seddon, K. R. *Nature (Materials)* **2003**, *2*, 363.

113. Muzart, J. *Ad*v. *Synth. Catal.* **2006**, *348*, 275.

114. Shetty, P. H.; Poole, S. K.; Poole, C. F. *Anal. Chim. Acta* **1990**, *236*, 51.

115. Armstrong, D. W.; Zhang, L.-K.; He, L.; Gross, M. L. *Anal. Chem.* **2001**, *73*, 3679.

116. Li, Y. L.; Gross, M. L. *J Am Soc Mass Spectrom* **2004**, *15*, 1833.

117. Garlitz, J. A.; Summers, C. A.; Flowers, R. A.; Borgstahl, G. E. O. *Act Crystallogr., Sect D* **1999**, *55*, 2037.

118. Ranu, B. C.; Banerjee, S. *Org. Lett.,* **2005**, *7*, 3049.

119. Castner, E. W. Jr.; Margulis, C. J.; Maroncelli, M.; Wishart, J. F. *Ann. Rev. Phys. Chem.* **2011**, *62, 85.*

120. Armand, M.; Endres, F.; MacFarlane, D. R.; Ohno, H.; Scrosati, B. *Nat. Mater.* **2009**, *8*, 621.

121. Ding, J.; Zhou, D.; Spinks, G.; Wallace, G.; Forsyth, S.; Forsyth, M.; MacFarlane, D. *Chem. Mater.* **2003**, *15*, 2392.

122. Qu, J.; Truhan, J. J.; Dai, S.; Luo, H.; Blau, P. J. *Tribol. Lett.* **2006**, *22*, 207.

123. Janus, E.; Goc-Maciejewska, I.; Lozynski, M.; Pernak, J. *Tetrahedron Lett.* **2006**, *47*, 4079.

124. Surette, J. K. D.; Green, L.; Singer, R. D. *Chem. Commun.* **1996**, 2753.

125. Huang, K.; Zhang, X. M.; Li, Y. X.; Wu, Y. T.; Hu, X. B. *J. Membr. Sci.* **2014**, *471*, 227.

126. Anderson,J. L.;Ding,R.;Ellern,A.;Armstrong,D. W. *J. Am. Chem. Soc.* **2005**, *127*, 593.

127. Payagala, T.; Huang, J.; Breitbach, Z. S.; Sharma, P. S.; Armstrong, D. W. *Chem. Mater.* **2007**, *19*, 5848.

128. Ding, Y.-S.; Zha, M.; Zhang, J.; Wang, S.-S. *Colloids Surf. A* **2007**, *298*, 201.

129. Sun, H.; Zhang, D.; Liu, C.; Zhang, C. *THEOCHEM* **2009**, *900*, 37.

130. Lall, S. I.; Mancheno, D.; Castro, S. B.; Cohen, J. I.; Engel, R. *Chem. Commun.* **2000**, 2413.

131. Engel, R.; Cohen'J. I.; Lall, S. I. *Phosphorus, Sulfur Silicon Relat. Elem*. **2000**, *177*, 1441.

132. Engel, R.; Cohen, J. I. *Curr. Org. Chem.* **2002,** *6*, 1453.

133. Wishart, J. F.; Lall-Ramnarine, S. I.; Raju, R.; Scumpia, A.; Bellevue, S.;Ragbir, R.; Engel, R. *Radiat. Phys. Chem.* **200**5, *72*, 99.

134. Yoshizawa, M.; Ito-Akita, K.; Ohno, H. *Electrochim. Acta* **2000**, *45*, 1617.

135. Ito, K.; Nishina, N.; Ohno, H. *Electrochim. Acta* **2000**, *45*, 1295.

136. Fang, D.; Yang, J. M.; Ni, C. J. *Heteroatom. Chem.* **2011**, *22*, 5.

137. Chinnappan, A.; Kim, H. *Chem. Eng. J.* **2012**, *187*, 283.

138. Fan, M. M.; Yang, J.; Jiang, P. P.; Zhang, P. B.; Li, S. S. *RSC Adv.* **2013**, *3*, 752.

139. Liu, X. F.; Xiao, L. F.; Wu, H. J. T.; Chen, J.; Xia, C. G. *Helv. Chim. Acta* **2009**, *92*, 1014.

140. Han, X. X.; Armstrong, D. W. *Org. Lett.* **2005**, *7*, 4205.

141. Pagano, F.; Gabler, C.; Zare, P.; Mahrova, M.; Dorr, N.; Bayon, R.; Fernandez, X.; Binder, W. H.; Hernaiz, M.; Tojo, E.; Igartua, A. *P. I. Mech. Eng. J.-J. Eng.* **2012**, *226*, 952.

142. Jin, C. M.; Ye, C. F.; Phillips, B. S.; Zabinski, J. S.; Liu, X. Q.; Liu, W. M.; Shreeve, J. M. *J. Mater. Chem.* **2006**, *16*, 1529.

143. Zhancy, Z. X.; Zhou, H.; Yang, L.; Tachibana, K.; Kamijima, K.; Xu, J. *Electrochim. Acta* **2008**, *53*, 4833.

144. Cho, W. J.; Yeom, C. G.; Kim, B. C.; Kim, K. M.; Ko, J. M.; Yu, K. H. *Electrochim. Acta* **2013**, *89*, 807.

145. Mandal, P. K.; Paul A.; Samanta, A. *J. Photochem. Photobiol*. **2006**, *182*, 113.

146. Paul, A.; Samanta*, A. J. Phys. Chem. B* **2008**, *112*, 16626

147. Patra, S.; Samanta, A. *J. Phys. Chem. B* **2012**, *116*, 12275.

148. E. Binetti, A. Panniello, L. Triggiani, R. Tommasi, A. Agostiano, M. L. Curri, M. Striccoli, *J. Phys. Chem. B*, **2012**, *116*, 3512.

149. Ghosh, A.; Chatterjee, T.; Mandal, P. K. *Chem. Commun.* **2012**, *48*, 6250.

150. Guo, J. Baker, G. A.; Hillesheim P. C.; Dai, S.; Shaw R. W.; Mahurin, S. M. *Phys. Chem. Chem. Phys.* **2011**, *13*, 12395.

151. Karmakar, R.; Samanta, A. *J. Phys. Chem. A* **2002**, *106*, 4447.

152. Karmakar, R.; Samanta, A. *J. Phys. Chem. A* **2003**, *107*, 7340.

153. Mandal, P. K.; Samanta, A. *J. Phys. Chem. B* **2005**, *109*, 15172.

154. Mandal, P. K.; Saha, S.; Karmakar, R.; Samanta, A. *Curr. Sci.* **2006**, *90*, 301.

155. Samanta, A. *J. Phys. Chem. B* **2006**, *110*, 13704.

156. Paul, A.; Samanta, A. *J. Phys. Chem. B* **2007**, *111*, 4724.

157. Paul, A.; Samanta, A. *J. Phys. Chem. B* **2008**, *112*, 947.

158. Samanta, A. *J. Phys. Chem. Lett.* **2010**, *1*, 1557.

159. Khara, D. C.; Samanta, A. *J. Phys. Chem. B* **2012**, *116*, 13430.

160. Ingram, J. A.; Moog, R. S.; Ito, N.; Biswas, R.; Maroncelli, M. *J. Phys. Chem. B* **2003**, *107*, 5926.

161. Ito, N.; Arzhantsev, S.; Maroncelli, M. *Chem. Phys. Lett.* **2004**, *396*, 83.

162. Ito, N.; Arzhantsev, S.; Heitz, M.; Maroncelli, M. *J. Phys. Chem. B* **2004**, *108,* 5771.

163. Arzhantsev, S.; Jin, H.; Baker, G. A.; Maroncelli, M. *J. Phys. Chem. B* **2007**, *111*, 4978.

164. Jin, H.; Li, X.; Maroncelli, M. *J. Phys. Chem. B* **2007**, *111*, 13473.

165. Jin, H.; Baker, G. A.; Arzhantsev, S.; Dong, J.; Maroncelli, M. *J. Phys. Chem. B* **2007**, *111*, 7291.

166. Roy, D.; Patel, N.; Conte, S.; Maroncelli, M. *J. Phys. Chem. B* **2010**, *114*, 8410.

167. Roy, D.; Maroncelli, M. *J. Phys. Chem. B* **2010**, *114*, 12629.

168. Maroncelli, M.; Zhang, X. X.; Liang, M.; Roy, D.; Ernsting, N. P. *Disc. Faraday Soc.* **2012**, *154*, 409.

169. Zhang, X. X.; Liang, Min.; Ernsting, N. P.; Maroncelli, M. *J. Phys. Chem. B* **2013**, 117, 4291.

170. Zhang, X. X.; Liang, M.; Ernsting, N. P.; Maroncelli, M. *J. Phys. Chem. Lett.* **2013**, *4,* 1205.

171. Chakrabarty, D.; Chakraborty, A.; Seth, D.; Hazra, P.; Sarkar, N. *Chem. Phys. Lett.* **2004**, *397*, 469.

172. Chakrabarty, D.; Chakraborty, A.; Seth, D.; Sarkar, N. *J. Phys. Chem. A* **2005**, *109*, 1764.

173. Chakraborty, A.; Seth, D.; Chakrabarty, D.; Setua, P.; Sarkar, N. *J. Phys. Chem. A* **2005**, *109*, 11110.

174. Chakrabarty, D.; Hazra, P.; Chakraborty, A.; Seth, D.; Sarkar, N. *Chem. Phys. Lett.* **2003**, *381*, 697.

175. Seth, D.; Sarkar, S.; Sarkar, N. *J. Phys. Chem. B* **2008**, *112*, 2629.

176. Pramanik, R.; Rao, V. G.; Sarkar, S.; Ghatak, C. ; Setua, P.; Sarkar, N. *J. Phys. Chem. B* **2009**, *113*, 8626.

177. Sarkar, S.; Pramanik, R.; Ghatak, C.; Setua, P.; Sarkar, N. *J. Phys. Chem. B* **2010**, *114*, 2779.

178. Chowdhury, P. K.; Halder, M.; Sanders, L.; Calhoun, T.; Anderson, J. L.; Armstrong, W. D.; Song, X.; Petrich, J. W. *J. Phys. Chem. B* **2004**, *108*, 10245.

179. Carlson, P. J.; Bose, S.; Armstrong, D. W.; Hawkins, T.; Gordon, M. S.; Petrich, J. W. *J. Phys. Chem. B* **2012**, *116*, 503.

180. Kashyap, H. K.; Biswas, R. *J. Phys. Chem. B* **2008**, *112*, 12431.

181. Kashyap, H. K.; Biswas, R. *J. Phys. Chem. B* **2010**, *114*, 254.

182. Kashyap, H. K.; Biswas, R. *J. Phys. Chem. B* **2010**, *114*, 16811.

183. Daschakraborty, S.; Biswas, R. *J. Phys. Chem. B* **2011**, *115*, 4011.

184. Daschakraborty, S.; Biswas, R. *Chem.Phys. Lett.* **2011**, *510*, 202.

185. Das, S. K.; Sahu, P. K.; Sarkar, M. *J. Phys. Chem. B* **2013**, *117*, 636.

186. Das, S. K.; Sarkar, M. *J. Lumin.* **2012**, *132*, 368.

187. Sahu, P. K.; Das, S. K.; Sarkar, M. *J. Appl. Sol. Chem. Model.*, **2013**, *2*, 47.

188. Sahu, P. K.; Das, S. K.; Sarkar, M. *Phys. Chem. Chem. Phys.* **2014**, *16*, 12918.

189. Sahu, P. K.; Ghosh A.; Sarkar, M. *J. Phys. Chem. B* **2015**, *119*, 14221.

190. Sahu, P. K.; Das, S. K.; Sarkar, M. *J. Phys. Chem. B* **2014**, *118*, 1907.

191. Sahu, P. K.; Sarkar, M. *Chem. Phys. Lett.,* **2016**, *652*, 177.

192. Khara, D. C.; Samanta, A. *Phys. Chem. Chem. Phys.* **2010**, *12*, 7671.

193. Fruchey, K.; Fayer, M. D. *J. Phys. Chem. B* **2010**, *114*, 2840.

194. Mali, K. S.; Dutt, G. B.; Mukherjee, *J. Chem. Phys*. **2008**, 128, 054504.

195. Dutt, G. B. *J. Phys. Chem. B* **2010**, *114*, 8971.

196. Dutt, G. B. *Indian J. Chem*. **2010**, *49A*, 705.

197. Karve, L.; Dutt, G. B. *J. Phys. Chem. B* **2011**, *115*, 725.

198. Karve, L.; Dutt, G. B. *J. Phys. Chem. B* **2012**, *116*, 1824.

199. Karve, L.; Dutt, G. B. *J. Phys. Chem. B* **2012**, *116*, 9107.

200. Das, S. K.; Sarkar, M. *J. Phys. Chem. B* **2012**, *116*, 194.

201. Gangamallaiah V.; Dutt, G. B. *J. Phys. Chem. B* **2012**, *116*, 12819.

202. Gangamallaiah V.; Dutt, G. B. *J. Phys. Chem. B* **2014**, *118*, 13711..

203. Prabhu S. R.; Dutt, G. B. *J. Phys. Chem. B* **2014**, *118*, 9420.

204. Khara D. C., Kumar J. P., Mondal N., Samanta A. *J. Phys. Chem. B* **2013**, *117*, 5156.

205. B. Li, M. Qiu, S. Long, X. Wang, Q. Guo, A. Xia, *Phys. Chem. Chem. Phys*. **2013**, *15*, 16074.

206. Shim, Y.; Duan, J. S.; Choi, M. Y.; Kim, H. J. *J. Chem. Phys.* **2003**, *119*, 6411.

207. Kobrak, M. N.; Znamenskiy, V. *Chem. Phys. Lett.* **2004**, *395*, 127.

208. Znamenskiy, V.; Kobrak, M. N. *J. Phys. Chem. B* **2004**, *108*, 1072.

209. Shim, Y.; Choi, M. Y.; Kim, H. J. *J. Chem. Phys.* **2005**, *122*, 044511.

210. Bargava, B. L.; Balasubramanian, S. *J. Chem. Phys*. **2005**, *123*, 144505.

211. Bargava, B. L.; Balasubramanian, S. *J. Chem. Phys.* **2006**, *417*, 486.

212. Lockard, J. V.; Wasielewski, M. R. *J. Phys. Chem. B* **2007,** *111,* 11638.

213. Santosh, K.; Samanta, A. *J. Phys. Chem. B* **2010,** *141,* 11638.

214. Santosh, K.; Samanta, A. *ChemPhyschem* **2012,** *13,* 1956.

215. Li, X.; Maroncelli, M. *J. Phys. Chem. A* **2011,** *115,* 11638.

216. Wu, H.; Wang, H.; Xue, L.; Shi, Y.; Li. X. *J. Phys. Chem. B* **2010,** *114,* 14420.

217. Lee, H. Y.; Issa, J. B.; Isied, S. S.; Castner, E. W. Jr.; Pan, Y.; Hussey, C. L.; Lee, K. So.; Wishart J. F. *J. Phys. Chem. C* **2012**, *116*, 5197

218. Bhattacharya, B.; Samanta, A. *J. Phys. Chem. B* **2008**, *112*, 10101.

219. Kumar, V.; Pandey, S. *ChemPhysChem* **2013**, *14*, 491.

220. Kumar, V.; Rai, R.; Pandey, S. *RSC Adv.* **2013**, *3*, 11621.

221. Skrzypczak, A.; Neta, P. *J. Phys. Chem. A* **2003,** *107,* 7800.

222. Paul, A.; Samanta, A. *J. Phys. Chem. B* **2007,** *111,* 1957.

223. Sarkar, S.; Pramanik, R.; Ghatak, C.; Rao, V. G.; Sarkar, N. *Chem. Phys. Lett.* **2011,** *506*, 211.

224. Das, K.; Mondal, T.; Sen Mojumdar, S.; Bhattacharyya, K. *J. Phys. Chem. B* **2011,** *115,* 4680.

225. Liang, M.; Kaintz, A.; Baker, G. A.; Maroncelli, M. *J. Phys. Chem. B* **2012,** *116,* 1370.

226. Koch, M.; Rosspeintner, A.; Angulo, G.; Vauthey, E. *J. Am. Chem. Soc.* **2012**, *134*, 3729.

227. Birks, J. B. *Photophysics of Aromatic Molecules*; Wiley-Inter-Science: London, 1970.

228. Demchenko, A. P. *Luminescence* **2002**, *17*, 19.

229. Demchenko, A. P. *In Topics in Fluorescence Spectroscopy*; Lakowicz, J. R., Ed.; Plenum Press: New York, 1991; Vol. 3.

230. Lakowicz, J. R.; Nakamoto, S. K. *Biochemistry* **1984**, *23*, 3013.

231. Valeur, B.; Weber, G. *Chem. Phys. Lett.* **1977**, *45*, 140.

232. Weber, G.; Shinitzky, M. *Proc. Natl. Acad. Sci. U.S.A.* **1970**, *65*, 823.

233. Itoh, K.; Azumi, T. *J. Chem. Phys.* **1975**, *62*, 3431.

234. Chattopadhyay, A.; Mukherjee, S. *Biochemistry* **1993**, *32*, 3804.

235. Bagchi, B.; Jana, B. Chem. Soc. Rev. **2010,** *39*, 1936.

236. Bhattacharyya, K. *Acc. Chem. Res.* **2003**, *36*, 95.

237. Adhikari, A.; Sahu, K.; Dey, S.; Ghosh, S.; Mandal, U.; Bhattacharyya, K. *J. Phys. Chem. B* **2007**, *111*, 12809.

238. Lakowicz, J. R. *Principles of Fluorescence Spectroscopy, 3rd edition*; Springer: New York, 2006.

239. Dutt, G. B. *ChemPhysChem* **2005**, *6*, 413.

240. Hu, C. M.; Zwanzig, *R. J. Chem. Phys.* **1974**, *60*, 4354.

241. Gierer, A.; Wartz, K. Z. *Naturforsch A* **1953**, *8*, 532.

242. Dote, J. L.; Kivelson, D.; Schwart, R. N. *J. Phys. Chem.* **1981**, *85*, 2169.

243. Spears, K.G; Cramer, L.E. *J. Chem. Phys.* **1978**, *30*, 1.

244. Nee, T.-W.; Zwanzig, R. *J. Chem. Phys.* **1970**, *52*, 6353.

245. Julliard, M.; Chanon, M. *Chem. Rev.* **1983**, *83*, 425.

246. Whitten, D. G. *Acc. Chem. Res.* **1980**, *84*, 981.

247. Kondratenko, M.; Moiseev, A. G.; Perepichka, D. F. *J. Mater. Chem.* **2011**, *21*, 1470.

248. Liang, M.; Kaintz, A.; Baker, G. A.; Maroncelli, M. *J. Phys. Chem. B* **2012,** *116,* 1370.

249. Koch, M.; Rosspeintner, A.; Angulo, G.; Vauthey, E. *J. Am. Chem. Soc.* **2012**, *134*, 3729.

250. Damodaran, K. *Annual Reports on NMR Spectroscopy* **2016**, 88, 215.

251. Dias, N.; Shimizu, K.; Morgado, P.; Filipe, E.J.M.; Canongia Lopes, J. N.; F. Chavez, V. *J. Phys. Chem. B* **2014**, *118*, 5772.

252. Kruk, D.; Meier, R.; Rachocki, A.; Korpala, A.; Singh, R. K.; Rossler, E.A. *J. Chem. Phys.* **2014**, *140*, 244509.

253. Forse, A.C.; Griffin, J. M.; Merlet, C.; Bayley, P. M.; Wang, H.; Simon, P.; Grey, C.P. *J. Am. Chem. Soc.* **2015**, *137*, 7231.

254. Judeinstein, P.; Huet, S.; Lesot, P. *RSC Adv.* **2013**, *3*, 16604.

255. Herriot, C.; Khatun, S.; Fox, E.T.; Judeinstein, P.; Armand, M.; Henderson, W.A.; Greenbaum, S. *J. Phys. Chem. Lett.* **2012**, *3*, 441.

256. Cifelli, M. *Magn. Reson. Chem.* **2014**, *52*, 640.

257. Saihara, K.; Ohta, S.; Shimizu, A.; Yoshimura, Y. *Sci. Rep.* **2015**, *5*, 10619.

258. Rupp, A.B.A.; Welle, S.; Klose, P.; Scherer, H.; Krossing, I. *ChemPhysChem* **2015**, *16*, 1940.

259. Filippov, A.; Azancheev, N.; Taher, M.; Shah, F. U.; Rabet, P.; Glavatskih, S.; Antzutkin, O. N. *Magn. Reson. Chem.* **2015**, *53*, 493.

260. Liang, M.; Khatun, S.; Castner, E. W.; *J. Chem. Phys.* **2015**, *142*, 121101.

261. Radhi, A.; Le, K. A.; Ries, M. E.; Budtova, T. *J. Phys. Chem. B* **2015**,*119*, 1633.

262. Marekha, B. A.; Kalugin, O. N.; Bria, M.; Buchner, R.; Idrissi, A. *J. Phys. Chem. B* **2014**, *118*, 5509.

263. Simons, T. J.; Bayley, P. M.; Zhang, Z.; Howlett, P. C.; MacFarlane, D. R.; Madsen, L. A.; Forsyth, M. J. *Phys. Chem. B* **2014**, *118*, 4895.

264. Pereiro, A. B.; Araujo, J. M. M.; Oliveira, F. S.; Esperanca, J. M. S. S.; Canongi Lopes, J.N.; Marrucho, I. M.; Rebelo, L. P. N.; *J. Chem. Thermodyn.* **2012**, *55*, 29.

265. Hayamizu, K.; Tsuzuki, S.; Seki, S.; Umebayashi, Y. *J. Chem. Phys.* **2011**, *135*, 084505.

266. Hayamizu, K.; Tsuzuki, S.; Seki, S.; Umebayashi, Y. *J. Phys. Chem. B* **2012**, *116*, 11284.

267. Alam, T. M.; Dreyer, D. R.; Bielwaski, C.W.; . Ruoff, R. S *J. Phys. Chem. A* **2011**, *115*, 4307.

268. Antony, J. H.; Mertens, D.; Doelle, A.; Wasserscheid, P.; Carper, W. R. *ChemPhysChem* **2003**, *4*, 588.

269. Wahlbeck, P. G.; Carper, W. R. *Chem. Eng. Commun*. **2007**, *194*, 1160.

270. Han, K. S.; Li, S.; Hagaman, E. W.; Baker, G. A.; Cummings, P.; Dai, S. *J. Phys. Chem. C* **2012**, *116*, 20779.

271. Garaga, M. N.; Nayeri, M.; Martinelli, A. *J. Mol. Liq.* **2015**, *210*, 169.

272. Matveev, V. V.; Markelov, D. A.; Chizhik, V. I.; Ingman, P.; Lahderanta, E. *Russ. Chem. Bull.* **2013**, *62*, 1985.

273. Driver, G. W.; Ingman, P. *ChemPhysChem* **2011**, *12*, 757.

274. Endo, T.; Imanari, M.; Seki, H.; Nishikawa, K. *J. Phys. Chem. A* **2011**, *115*, 2999.

275. Endo, T.; Sen, S. *J. Phys. Chem. B* **2014**, *118*, 14888.

276. Nockemann, P.; Thijs, B.; Parac-Vogt, T. N.; Hecke, K. V.; Meervelt, L. V.; Tinant, B.; Hartenbach, I.; Schleid, T.; Ngan, V. T.; Nguyen, M. T.; Binnemans, K. *Inorg. Chem.* **2008**, *47*, 9987.

277. Pham, T. P. T.; Cho, C-W.; Yun, Y-S. *Water Research* **2010**, *44*, 352.

278. Deetlefs, M.; Seddon, K. R. *Green Chem.* **2010**, *12*, 17.

279. Smith, E. L.; Abbott, A. P.; Ryder, K. S. *Chem. Rev.* **2014**, *114*, 11060.

280. Gilbert, A.; Baggott, J.; Wagner, P. J. *Essential of Molecular Photochemistry*; Blackwell science Inc.: Cambridge, USA, 1991.

281. Rohatgi-Mukherjee, K. K. *Fundamentals of Photochemistry*; Wiley Eastern Ltd: India, 1986.

282. Becker, W. *Advanced time correlated single photon counting technique*; Springer: New York, 2005.

283. Demas, J. N. *Excited state lifetime measurement*; Academic press: New York, 1983.

284. O'Connor, D. V.; Phillips, D. *Time Correlated Single Photon Counting*; Academic: New York, 1984.

285. Ware, W. R. *Creation and detection of the Excited State*; Lamola, A. A., Ed.; Marcel Dekker: New York, 1971; Vol. 1, Part A.

286. Bevington, P. R. *Data Reduction and Error Analysis for the Physical Sciences*; McGraw-Hill: New York, 1969.

287. McKinnon, A. E.; Szabo, A. G.; Miller, D. R. *J. Phys Chem.* **1977**, *81*, 1564.

288. O'Connor, D. V.; Ware, W. R.; Andre, J. C. *J. Phys. Chem.* **1979**, *83*, 1333.

289. Ware, W. R.; Doemeny, L. J.; Nemzek, T. L. *J. Phys Chem.* **1973**, *77*, 2083.

290. Horng, M. L.; Gardecki, J.; Papazyan, A.; Maroncelli, M. *J. Phys. Chem.* **1995**, *99*, 17311.

291. Fee, R. S.; Maroncelli, M. *Chem. Phys.* **1994**, *183*, 235.

292. Fukushima, E.; Roeder, S. B. W. *Experimental Pulse NMR: A Nuts and Bolts Approach*; Addision-Wesley Publishing Company: Reading, MA, 1981.

293. Abragam, A. *The Principles of Nuclear Magnetism*; Oxford University Press: New York, 1961.

294. Amyes, T. L.; Diver, S. T.; Richard, J. P.; Rivas, F. M.; Toth, K. *J. Am. Chem. Soc.* **2004**, *126*, 4366.

295. McLean, A. J.; Muldoon, M. J.; C.M. Gordon, Dunkin, I. R. *Chem. Commun.* **2002**, 1880.

296. Okoturo, O. O.; VanderNoot, T. J. *J. Electroanal. Chem*. **2004**, *568*,167.

297. Izgorodina, E. I.; Maganti, R.; Armel, V.; P. Dean, M.; Pringle, J. M.; Seddon, K. R.; MacFarlane, D. R. *J. Phys. Chem. B* **2011**, *115*, 14688.

298. Dutt, G. B.; *ChemPhysChem* **2005**, *6*, 413.

299. Rilo, E.; Vila, J.; García-Garabal, S.; Varela, L. M.; Cabeza, O. *J. Phys. Chem. B* **2013**, *117*, 1411.

300. Ab Rani, M. A.; Brant, A.; Crowhurst, L.; Dolan, A.; Lui, M.; Hassan, N. H.; Hallett, J. P.; Hunt, P. A.; Niedermeyer, H.; Perez-Arlandis, J. M.; Schrems, M.; Welton, T.; Wilding, R. *Phys. Chem. Chem. Phys.,* **2011**, *13*, 16831.

301. Fumino, K.; Wulf, A.; Ludwig, R. *Angew. Chem., Int. Ed.* **2008**, *47*, 8731.

302. Peppel, T.; Roth, C.; Fumino, K.; Paschek, D.; Kckerling, M.; Ludwig, R. *Angew. Chem. Int. Ed.* **2011**, *50*, 6661.

303. Noack, K.; Schulz, P. S.; Paape, N.; Kiefer, J.; Wasserscheid, P.; Leipertz, A. *Phys. Chem. Phys. Chem.* **2010**, *12*, 14153.

304. Sureshkumar, M.; Lee, C. K. *J. Mol. Catal. B: Enzym.* **2009**, *60*, 1.

305. Paczal, A.; Kotschy, A. *Monatsh. Chem.* **2007**, *138*, 1115.

306. Harjani, J. R.; Naik, P. U.; Nara, S. J.; Salunkhe, M. M. *Curr. Org. Synth.* **2007**, *4*, 354.

307. Li, Z. J.; Chang, J.; Shan, H. X.; Pan, J. M. *Rev. Anal. Chem.* **2007**, *26*, 109.

308. Hagiwara, R.; Lee, J. S. *Electrochemistry* **2007**, *75*, 23.

309. Frisch, M. J. et al., *Gaussian 09 Rev 09.A0*, Gaussian, Inc.,Wallingford, CT, **2009.**

310. Horng, M.-L.; Gardecki, J. A.; Maroncelli, M. *J. Phys. Chem. A* **1997**, *101*, 1030.

311. Kurnikova, M. G.; Balabai, N.; Waldeck D. H.; Coalson, R. D. *J. Am. Chem. Soc.,* **1998**, *120*, 6121.

312. Hunt, P. A.; Kirchner, B.; Welton, T. *Chem. Eur. J.* **2006**, *12*, 6762.

313. Vieira, R. C.; Falvey, D. E. *J. Phys. Chem. B* **2007**, *111*, 5023.

314. Li, X.; Liang, M.; Chakraborty, A.; Kondo, M.; Maroncelli, M. *J. Phys. Chem. B* **2011**, *115*, 6592.

315. Bose, S.; Wijeratne, A. B.; Thite, A.; Kraus, G. A.; Armstrong,D. W.; Petrich, J. W. *J. Phys.Chem. B* **2009**, *113*, 10825.

316. Tahara, H.; Yonemura, H.; Harada, S.; Nakashima, A.; Yamada, S. *Chem. Phys. Lett.* **2012**, *524*, 42.

317. DeVine, J. A.; Labib, M.; Harries, M. E.; Rached, R. A. M.; Issa, J.; Wishart, J. F.; Castner Jr., E.W. *J. Phys. Chem. B* **2015**, *119*, 11336.

318. Boulton, A. J.; Ghosh, P. B.; Katritzky, A. R. *J. Chem. Soc. B* **1966**, 1004.

319. Ramachandram, B.; Samanta, A. *Chem. Commun.* **1997**, 1037.

320. Ramachandram, B.; Samanta, A. *Chem. Phys. Lett.* **1998**, *290*, 9.

321. Ramachandram, B.; Samanta, A. *J. Phys. Chem. A* **1998**, *102*, 10579.

322. Karmakar, R.; Samanta, A. *J. Am. Chem. Soc.* **2001**, *123*, 3809.

323. Badugu, R. *Chem. Lett.* **2002**, *31*, 52.

324. Bhattacharjee, U.; Beck, C.; Winter, A.; Wells, C.; Petrich, J. W. *J. Phys. Chem. B* 2014, *118*, 8471.

325. Rechthaler, K.; Ko¨hler, G. *Chem. Phys.* 1994, *189*, 99.

326. Pal, T.; Biswas, R. *J. Chem. Phys.* **2014**, 141, 164502.

327. Pal, T.; Biswas, R. *J. Chem. Phys.* **2014**, 141, 104501.

328. Van der Auweraer, M.; Gilbert, A.; De Schryver, F. C. *J. Am. Chem. Soc*. **1980**, *102*, 4007.

329. Swimen, A. M.; Van der Auweraer, M.; De Schryver, F. C.; Nakatani, K.; Okada, T.; Mataga, N. *J. Am. Chem. Soc.* **1987**, *109*, 321.

330. Sahu, K.; Kern, S. J.; Berg, M. A. *J. Phys. Chem. A* **2011**, *115*, 7984.

331. Singh, T.; Kumar, A. *J. Phys. Chem. B* **2008**, *112*, 12968.

332. Cote, J.-F.; Brouillette, D.; Desnoyers, J. E.; Rouleau, J.-F.; St.-Arnaud, J.-M.; Perron, G.; *J. Solution Chem.* **1996**, *25*, 1163.

333. Zusman, L. D. *Chem. Phys.* 1980, *49*, 295.

334. Marcus, R. A. *Rev. Mod. Phys.* 1993, *65*, 599.

335. Marcus, R. A. *J. Chem. Phys.* **1956**, *24*, 979.

336. Sasmal, D. K.; Mandal, A. K.; Mondal, T.; Bhattacharyya, K. *J. Phys. Chem. B*, **2011**, *115*, 7781.

337. Rao, V. G.; Ghatak, C.; Ghosh, S.; Mandal, S.; Sarkar. N. *J. Phys. Chem. B*, **2012**,*116*, 3690.

338. Nanda, R.; Rajamohanan, P. R.; Kumar, A. *ChemPhysChem*, **2015**, *16*, 2936.

339. Ivanov, D. A.; Petrov, N. K.; Klimchuk, O.; Billard, I. *Chem. Phys. Lett*. **2012**, *551*, 111.

340. Gomes, M. C.; Lopes, J. N. C.; Padua, A. A. H. *Thermodynamics and Micro Heterogeneity of Ionic Liquids, (Ed. B. Kirchner)*, Springer, Berlin Heidelberg, **2010**, *290*, 161.

341. Sahu, P. K.; Ghosh A.; Sarkar, M. *J. Phys. Chem. B* **2015**, *119*, 14221.

342. Jiang, W.; Wang, Y.; Voth, G. A. *J. Phys. Chem. B*, **2007**, *111*, 4812.

343. Shirota, H. Biswas, R. *J. Phys. Chem. B* **2012**, *116*, 13765.

344. H. Shirota, *J. Phys. Chem. B* **2013**, *117*, 7985.

345. Shi, W.; Damodaran, K.; Nulwala, H. B.; Luebke, D. R. *Phys. Chem. Chem. Phys.* **2012**, *14*, 15897.

346. Allen, J. J.; Bowser, S. R.; Damodaran. K. *Phys. Chem. Chem. Phys.* **2014**, *16*, 8078.

347. Anouti, M.; Jacquemin, J.; Porion. P.; *J. Phys. Chem. B* **2012**, *116*, 4228.

348. Singh, T.; Kumar, A. *J. Phys. Chem. B*, **2007**, *111*, 7843.

349. Russina, O.; . Sferrazza, A.; Caminiti, R. Triolo, A. *J. Phys. Chem. Lett.* **2014**, *5*, 1738.

350. Pal, T.; Biswas, R. *J. Phys. Chem. B* **2015**, *119*, 15683.

351. Nakakoshi, M.; Ishihara, S.; Utsumi, H.; Seki, H.; Koga, Y.; Nishikawa, K. *Chem. Phys. Lett.* **2006**, *427*, 87.

352. Sun, B. Jin, Q.; Tan, L.; Wu, P.; Yan,.F. *J. Phys. Chem. B*, **2008**, *112*, 14251.

353. Sun, X.-G.; Liao, C.; Baggetto, L.; Guo, B.; Unocic, R. R.; Veith, G. M.; Dai, S. *J. Mat. Chem. A*, **2014**, *2*, 7606.

354. Wu, F.; Zhu, Q.; Chen, R.; Chen, N.; Chen, Y.; Li, L. *Nano Energy*, **2015**, *13*, 546-553.

355. Zăgar, E.; Z ǐgon, M. *Polymer* **2000**, *41*, 3513.

356. Borrmann, H.; Persson, I.; Sandstro¨m, M.; Stålhandske, C. M. V. *J Chem Soc Perkin Trans 2* **2000**, 393.

357. Deetlefs, M.; Hardacre, C.; Nieuwenhuyzen, M.; Sheppard, O.; Soper, A. K. *J. Phys. Chem. B*, **2005**, *109*, 1593.

358. Shimomura, T.; Takamuku, T.; Yamaguchi, T. *J. Phys. Chem. B* **2011**, *115*, 8518.

359. Takamuku, T.; Shimomura, T.; Sadakane, K.; Koga, M.; Seto, H. *Phys. Chem. Chem. Phys.* **2012**, *14*, 11070.

360. Noda, A.; Hayamizu, K.; Watanabe, M. *J. Phys. Chem. B*, **2001**, *105*, 4603.

361. Klinger, J. Friedrich, T. *Biophys J.* **1997**, *73*. 2195.

362. Yeganegi, S.; Soltanabadi, A.; Farmanzadeh, D. *J. Phys. Chem. B* **2012**, *116*, 11517.

363. Ishida, T.; Shirota, H. *J. Phys. Chem. B* **2013**, *117*, 1136.

364. Bhargava, B. L.; Klein, M. L. *J. Chem. Theory Comput*. **2010**, *6*, 873.

365. Bodo, E.; Chiricotto, M.; Caminiti, R. *J. Phys. Chem. B* **2011**, *115*, 14341.

366. Li, S.; Feng, G.; Ban˜uelos, J. L.; Rother, G.; Fulvio, P. F.; Dai, S.; Cummings, P. T. *J. Phys. Chem. C* **2013**, *117*, 18251.

367. Li, S.; Van Aken, K. L.; Aken, V.; McDonough, J. K.; Feng, G.; Gogotsi, Y.; Cummings, P. T. *J. Phys. Chem. C* **2014**, *118*, 3901.

368. Shirota, H.; Ishida, T. *J. Phys. Chem. B* **2011**, *115*, 10860.

369. Turro, N. J. *Modern Molecular Photochemistry*; Benjamin/Cummings: San Francisco, 1978.

370. Davydov, A. S. *Theory of Molecular Excitons*; Springer: New York, 1971.

371. Inamura, Y.; Yamamuro, O.; Hayashi, S.; Hamaguchi, H. *Phys. B* **2006**, *385*, 732.

372. Mao, Y.; Damodaran, K. *Chem. Phys.* **2014**, *440*, 87.

373. Lovelock, K. R. J.; Ejigu, A.; Loh, S. F.; Men, S.; Licence, P.; Walsh, D. A. *Phys. Chem. Chem. Phys.* **2011**, *13*, 10155.

374. Seyedlar, A. O.; Stapf, S.; Mattea, C. *Phys. Chem. Chem. Phys.* **2015**, *17*, 1653.

375. Mukherjee, K.; Das, A.; Choudhury, S.; Barman, A.; Biswas, R. *J. Phys. Chem. B* **2015**, *119*, 8063.

376. Habasaki, J.; Ngai, K. L. *J. Chem. Phys.* **2008**, *129*, 194501.

377. Tsuzuki, S. *ChemPhysChem* **2012**, *13*, 1664.

378. Das, S. K.; Sarkar, M. *ChemPhysChem* **2012**, *13*, 2761.

379. Maroncelli, M.; Fleming, G. R. *J. Chem. Phys.* **1987**, *86*, 6221.

380. Halder, A.; Sen, S.; Das Burman, A.; Patra, A.; Bhattacharyya, K. *J. Phys. Chem. B* **2004**, *108*, 2309.

381. Halder, M.; Headley, L. S.; Mukherjee, P.; Song, X.; Petrich, J. W. *J. Phys. Chem. A* **2006**, *110*, 8623.

.